TAMPEREEN TEKNILLINEN YLIOPISTO
TAMPERE UNIVERSITY OF TECHNOLOGY

Markus Rokala

Analysis of Slipper Structures in Water Hydraulic Axial Piston Pumps

Julkaisu 1055 • Publication 1055

Tampere 2012

Tampereen teknillinen yliopisto. Julkaisu 1055
Tampere University of Technology. Publication 1055

Markus Rokala

Analysis of Slipper Structures in Water Hydraulic Axial Piston Pumps

Thesis for the degree of Doctor of Science in Technology to be presented with due permission for public examination and criticism in Konetalo Building, Auditorium K1702, at Tampere University of Technology, on the 21st of June 2012, at 12 noon.

Tampereen teknillinen yliopisto - Tampere University of Technology
Tampere 2012

ISBN 978-952-15-2867-5 (printed)
ISBN 978-952-15-2872-9 (PDF)
ISSN 1459-2045

Rokala, M., **Analysis of Slipper Structures in Water Hydraulic Axial Piston Pumps,** Tampere, 2012, 97 p.

Keywords: Slipper structure, Slipper deformations, Slipper-swashplate contact, Water hydraulics, Axial piston pump

ABSTRACT

This thesis is focused on slipper behaviour during operation, slipper behaviour during swashplate turning and especially the impact of the slipper deformations in water hydraulic axial piston pumps. Experimental research, numerical methods, like computational fluid dynamics and fluid-structure interaction, and simulation are used as research methods. The main target is to find methods to achieve a higher power density of water hydraulic axial piston pumps because better components are necessary to obtain a wider range of applications for water hydraulics. The work is primarily basic research, not the development of an actual water hydraulic pump.

Two different basic structures of slippers with different material combinations are studied and compared through the work. It is shown that it is possible to follow the maximum PV-rate of the material. However, that means that the sizing of the slipper is designed near the limit of the hydrostatic balance. The problem is that the deformations should be accurately known in order to be able to do that.

Basic theory shows the physical base and also that numerical methods are needed if deformation is taken into account. Measurements show that slipper behaviour is smooth during swashplate turning and the problems of realizing a variable displacement pump are not from slipper-swashplate contact. Restrictions in achieving a higher pressure level are the deformation and PV-rate of the material. It is possible to size the slipper near the limit of the hydrostatic balance, which helps to obtain acceptable PV-rate values. In this case the deformations of the slipper have to be accurately known to avoid slipper lift from the surface.

Sliding surface deformations are one of the key factors in industrial plastic-made slipper design. Deformations are so big that the pressure profiles are totally different from the basic equations expected. Consequently, the leakage flow is also higher than expected. The difference of the force of the sliding surface between basic equation and FSI calculation arises when the pressure level rises. With one slipper with a steel core, for example, the force is 11.4 % higher at a pressure level of 10 MPa and 27.1 % higher at a pressure level of 40 MPa than is calculated with the basic equations. Nowadays the power loss is one significant reason to decide the dimensions of the slipper. The optimum ratio is, however, calculated based on the basic equations, the results of which are incorrect.

The results of the study show that FSI calculations are necessary to make the right decisions in slipper design. However, it is not needed to calculate all different situations because the behaviour of the slipper is logical. Slipper behaviour can be predicted with sufficient accuracy with the simulation model based on a few FSI calculations, basic theory and measurements. In this thesis, a simple simulation model is developed to predict the behaviour of two types of slipper structures.

PREFACE

The study was carried out at the Department of Intelligent Hydraulics and Automation (IHA), Tampere University of Technology (TUT), during 2006-2012 and was partly funded by The Academy of Finland and the TUT Graduate School.

I am grateful to the advisor of my studies and this thesis, Professor Kari T. Koskinen, for his dedicated support and advice. I am also grateful to Professor Matti Vilenius, former Head of Department, and Kalevi Huhtala, Head of Department, for providing excellent facilities for this study.

Thanks are also due to the whole staff of IHA for their help, support and discussions, particularly to the laboratory staff and the research group of water hydraulics. I wish to thank Olof Calonius from Aalto University/Engineering Design and Production for numerous discussions. I am also thankful to the company Danfoss A/S for support.

For the revision of the English manuscript I would like to thank John Shepherd.

My wife, Terhi, and my daughter, Reetta: I want especially to thank you for your love, support and understanding. Finally, I would like to thank my parents, Sinikka and Kari, for their support during this study and the whole of my life.

Tampere, 2012

Markus Rokala

CONTENTS

NOMENCLATURE

LATIN ALPHABETS

$A_{slipper}$	Area of the sliding surface of the slipper	[m^2]
A_{piston}	Piston area	[m^2]
a	Acceleration	[m/s^2]
C_1	Integration constant	[-]
C_2	Integration constant	[-]
c_f	Friction coefficient between slipper and swashplate	[-]
D_i	Slipper inner diameter	[m]
D_o	Slipper outer diameter	[m]
D_{piston}	Piston diameter	[m]
F_c	Centrifugal force of the slipper	[N]
$F_{friction}$	Friction force between slipper and swashplate	[N]
F_{hold_down}	Force from the slipper hold-down mechanism	[N]
$F_{inertia}$	Inertia force of the piston / slipper	[N]
$F_{p\_friction}$	Friction force between piston and cylinder	[N]
F_{piston}	Piston force against slipper	[N]
$F_{pressure}$	Pressure force on piston	[N]
F_{pts}	Force from piston to slipper	[N]
$F_{sealing}$	Lifting force of the sliding surface	[N]
$F_{slipper}$	Lifting force of the slipper	[N]
F_{stp}	Force from slipper to piston	[N]
F_{sp}	Reaction force of the swashplate	[N]
H	Power loss	[W]
H_p	Pumping loss	[W]
H_v	Viscous dissipation	[W]
h	Lubrication film thickness	[m]
h_1, h_2, h_3	Gap height at slipper outer edge	[m]

$\hat{h}$	Dimensionless lubrication film thickness	[-]
h_{CG}	Height of the slipper CG	[m]
h_{min}	Minimum gap height	[m]
h_r	Height of the deformation of the sliding surface	[m]
K	Slipper inner radius deformation coefficient	[-]
L_r	Width of the sliding surface	[m]
m_{piston}	Mass of the piston	[kg]
$m_{slipper}$	Mass of the slipper	[kg]
n	Rotational speed	[s^{-1}]
p	Pressure	[Pa]
p_{piston}	Pressure above piston	[Pa]
$p_{slipper}$	Pressure into the slipper pocket	[Pa]
$PV_{slipper}$	Pressure-velocity-rate of the slipper centre point	[MPa m/s]
q	Hydrostatic balance of the piston-slipper assembly	[-]
q'_{leak}	Volumetric flow rate per unit width	[m^2/s]
q_{leak}	Leakage flow	[m^3/s]
r	Radial dimension	[m]
r, θ, z	Cylindrical polar coordinates	[-]
r_i	Slipper inner radius	[m]
r_o	Slipper outer radius	[m]
R_{rot}	Radius of the rotation circle	[m]
t	Time	[s]
u	Velocity in x direction	[m/s]
u_a	Velocity of the a-surface	[m/s]
u_b	Velocity of the b-surface	[m/s]
v	Velocity in y direction	[m/s]
v_a	Velocity of the a-surface	[m/s]
v_b	Velocity of the b-surface	[m/s]
v_r	Velocity in r direction of polar coordinates	[m/s]
v_θ	Velocity in θ direction of polar coordinates	[m/s]
w	Velocity in z direction	[m/s]
X_a, Y_a, Z_a	Body forces in Cartesian coordinates	[m/s^2]
x, y, z	Cartesian coordinates	[-]

GREEK ALPHABETS

β	Swashplate angle	[deg]
ρ	Force density	[N·s^2/m^4]
δ	Slope of deformation	[-]
$\hat{\delta}$	Slope of deformation	[-]
ξ	Dilatation	[s^{-1}]
η	Dynamic viscosity	[Pa·s]
ω	Angular velocity	[s^{-1}]

ABBREVIATIONS

CFD	Computational fluid dynamics
CG	Center of gravity
DLC	Diamond-like carbon
FEM	Finite element method
FSI	Fluid-structure interaction
HB	Hydrostatic balance
HFA	Oil-in-water emulsions
PEEK	Polyetheretherketone
PTFE	Polytetrafluoroethylene

1 INTRODUCTION

1.1 Water hydraulics today

Although water hydraulics is a very old technology and the earliest hydraulic systems used water as the pressure medium, powerful technical development and research was started only in the 1980s. The research and development of water hydraulics is a multi-technical challenge. Research is a combination of hydraulics, mechanical design, tribology, control technology and material science. Also it is important to consider the water properties and the quality of the water.

Modern water hydraulics should provide fluid power components that operate with pure water and thus represent an environmentally friendly alternative to the ubiquitous oil hydraulics. In many areas of application there are requirements that the medium be non-flammable and, as leakages must be taken into account, non-harmful to products being made. In addition, if relatively high power density is required water hydraulics has an advantage over pneumatics.

Consequently, water hydraulics is particularly well suited for industrial activities such as food processing, sea water desalination, steel production, mining, packaging industry, the pulp and paper industry, nuclear power generation and for producing mobile machinery for environmentally sensitive areas. Offshore industry uses water hydraulic systems with seawater.

Technologically, however, there are challenges to be met in order to make water hydraulic systems more competitive and more reliable compared to oil hydraulic or pneumatic systems. The physical and chemical properties of the water produce challenges which mean that the components and the hydraulic systems should be redesigned. In fact, there are different types of technologies within water hydraulics because the pressure levels of the system can vary from low pressure to very high pressures.

Water is a poor lubricant. Compared to mineral oil, the lower viscosity and the lower viscosity-pressure coefficient of water makes lubrication more difficult. Water as a pressure medium requires that all materials should be non-corrosive and all clearances smaller than in oil hydraulic units. Sliding pairs of pumps are usually made of stainless steel and some type of reinforced industrial plastic, for example PEEK. All bearings are sliding bearings because adequate ball or roller bearings are not yet available. Various materials have been tested in pumps in recent years and at least water hydraulic pumps with ceramic pistons are available. Because of the requirements of special design and materials water hydraulic components, including pumps, are generally more expensive than oil hydraulic components. Costs are high also because the amount of production is rather low.

Research activities in the water hydraulics are going all the time but the biggest effort has already been made. However, the technical challenges and demands of the applications create a need for continued water hydraulic research. Advantages of water hydraulics are mostly related to the processes of the end user and the challenges are directly related to the water hydraulic system and especially component design. However, human friendliness and environmental safety are powerful global trends which ensure that water hydraulics will have an important role in the future.

1.2 Basic structure of water hydraulic axial piston pump

Axial piston pumps and motors are commonly used in hydraulic applications because of their compact size, wide operating range and controllability. On the other hand, these types of pumps and motors are quite complex.

The basic structure of the axial piston pump is shown in Figure 1. The axial piston pump usually contains 7 or 9 pistons in the rotating cylinder block. The pistons execute linear movements into the cylinders. During one revolution the pistons execute the full stroke. The pistons are connected to the swashplate with slippers, which allows rotating motion against the swashplate. The swashplate has an inclination angle which defines the stroke of the pistons. The theoretical flow of the pump is worked out with the piston area, stroke of the pistons, number of the pistons and the rotation speed of the cylinder block.

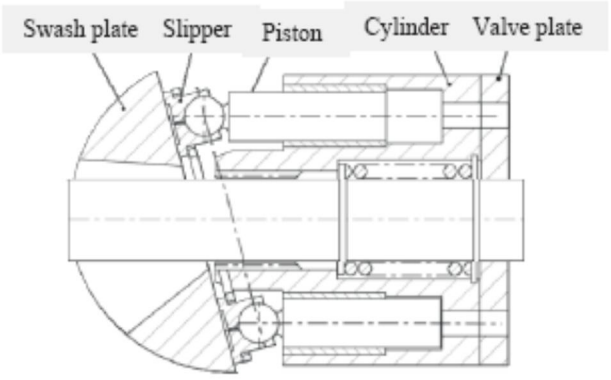

Figure 1. Structure of axial piston pump. [Pelosi 2009]

The other end of the cylinder block is connected to the valve plate as Figure 1 shows. The valve plate realizes the connection of the piston chambers to the suction and pressure ports. Usually, the swashplate and the valve plate are fixed and the cylinder block is the rotating part. The whole package shown in Figure 1 is in water inside the housing.

There are several sealing and bearing gaps in axial piston pumps. All the gaps, the gap between valve plate and cylinder, cylinder and piston, piston and slipper and also the gap between slipper and swashplate, are important for desirable pump working. The gap design affects the function of the bearing and sealing. Also the energy losses and therefore efficiency of the pump are dependent on gap design. It is noticed that a significant part of the leakage happens through the slipper in axial piston pumps and the good performance of the pump is directly dependent on smooth slipper-swashplate motion. The volumetric, hydraulic and mechanical efficiencies in water hydraulic axial piston pumps are all affected by slipper performance.

To increase the overall efficiency of the system, variable displacement axial piston units are currently widely used basic components in oil hydraulics. In variable displacement pumps the angle of the swashplate is adjustable. The movement of the pistons changes as a function of the swashplate angle and it is possible to control the flow of the pump. In mobile machines most of the units are currently axial piston design. Axial piston type units are very competitive also in modern water hydraulic pumps and motors. However, there is only one commercial variable axial piston pump for water hydraulics, which is a challenge in certain applications. All in all the commercial range of water hydraulic components is very limited.

In axial piston machines the piston forces should transmit to the swashplate with low friction connection. Pistons with slippers are commonly used in water hydraulic axial piston pumps to realize that connection. The objective of the slipper is to maintain bearing between the static swashplate and the rotating cylinder barrel. The slipper is also a sealing part and it compensates part of the piston pressure. The slipper and the swashplate are usually connected with a ball joint. The structure of the slipper-swashplate contact is shown in Figure 2.

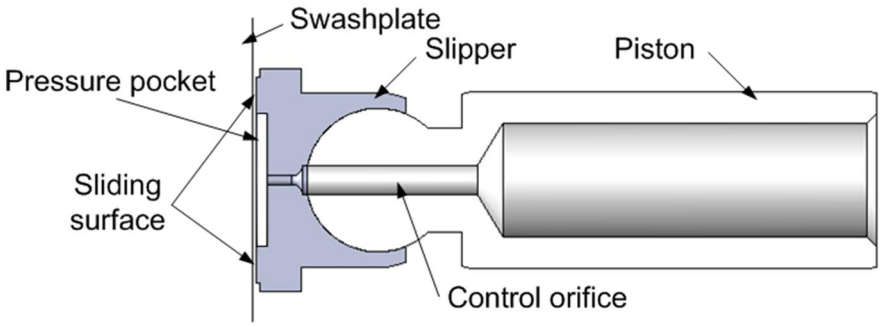

Figure 2. Cross-section of the structure of the slipper swashplate contact.

The idea is that the pressurized fluid into the cylinder chamber is connected to the slipper pressure pocket through the orifice. The fluid flows through the gap between the slipper and the swashplate and maintains the lubrication. Also the lubrication of the ball joint is made with fluid. The slippers are pushed against the swashplate with a slipper hold-down device to produce continuous contact and smooth operation between slipper and swashplate. That is needed because during the suction stroke there is no pushing pressure force. The slipper hold-down mechanism is usually spring-loaded.

Hydrostatic force is the product of hydraulic pressure and area. The balancing hydrostatic force is achieved by exposing opposing areas to the same pressure. In axial piston pumps the pressure force on the piston pushes the slipper to the swashplate. Opposite force is generated on the slipper and this force moves the slipper away from the swashplate. Theoretical hydrostatic balance of the piston-slipper assembly can be calculated by piston and slipper dimensions as Equation 1 shows [Donders 1997]. The derivation of Equation 1 is shown in Chapter 3.3.

$$q = \frac{D_i^2 - D_o^2}{2D_{piston}^2 \ln\left(\frac{D_i}{D_o}\right)} \tag{1}$$

The theoretical calculation assumes that there is a narrow and parallel gap between the slipper and swashplate. Hydrostatic balance values below 1 means that the pushing force is bigger than the lifting force. Also the term clamping ratio is used to describe hydrostatic balance. If the lifting force is greater than the piston load the slipper is underclamped, otherwise the slipper is overclamped.

1.3 Objectives of the thesis

The main reason for this work is the need for more efficient and durable water hydraulic components with higher power density. Better components are necessary to obtain a wider range of applications. This thesis is focused on the slipper-swashplate contact in axial piston pumps and obtains important information

necessary to operationalize a water hydraulic axial piston pump with higher pressure level and a variable displacement pump, which is one of the key components in producing more efficient systems.

The objectives of the study can be summarized as follows:

- to analyse the behaviour of different slippers experimentally
- to analyse slipper behaviour with numerical methods
- to build a semi-empirical model of slipper behaviour
- to predict the behaviour of the slipper with a semi-empirical model
- to define the restrictions and guidelines of slipper design

Several scientific papers were published during this research. The theoretical examination, experiments and the structure of the test rig are presented in [Rokala 2008a] and [Rokala 2008b]. A comparison of three different slipper structures is shown in [Rokala 2010]. [Rokala 2011] concentrates on the impact of the slipper PV-rate.

1.4 Structure of the thesis

This thesis contains seven chapters. The contents of the chapters are briefly as follows:

Chapter 1 introduces water hydraulic and axial piston pumps. Also the motivation of the study and objectives are presented.

Chapter 2 provides an overview of research going on concerning water hydraulic axial piston pumps and slipper-swashplate interaction generally in the hydraulic area. Chapter 2 also introduces commercial water hydraulic axial piston pumps on the market.

Chapter 3 concentrates on the theoretical aspect of slipper-swashplate contact. The slipper structures used in this study are introduced in this chapter. Different aspects of slipper behaviour are studied and lubrication theory is applied to the slipper-swashplate contact.

Chapter 4 introduces the test rig used in this study. Experimental results of the friction, lubrication gap, leakage and behaviour during operation are shown and discussed.

Chapter 5 includes deformation analysis of the slippers. Especially sliding surface deformations of the slippers and the pressure profile under the sliding surface are studied with numerical analysis.

Chapter 6 combines the results of the previous chapters. Based on the calculations, measurements, numerical analysis and water and material properties, a semi-empirical model of slipper behaviour is presented.

Chapter 7 concludes the study.

2 STATE OF THE ART OF WATER HYDRAULIC AXIAL PISTON PUMPS

Water has many good properties as a hydraulic medium but technological challenges still exist. More about water as a medium and water hydraulics in general can be found in references [Backé 1999], [Trostmann 1996] and [Urata 1999].

Water hydraulics have been studied during recent decades and publications about water hydraulic axial piston pumps are reviewed. Oil hydraulic axial piston pumps are very widely studied and the number of publications is very large. Also the interaction between slipper and swashplate has been widely studied. The following chapters are a brief summary of the most significant publications concerning this research field.

2.1 Water hydraulic axial piston pump research

Water hydraulic pumps have mainly been in-line piston pumps until the 1980's. Some developments of water hydraulic axial piston machines have been made around world during the past three decades. Design, development and testing of one kind of sea water hydraulic axial piston pump and power pack was made under the Eureka-program during 1994-1996. The research included material research, pump design and pump tests, including life time tests. The development is described in references [Terävä 1995] and [Pohls 1999].

In reference [Usher 1998a] water hydraulic pump and motor development during 10 years is shown. The changes in slipper design, material selections and power pack development are discussed.

Bech et al. introduced general design lines for water hydraulic pumps in reference [Bech 1999]. They also developed vane and gear pumps for mini-power packs during the project. The design of the pumps, material of the pumps and test results are also discussed. The combination of stainless steel and coal fibre reinforced PEEK has proven to be successful in water hydraulic pumps.

The problems of water hydraulic axial piston pumps are studied in reference [Dong 2001]. Material selection, optimizing structure and manufacturing are recognized as the key problems. The article also includes experimental work for pump design and the results for pump measurements. In reference [Petrovic 2011] novel axial piston pumps with low lateral forces are researched with a mathematical model and experimental tests.

Material research is an important part of water hydraulic component research. Materials for friction pairs are experimentally studied in references [Brookes 1995] and [Jiao 2003]. In [Jiao 2003] the test system and conditions are described and the results reported. The wear mechanism of ceramic-ceramic contact is fatigue and surface fracture. In stainless steel-polymer combinations the wear mechanism of the PEEK composites is fatigue when the load is lighter and micro-cutting and plastic deformation when the load is heavier. The conclusion is that metal-polymer combinations are more suitable to be friction pairs in water hydraulic piston pumps, but that ceramic-ceramic combinations also have potential. Yang et al. have studied piston and cylinder materials in water hydraulic pumps [Yang 2003]. They concluded that it is more

suitable to use stainless steel and engineering plastics than stainless steel and ceramics. DLC coating in water hydraulic pumps is studied in reference [Yuge 2006] by simulation and experimental tests. The authors conclude that DLC coatings can improve the tribological property of stainless steel in water.

In reference [Zhou 1999] cavitation inception in water hydraulic piston pumps has been studied. The topic is important because cavitation damage is likely to occur in water hydraulics components. Signal analysis of the outlet pressure is used to identify the cavitation inception.

Companies have some patents concerning water hydraulic axial piston pumps [Kuikko 1997], [Olsen 2008] and [Usher 1998b]. Key elements of the patents are the structure and materials of the slipper. Stainless steel and industrial plastics combinations are used in all the inventions.

Some axial piston pump papers, without water aspect, are also very important to note. Papers concerning pump in general, for example control of pumps or numerical methods, can easily applied in water hydraulics also. The principles are usually common to all fluids and some methods and tools for axial piston pump research are developed in references [Pelosi 2008], [Pelosi 2009] and [Wieczoreck 2000].

2.2 Slipper-swashplate contact research

In axial piston pumps slippers are key components which have been widely researched. Lubrication conditions between the swashplate and the slipper pad have been studied in many research projects. Most of the research, such as [Hooke 1988] and [Koc 1992], was performed using oil as pressure medium. In [Hooke 1988] oil film thickness is measured and it is proved that the thickness can be predicted with reasonable accuracy. In [Kazama 1993a] optimum design of the bearing and seal parts of the hydraulic equipment have been studied.

Koc et al. [Koc 1997] show that for successful slipper operation, slippers require a slightly convex surface on the running face. Also the slippers examined seemed to run satisfactorily, with no control orifice, and to have their greatest resistance to tilting couples. In [Koc 1996] Koc and Hooke concluded that the slippers are very sensitive to the overclamp ratio and orifice size. They also say that the behaviour of the slipper is not the same at low and high pressures.

Harris et al. [Harris 1996] describe dynamic model to predict slipper lift and tilt behavior. According the study, the contact between slipper and swashplate can occur as the piston makes the transition between suction and delivery. Hydrodynamic and hydrostatic aspects of slipper bearing are studied in [Carbone 2002]. In [Borghi 2009] the critical speed of slipper bearing is studied. The effect of different factors are showed and discussed.

Research has also been carried out with water based fluids. In references [Li 1991], [Donders 1997], [Huanlong 2006] and [Kazama 2005] lubricating conditions have been studied using water or HFA-fluid in axial piston pumps. In [Li 1991] experimental friction measurements were made. The authors concluded that water-based slippers run with much lower film thickness than with oil operation, but, however, after run-in they operate with full film lubrication and the analyses developed for oil-based slippers are valid for water-lubricated systems. They also concluded that successful operation of the composite slippers appears to depend on the ability of the slippers and swashplate materials to polish to a combined surface roughness below that of the film thickness.

Donders and Backé [Donders 1997] worked with axial piston pumps and high water based fluids. Experimental tests with two different slippers were made. They concluded that slipper types with just one sealing land give better results in terms of efficiency and resistance against wear. They also concluded that even when conventional materials are being used for swashplate and slipper, satisfactory efficiency and lifetime can be achieved.

In [Huanlong 2006] the lubrication characteristics of water hydraulic friction pairs have been studied with simulations and experiments. The authors conclude that the three-cavity independent supporting slipper can improve the anti-turnover ability of the slipper. They noticed that the surface roughness has an important role for leakage flow and classical theory gives too high leakages.

In [Kazama 1993b] the characteristics of the hydrostatic bearing on mixed lubrication are studied. The results show that minimum power loss on mixed lubrication is achieved when the ratio of hydrostatic balance becomes close to unity. In [Kazama 2005] a time-dependent mathematical model of hydrostatic and hydrodynamic bearings under mixed and fluid film lubricating conditions was developed. The results tell that an eccentric load causes local contacts, the preceding change in the load poses a larger motion of the bearing, and as the recess volume increases the bearing stiffness decreases.

In [Wang 2002] the characteristics of hydrostatic bearings are studied with experiment and theory. The conclusions are that materials more compressible than stainless steel can improve the load carrying capacity of the hydrostatic bearing. Also the tribological behaviour of the slipper in water hydraulic axial piston motors has been studied at least in [Nie 2006].

In [Manring 2002] the impacts of concave and convex deformations were investigated. Bearing deformation causes the required flow rate to increase and bearing deformations have a larger impact on the flow rate than they do on the load carrying capacity. The authors noticed that a concave deformation causes more bearing leakage than an equal amount of convex deformation. They also concluded that bearings with large pockets are less sensitive to bearing deformations than bearings with small pockets. Reference [Manring 2004] discusses linear deformations of the slipper and the performance characteristics of similar slipper bearings using different socket geometries. The authors concluded among other things that the majority of the bearing deformation occurs at low pressure and does not generally change much for pressures that exceed 14 MPa.

In reference [Canbulut 2009] frictional power loss of the hydrostatic slipper bearings is discussed. Experimental analysis was done and the authors concluded that the least power loss occurred with slipper surface roughness of 1.5 µm. The research also indicated that the power loss increased between velocities 0.52 and 1.08 m/s and decreased between 1.08 and 3.34 m/s for all supply pressures. The measurements were done in oil lubrication.

It is interesting to note that although slipper swashplate contact has been commonly researched, all the presented articles discuss slipper-swashplate contact with a constant swashplate angle. Changing of the swashplate angle and behaviour during changing has not been of interest.

2.3 Available water hydraulic axial piston pumps on the market

There are several different water hydraulic pumps on the market at the moment. Most of the pumps are oil lubricated piston pumps which are driven by a crankshaft mechanism. Only a few of the pumps on the

market are totally water lubricated. Water lubricated pumps are usually axial piston pumps with non-adjustable swashplate. In this research only water lubricated axial piston pumps are studied.

Water as a pressure medium requires that all materials should be non-corrosive and all clearances are smaller than in oil hydraulic units. Sliding pairs of pumps are usually made of stainless steel and some type of reinforced industrial plastic, for example PEEK. All bearings are sliding bearings because adequate ball or roller bearings are not yet available. Various materials have been tested in pumps in recent years and at least water hydraulic pumps with ceramic pistons are available. Because of the requirements of special design and materials, water hydraulic components, including pumps, are generally more expensive than oil hydraulic components. Costs are high also because the amount of production is rather low. All in all, manufacturing of the water hydraulic components is very demanding, which partly accounts for the low number of water hydraulic component manufacturers.

Usually the maximum pressure level of the water hydraulic axial piston pump is 16 MPa, but there is also at least one commercial pump at a pressure level of 21 MPa. The water flow of the pump varies from a few litres per minute to a few hundred litres per minute. The pump body can be the same in pumps with different displacements, the only difference being the angle of the swashplate. However, there is only one variable displacement pump available on the market (2011).

One series of commercial pumps consists of several axial piston pumps for tap water and for seawater applications. The continued pressure level is maximum 16 MPa and the size of the pumps varies from 2-100 cm^3/rev. The nominal flow of the pumps ranges from 1 up to 150 l/min. Small pumps include five pistons and the bigger ones are manufactured with nine pistons. The slipper sliding surfaces are made of PEEK and swashplate and the pistons are made of stainless steel (1.4057). Valve plate of the pump is made of PEEK. [Anon 2010b]

On the market there are axial piston pump series for both tap water and seawater applications. The maximum continuous pressure level is 16 MPa or 21 MPa. The pump sizes are 20, 31 and 40 cm^3/rev. The pumps include nine pistons. The slipper sliding surfaces are made of PEEK and swashplate and the pistons are made of stainless steel (AISI 316). [Anon 2000]

One commercial manufacturer provides six different sizes of water hydraulic axial piston pumps. The pressure levels of the pumps are 16 MPa. The sizes of the pumps are from 0.8 to 225 cm^3/rev. Water flow is up to 430 l/min. The pumps include nine pistons. These are manufactured in AISI 316 stainless steel and the slipper sliding surfaces are some softer material, probably PEEK. In 2011 the company introduced a water hydraulic variable displacement pump. The displacement of the pumps can be controlled by electrical, hydraulic or mechanical means. The pressure level is 16 MPa and maximum flow is 330 l/min. [Anon 2011]

3 THEORETICAL ASPECTS OF SLIPPER-SWASHPLATE CONTACT

The basic theory of slipper behaviour is reviewed in this chapter. Many different things affect the slipper-swashplate contact in water hydraulic axial piston pumps. In this chapter the impact of water, generally used materials, the dimensions of the slipper and other important aspects are treated from the point of view of slipper-swashplate contact.

Although the basic equations are partly too simple, a good analytical understanding of the slipper behaviour in axial piston pumps is very important to achieve good design. Theoretical base is needed to build a mathematical model and to understand the results of the numerical calculations. PV-rate and deformations are widely studied because those are significant in water hydraulic pumps, if the industrial plastics are used.

3.1 Slipper structures used in this study

Six different slippers and three different slipper structures are investigated in this study. The outside dimensions of slipper types are quite close to each other, which makes comparison acceptable. The main dimensions of all six slippers are shown in Figure 3.

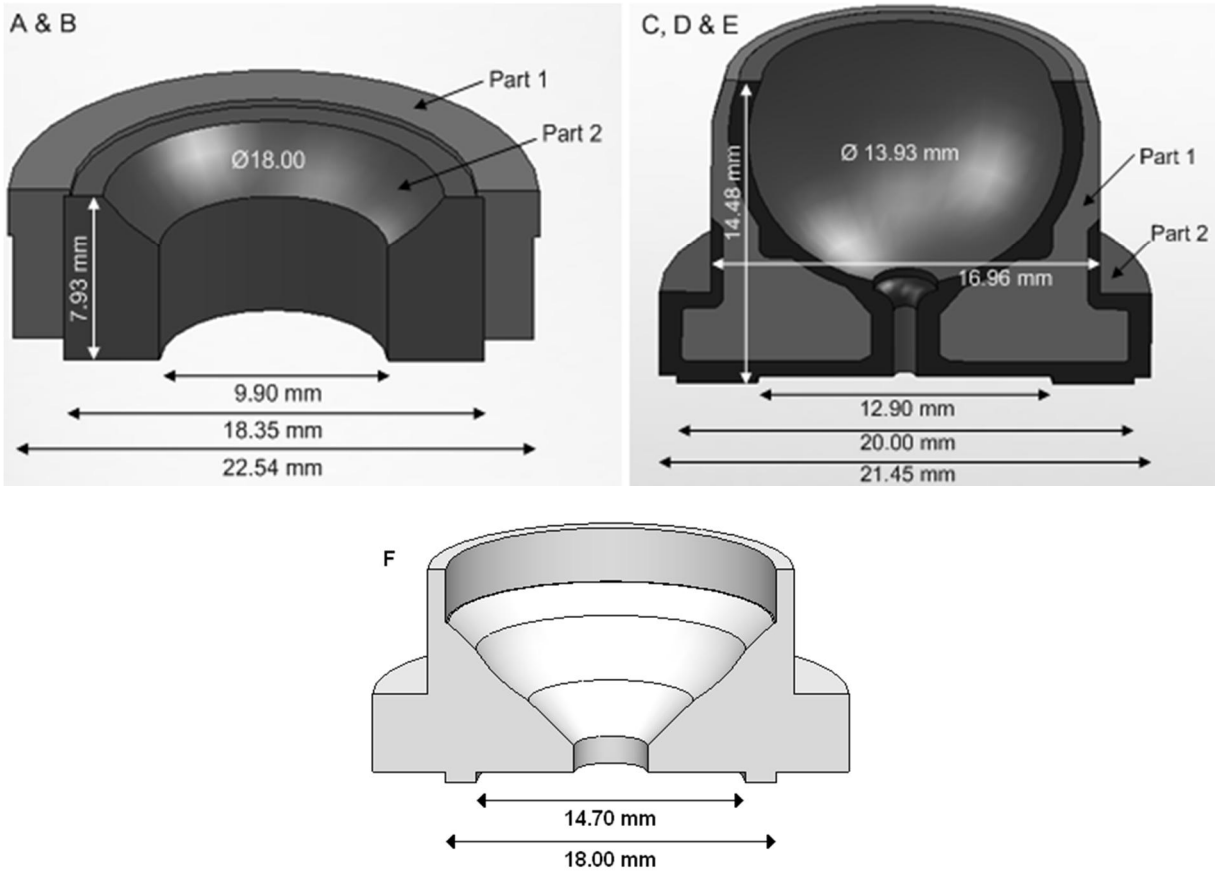

Figure 3. Structure and dimensions of the slipper types.

Three of the investigated slippers are made from PEEK; one is made from stainless steel and other two are a combination of PEEK and stainless steel, as Table 1 shows. Slippers B and D, which are made from PEEK and stainless steel, are of a similar kind to the slippers in commercial pumps. Both slippers are designed so that both contact surfaces are made by PEEK and the structure is reinforced by stainless steel. However, the structures of the slippers are remarkably different, as Figure 3 shows. The structure of slipper B can be machined, but the PEEK part of the slipper D must be manufactured by moulding. In real use slipper B includes an additional PEEK part outside the steel part to take care of the contact to the slipper hold down mechanism, but that additional part need not be taken into account because of the loose fit.

Table 1 shows the important parameters of the slippers.

	A	B	C	D	E	F
Material of part 1	PEEK1	Steel	PEEK2	Steel	Steel	PEEK1
Material of part 2	PEEK1	PEEK1	PEEK2	PEEK2	Steel	-
Piston diameter [mm]	16.29	16.29	16.96	16.96	16.96	16.29
Hydrostatic balance [-]	0.729	0.729	0.923	0.923	0.923	1.029
Mass [g]	6.89	13.23	3.48	13.59	20.88	4.51
Centre of gravity [mm] (below centre of piston ball)	6.52	7.39	6.27	6.25	6.27	~7.00
Orifice diameter [mm]	2.00	2.00	0.85	0.85	0.85	-
Orifice length [mm]	3.00	3.00	2.90	2.90	2.90	-
Inner radius / Outer radius [-]	0.540	0.540	0.645	0.645	0.645	0.817
Surface pressure (10 MPa) without HB [MPa]	7.01	7.01	5.23	5.23	5.23	22.00
PV-rate (10 MPa, 1500 rpm) without HB [MPa m/s]	44.05	44.05	32.89	32.89	32.89	138.22
PV-rate (10 MPa, 1500 rpm) with HB [MPa m/s]	19.14	19.14	5.96	5.96	5.96	-

Table 1. Properties of different slippers.

Table 1 shows that the design principle of the three structures is different. The compensated part of the piston force is significantly higher with slippers C, D and E. The term hydrostatic balance from [Donders 1997] is used here. Also the ratio of the inner and outer radius and PV-rate are different between slipper types. Slipper F is special because it is made only for PV-testing and its properties cannot be compared directly to the other slippers.

3.2 Dimensions of the slipper

The dimensions of the slipper and piston affect all the important properties of the slipper. Basically, the slipper design includes structure determination, exact dimensioning and material selection of the slipper. The load carrying capacity, leakage, surface pressure, PV-rate and friction forces are all related to the slipper dimensions. Also the mechanical structure, size of the pump and the piston and the manufacturing process give boundary conditions to the slipper dimensions. The dimensions of the slipper are always a compromise.

The most important dimensions of the slippers are the inner and outer radius of the sliding surface. These have to be designed so that the hydrostatic balance and the PV-rate of the slipper are appropriate. It requires that the diameter of the piston should be taken into account. To get the idea of the slipper

properties, the hydrostatic balance and the surface pressure of the studied slippers are presented in Table 1 at a pressure level of 10 MPa and 1500 rpm rotation speed.

If the inner radius of the sliding surface is constant and the ratio between the inner and the outer radius of the sliding surface decreases, the consequences can be summarised as follows:

- Outer radius increases
- Load capacity rises
- Leakage flow decreases
- Hydrostatic balance increases
- PV-rate decreases

The height of the slipper is not so significant, but it should be noticed that the height affects the position of the centre of gravity of the slipper. The position of the centre of gravity is needed to calculate the tilting moment caused by the centrifugal force. Figure 4 clarifies that.

The structure, geometry and material thickness of the slipper include dimensions which affect the slipper properties via deformations and the durability of the pressure cycle. That is why it is very important that these dimensions are taken into account in the dimensioning process.

Notable dimensions are also the diameter and the length of the control orifice. The mission of the control orifice is to lead the flow to the slipper pocket to realize the hydrostatic bearing and keep the hydrostatic balance of the slipper in the right values to avoid too high loading of the slipper. Reference [Koc 1997] shows that the control orifice slightly increases the minimum film thickness, but also reduces the slipper´s resistance to tilting couples. The control orifice in both slipper structures B and D is so loose that there is no pressure drop over the control orifice if the leakage of the slipper is low.

In water hydraulic axial piston pumps a control orifice is needed because without the control orifice the PV-rate is too high with a reasonable pressure level. Without a control orifice (without pressure pocket) the maximum pressure level of the slipper B is 3.6 MPa with the maximum PV-rate 18 MPa m/s. It is obvious that a 3.6 MPa pressure level is too low for axial piston pumps and the slipper without a control orifice is not usually a realistic option in water hydraulic axial piston pumps.

The slipper hold-down mechanism causes restrictions to the size and geometry of the slipper. The bearing between the hold-down mechanism and slipper needs the outer surface or the slipper or contact surface of the hold-down mechanism to be made from PEEK or other material which has good bearing properties.

3.3 Forces in piston-slipper assembly

Many forces are subjected to the slipper of the axial piston pump. Piston forces like the pressure force of the piston are coming via the spherical joint between piston and slipper. Also centrifugal force, inertial force, gravitational force, friction force between swashplate and slipper, friction force in the spherical joint and force from the slipper hold down mechanism affect the slipper. The magnitude and the direction of the force resultant are dependent on many different factors, for example pressure level, rotation speed of the cylinder group, swashplate angle and the dimension of the slipper.

Forces affecting the piston and the slipper are shown in Figure 4.

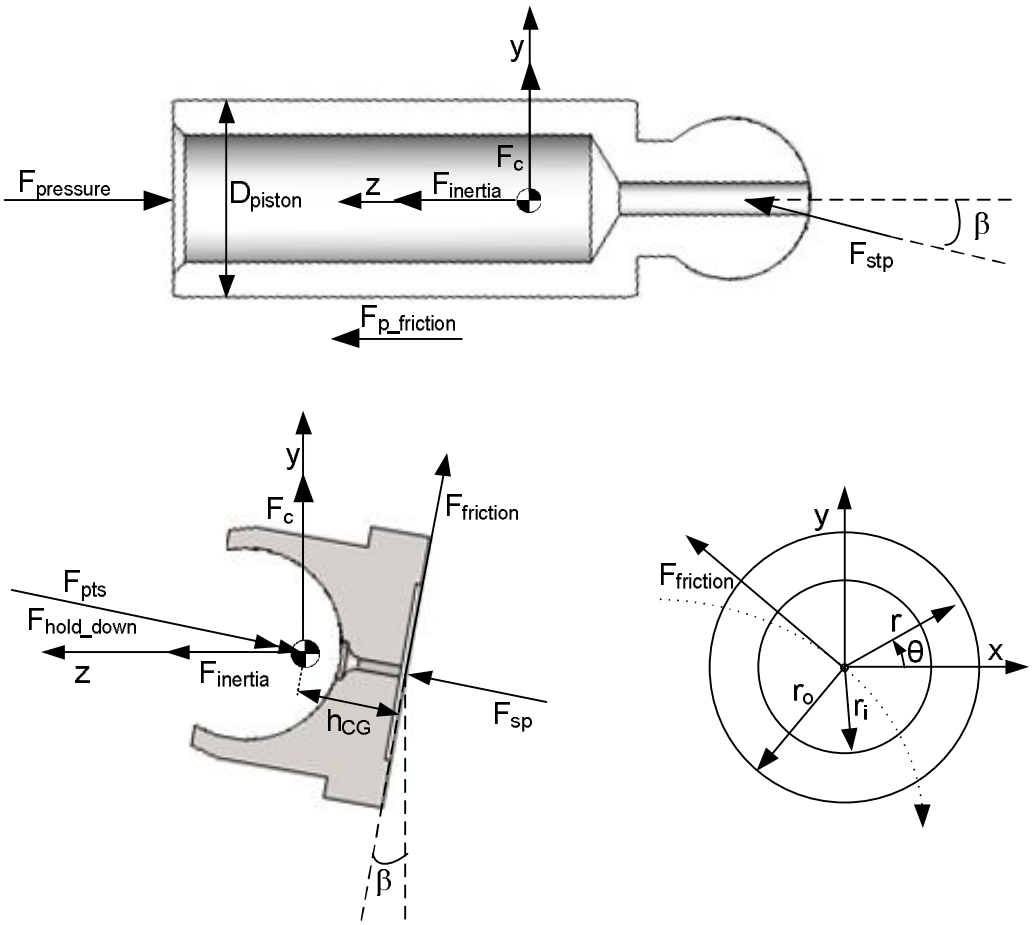

Figure 4. Main dimensions and forces acting on piston and slipper. Cartesian and polar coordinate systems are presented.

Forces in axial piston pumps can be grouped into two types: pressure dependent and pressure independent forces. Pressure dependent forces are dominant in axial piston pumps and all other forces can often be neglected in simplified calculations. Pressure dependent forces can be compensated by the hydrostatic bearings. [Ivantysyn 2001]

Pressure force on the piston is given in Equation 2.

$$F_{pressure} = A_{piston} p_{piston} = \frac{\pi}{4} D_{piston}^2 p_{piston} \tag{2}$$

Inertia force and friction force between the piston and cylinder also affect the slipper via the spherical joint, but the impact of these forces is quite low in high pressure pumps. In the simulation model, shown in Chapter 6, inertia and friction forces are taken into account, but the following procedure is made without these. Also the slipper hold-down device causes force on the piston-slipper assembly, but it is not taken into account. Because only pressure force is deal with, the pressure force is equal to piston force, F_{piston}.

Against that, pressure force affects the lifting force of the slipper. The slipper lifting force consists of pocket force and the hydrostatic and hydrodynamic force of the sliding surface. If only the hydrostatic forces are

taken into account, Equation 3 shows the force. Note that assumptions are made that the film thickness is the same in any radial or angular position and the pressure does not vary in the angular direction.

$$F_{slipper} = \pi r_i^2 p_{slipper} + \int_{r_i}^{r_o} \frac{p_{slipper} \ln\left(\frac{r}{r_o}\right)}{\ln\left(\frac{r_i}{r_o}\right)} 2\pi r \, dr \tag{3}$$

$$F_{slipper} = \pi r_i^2 p_{slipper} + \frac{2\pi p_{slipper}}{\ln\left(\frac{r_i}{r_o}\right)} \int_{r_i}^{r_o} \ln\left(\frac{r}{r_o}\right) r \, dr \tag{4}$$

Integrating the previous Equation 4 over the sliding area by parts, as Equation 5 shows, with the assumptions shown in Equations 6 gives Equation 7. [Riley 1974], [Hamrock 1994]

$$\int uv' \, dx = uv - \int u'v \, dx \tag{5}$$

$$\begin{cases} u = \ln\left(\frac{r}{r_o}\right) \\ du = \frac{r_o}{r_o r} dr = \frac{1}{r} dr \\ v = \frac{r^2}{2} \\ dv = r \, dr \end{cases} \tag{6}$$

$$F_{slipper} = \pi r_i^2 p_{slipper} + \frac{2\pi p_{slipper}}{\ln\left(\frac{r_i}{r_o}\right)} \left[\frac{1}{2} \ln\left(\frac{r}{r_o}\right) r^2 \Big|_{r_i}^{r_o} - \int_{r_i}^{r_o} \frac{r}{2} dr \right] \tag{7}$$

$$F_{slipper} = \pi r_i^2 p_{slipper} + \frac{2\pi p_{slipper}}{\ln\left(\frac{r_i}{r_o}\right)} \left[\frac{1}{4}\left(r_i^2 - r_o^2\right) - \ln\left(\frac{r_i}{r_o}\right) \frac{r_i^2}{2} \right] \tag{8}$$

And finally, the slipper force can be expressed as

$$F_{slipper} = \frac{\pi}{2} p_{slipper} \frac{r_o^2 - r_i^2}{\ln\left(\frac{r_o}{r_i}\right)} = \frac{\pi}{8} p_{slipper} \frac{D_i^2 - D_o^2}{\ln\left(\frac{D_i}{D_o}\right)} \tag{9}$$

Equation 9 shows that slipper force in hydrostatic lubrication depends only on pressure level and the dimensions of the slipper and the piston. The characteristics of the fluid are not significant and therefore any available fluid is suitable for lubrication. That is why water is the most realistic lubrication fluid in water hydraulic axial piston machines.

If $p_{slipper}$ is equal to p_{piston}, which means that the control orifice of the piston is loose, then hydrostatic balance is force ratio as Equation 10 shows.

$$q = \frac{F_{slipper}}{F_{pressure}} = \frac{\frac{\pi}{8} p_{slipper} \frac{D_i^2 - D_o^2}{\ln\left(\frac{D_i}{D_o}\right)}}{\frac{\pi}{4} D_{piston}^2 p_{piston}} = \frac{D_i^2 - D_o^2}{2 D_{piston}^2 \ln\left(\frac{D_i}{D_o}\right)} \tag{10}$$

It is important to notice that slipper bearings in axial piston pumps are not totally hydrostatically balanced. Not-balanced pressure force and other pushing forces are compensated in other ways, for example speed difference causes hydrodynamic force between slipper and swashplate (if those are not parallel) and with water lubricated conditions even the contact between surfaces can carry load.

Contact between slipper and swashplate can carry only perpendicular load. Contact force between slipper and swashplate rises when the angle of the swashplate rises. That also means that the leakage is smaller if the swashplate angle is bigger. However, when the swashplate angle changes, the change in this perpendicular force is quite small. For example, in slippers A and B with 10 MPa, the force change between 0 and 10 degrees angle is 1.5 % (2084 N → 2116 N) according to Equation 11.

$$F_{sp} = \frac{F_{piston}}{\cos(\beta)} \tag{11}$$

Because the force change is not so significant, it is possible to use the same slippers with a different swashplate angle, which is realized in commercial pumps. That fact also makes it possible to adjust the angle of the swashplate during operation without significant changes in the slipper behaviour. Increasing the force affects the leakage flow; this reduces with higher swashplate angles.

It should be noticed that in a real situation F_{sp} consists of hydrostatic and hydrodynamic forces. Hydrostatic force is presented in Equation 9. Relative movement between the slipper and swashplate causes hydrodynamic force if they are not parallel so that a physical wedge exists. This phenomenon, together with squeeze effect, are the two most important aspects in hydrodynamic pressure generation. These are part of the Reynolds equation presented in Chapter 3.4.

In axial piston pumps there are many friction pairs. In Figure 4 friction forces $F_{p\_friction}$ and $F_{friction}$ are shown. Friction between the piston and cylinder consists of friction coefficient, force acting on the piston perpendicular to the piston axis and the velocity of the piston. The friction force between slipper and swashplate occurs because of the continuous relative movement between slipper and swashplate during operation. With sufficient water film the friction force can be determined according to Equation 12 [Ivantysyn 2001].

$$F_{friction} = \eta \omega \pi \frac{R_{rot}}{h} (r_o^2 - r_i^2) \tag{12}$$

In water applications friction is interesting because the water film is so thin that it is possible that there is contact between materials. If there is contact between slipper and swashplate, the friction force depends

on the material pair. An assumption of pure viscous friction between slipper and swashplate cannot be automatically made and possibility of mixed lubrication should take into account. However, if it is possible to make measurements, or if measurement data is available, it is possible to derive friction force also in the most simplified form, as shown in Equation 13.

$$F_{friction} = c_f (F_{piston} - F_{slipper}) \tag{13}$$

Centrifugal force is important because the centre of mass of the slipper is usually lower than the centre of the ball of the piston, which makes the slipper swing radially outwards. In water hydraulic pumps, it is possible to try to make the slipper so that the mass centre is close to the ball centre because of the steel PEEK combination. PEEK is much lighter than stainless steel, which makes the centrifugal force of the slipper lower in water hydraulic pumps.

To maintain the slipper contact with the swashplate, the slipper hold-down mechanism is used to push the slipper against the swashplate. Springs are commonly used to realize that, which means that there is continuous force pushing the slipper. The label of that force is F_{hold_down} in Figure 4.

Forces also cause a tilting moment of the slipper, which has to take into account. The tilting moment consists of centrifugal force, friction force between the swashplate and the slipper and the friction force between the piston and the slipper. Tilting moments cause the slipper to rotate in an inclined position against the swashplate. The tilting moment of the slipper is carried with hydrodynamic force. Because of the very thin lubricating film in water film lubrication, the tilting moments cause contact between the slipper and swashplate and it should be attempted to minimize this.

3.4 Water film lubrication

Water as a pressure medium is a challenging task, but because the load capacity is not viscosity dependent, as Equation 9 shows, water is from that point of view suitable for hydrostatic lubrication.

The theory of fluid film lubrication assumes that fluids are Newtonian fluids, which means that fluid has viscosity. The viscosity of a fluid is associated with its resistance to flow. If it is assumed that fluid behaviour is Newtonian and flow is laminar, fluid motion can be described by the Navier-Stokes equations shown in Equation 14 [Hamrock 1994].

$$\begin{aligned}
\rho\frac{Du}{Dt} &= \rho X_a - \frac{\partial p}{\partial x} - \frac{2}{3}\frac{\partial}{\partial x}(\eta\xi_a) + 2\frac{\partial}{\partial x}\left(\eta\frac{\partial u}{\partial x}\right) + \frac{\partial}{\partial y}\left[\eta\left(\frac{\partial u}{\partial y} + \frac{\partial v}{\partial x}\right)\right] + \frac{\partial}{\partial z}\left[\eta\left(\frac{\partial u}{\partial z} + \frac{\partial v}{\partial x}\right)\right] \\
\rho\frac{Dv}{Dt} &= \rho Y_a - \frac{\partial p}{\partial y} - \frac{2}{3}\frac{\partial}{\partial y}(\eta\xi_a) + 2\frac{\partial}{\partial y}\left(\eta\frac{\partial v}{\partial y}\right) + \frac{\partial}{\partial x}\left[\eta\left(\frac{\partial u}{\partial y} + \frac{\partial v}{\partial x}\right)\right] + \frac{\partial}{\partial z}\left[\eta\left(\frac{\partial v}{\partial z} + \frac{\partial w}{\partial y}\right)\right] \\
\rho\frac{Dw}{Dt} &= \rho Z_a - \frac{\partial p}{\partial z} - \frac{2}{3}\frac{\partial}{\partial z}(\eta\xi_a) + 2\frac{\partial}{\partial z}\left(\eta\frac{\partial w}{\partial z}\right) + \frac{\partial}{\partial x}\left[\eta\left(\frac{\partial u}{\partial z} + \frac{\partial w}{\partial x}\right)\right] + \frac{\partial}{\partial y}\left[\eta\left(\frac{\partial v}{\partial z} + \frac{\partial w}{\partial y}\right)\right]
\end{aligned} \tag{14}$$

The terms on the left side come from inertia effects. Those on the right side are body force, pressure gradient, and viscous terms, in that order. The Navier–Stokes equations are derived and shown in different forms in reference [Hamrock 1994].

The full Navier–Stokes equations are quite complicated, and analytical solutions are not possible in the most practical solutions. In fluid film lubrication problems pressure and viscous terms are dominant. The equation that describes the pressure distribution in fluid film lubrication is known as the Reynolds equation. The Reynolds equation can be derived in two different ways, from the Navier–Stokes and continuity equations and directly from the principle of mass conservation. Both ways to derive Reynolds equation are shown in reference [Hamrock 1994]. The Reynolds equation in general form is shown in Equation 15.

$$\frac{\partial}{\partial x}\left(-\frac{\rho h^3}{12\eta}\frac{\partial p}{\partial x}\right)+\frac{\partial}{\partial y}\left(-\frac{\rho h^3}{12\eta}\frac{\partial p}{\partial y}\right)+\frac{\partial}{\partial x}\left[\frac{\rho h\left(u_a+u_b\right)}{2}\right]+\frac{\partial}{\partial y}\left[\frac{\rho h\left(v_a+v_b\right)}{2}\right]$$
$$+\rho\left(w_a-w_b\right)-\rho u_a\frac{\partial h}{\partial x}-\rho v_a\frac{\partial h}{\partial y}+h\frac{\partial \rho}{\partial t}=0 \tag{15}$$

The first two terms of Equation 15 are Poiseuille terms, which describe the net flow rates due to the pressure gradients within the lubrication area. How to get the velocity profile of the flow between two parallel plates is shown in references [Hamrock 1994] and [Ivantysyn 2001]. Velocity profile is derived directly from Navier-Stokes equations. When the velocity profile is known, the volume flow rate per unit width can be written as Equation 16 shows.

$$q'=\int_0^h u\,dz \tag{16}$$

In conditions with parallel plates when the boundary conditions are taken into account, Equation 16 can be written as

$$q'=-\frac{h^3}{12\eta}\frac{dp}{dx}+\frac{u_a h}{2} \tag{17}$$

The first term on the right side of Equation 17 is the Poiseuille term, and the second is the Couette term. [Hamrock 1994]

The third and the fourth term of Equation 15 are the Couette terms and they describe the net entraining flow rates due the surface velocities. The Couette term leads to three distinct actions. The density wedge action is concerned with the rate at which lubricant changes in the sliding direction. The strength action considers the rate at which surface velocity changes in the sliding direction. The physical wedge action is important for pressure generation. For positive load carrying capacity the film thickness must decrease in the sliding direction. [Hamrock 1994]

The fifth, sixth and seventh terms of Equation 15 describe the net flow rates due to a squeezing motion. Normal squeeze action provides a cushioning effect when bearing surfaces tend to be pressed together. When the film thickness is decreased, positive pressure will be generated. Translation squeeze action results from the translation of inclined surfaces. [Hamrock 1994]

The last term of Equation 15 describes the net flow rate due local expansion. [Hamrock 1994]

It is important to be aware that the physical wedge and normal squeeze actions are the two major pressure generating devices in hydrodynamic or self-acting fluid film bearings.

If only the tangential motion is taken into account, Equation 15 reduces to Equation 18 [Hamrock 1994].

$$\frac{\partial}{\partial x}\left(\frac{\rho h^3}{12\eta}\frac{\partial p}{\partial x}\right)+\frac{\partial}{\partial y}\left(\frac{\rho h^3}{12\eta}\frac{\partial p}{\partial y}\right)=\frac{\partial}{\partial x}\left[\frac{\rho h\left(u_a+u_b\right)}{2}\right]+\frac{\partial}{\partial y}\left[\frac{\rho h\left(v_a+v_b\right)}{2}\right]+\frac{\partial\left(\rho h\right)}{\partial t} \tag{18}$$

And again, if the viscosity of the fluid is constant

$$\frac{\partial}{\partial x}\left(h^3\frac{\partial p}{\partial x}\right)+\frac{\partial}{\partial y}\left(h^3\frac{\partial p}{\partial y}\right)=6\eta\left[\frac{\partial}{\partial x}\left[h\left(u_a+u_b\right)\right]+\frac{\partial}{\partial y}\left[h\left(v_a+v_b\right)\right]+2\frac{\partial h}{\partial t}\right] \tag{19}$$

The Reynolds equation shown in Equation 19 on polar coordinates is shown in Equation 20 [Hamrock 1994], [Riley 1974].

$$\frac{1}{r}\frac{\partial p}{\partial r}h^3+\frac{\partial}{\partial r}\left(\frac{\partial p}{\partial r}h^3\right)+\frac{1}{r^2}\frac{\partial}{\partial\theta}\left(\frac{\partial p}{\partial\theta}h^3\right)=6\eta\left[\frac{\partial h}{\partial r}v_r+\frac{1}{r}\frac{\partial h}{\partial\theta}v_\theta+2\frac{\partial h}{\partial t}\right] \tag{20}$$

where

$$\begin{aligned} v_r &= v_{ra}+v_{rb} \\ v_\theta &= v_{\theta a}+v_{\theta b} \end{aligned} \tag{21}$$

If film thickness is the same in any radial or angular position and the pressure does not vary in the angular direction, the Reynolds equation reduces to Equation 22 [Hamrock 1994].

$$\frac{\partial}{\partial r}\left(r\frac{\partial p}{\partial r}\right)=0 \tag{22}$$

After integration

$$r\frac{\partial p}{\partial r}=C_1 \tag{23}$$

Integrating Equation 23 again gives

$$p=C_1\ln r+C_2 \tag{24}$$

Figure 11 shows the boundary conditions, which are

1. If the r = r_i the pressure p = $p_{slipper}$
2. If the r = r_o, the pressure p = 0

By solving C1 from boundary condition equations

$$\begin{aligned} p_{slipper} &= C_1\ln r_i+C_2 \\ 0 &= C_1\ln r_o+C_2 \end{aligned} \tag{25}$$

And putting that to Equation 24 gives

$$p = p_{slipper} \frac{\ln\left(\frac{r}{r_o}\right)}{\ln\left(\frac{r_i}{r_o}\right)} \tag{26}$$

Note that in the slipper case pressure from the inner edge to the outer edge is not reduced linearly like, for example, in pipes.

The radial volumetric flow is

$$q'_{leak} = -\frac{h^3}{12\eta}\frac{dp}{dr} = -\frac{h^3 p_{slipper}}{12\eta r \ln\left(\frac{r_i}{r_o}\right)} \tag{27}$$

Hence, the total flow rate is

$$q_{leak} = 2\pi r q'_{leak} = \frac{\pi h^3 p_{slipper}}{6\eta \ln\left(\frac{r_o}{r_i}\right)} \tag{28}$$

Water properties affect all parts in the hydraulic system and components. In water hydraulic pumps one of these is slipper-swashplate contact. Low dynamic viscosity, 0.7e-3 Ns/m^2, means that either leakage is high or manufacturing tolerances should be very tight. If the same dimensions and pressure as in the oil hydraulic is used and it is attempted to maintain leakage at the same value gap, then the height should be about one third of the gap in oil hydraulic. In other words, gap height is relative to the fluid viscosity, as Equation 28 shows.

In slipper-swashplate contact gaps are automatically smaller because of the very poor hydrodynamic or elastohydrodynamic film formation related to the low viscosity and pressure viscosity coefficient of water. A low dynamic pressure build-up of water is clearly shown in wedge gaps. This means that gaps have to be small to build up significant hydrodynamic bearing forces. That makes material contact between slipper and swashplate possible and in real pumps unavoidable.

Equation 28 shows that if the ratio between the inner and the outer radius of the sliding surface is constant, also the leakage flow is constant. This means that it is possible to increase the area of the sliding surface to obtain lower PV-rate without changes in the leakage flow. If the outer radius is constant and the inner radius is increased, the leakage flow is also increased. That is not the whole truth because the gap height is not constant.

Unclean water is a big challenge because PEEK is quite a soft material and particles cause scratches to the sliding surface and the pressure field under the slipper can easily change. It is known that unclean water can make the slipper lifetime dramatically shorter than expected. The design of the slipper cannot make the system safe if the quality of the water is low.

In the case of water, cavitation should always be remembered. However, cavitation in slipper-swashplate contact is unlikely to occur because of low leakage flow level. Cavitation damage is not shown in the slipper structures in the used pumps.

Water also causes corrosion, which has to be noticed when selecting materials for the water hydraulic pump. More about the water properties in hydraulic systems can be found in reference [Rydberg 2001].

3.5 Materials in piston-slipper assembly

Due to poor lubricating properties, erosion and corrosion, special materials are required in water hydraulic components. Especially sliding pairs are very critical because the poor properties of water film lubrication are known. In this study material properties are mainly examined from the point of view of slipper-swashplate contact.

Many different material combinations of water lubricated sliding pairs have been tested during the last two decades, see [Rämö 1999] and [Terävä 1995]**.** Polymers, especially PEEK, show good results with low friction, wear resistance and durability. Also cost and manufacturability are suitable and corrosion is not a problem with polymers. Water hydraulic pump manufacturers have decided to use PEEK and stainless steel in their pumps. Because there are many different kinds of PEEKs on the market, the main properties of the PEEKs used in calculations are shown in Table 2.

Property	PEEK 1	PEEK 2
Additives	10% carbon, 10% graphite, 10% PTFE	-
Young's modulus [MPa]	9500	3500
Poissons ratio [-]	0.394	0.400
Density [kg/m^3]	1480	1300
Tensile strength, Yield [MPa]	119	97
Compressive yield strength [MPa]	152	118
Maximum PV [MPa m/s]	18	2.4
Friction coefficient [-]	0.19	0.34

Table 2. Properties of PEEK 1 and PEEK 2.

Continuous pressure changes inside the slipper mean that it is under dynamic loading (25Hz at 1500 rpm). Reference [Anon 2010a] shows that the SN-curve of the PEEK is downward, which means that during dynamic cyclic loading PEEK will fail as stress level are substantially lower than the tensile stress during tensile testing. The number of load cycles the slipper material can stand is dependent on the stress amplitude, i.e. working pressure level in the pump. It has been noticed in experiments that slippers made totally in PEEK are not durable in the continuous pump operating cycle because of the tensile stress. In real pumps steel core or steel ring is used to support the slipper structure, which changes the tensile stress of the PEEK-part into compression stress.

The yield strength of PEEK is high enough for slipper use; for example, 97 MPa with PEEK 1 and the calculated surface pressure is 7.0 MPa under slipper B and 10.9 MPa in the spherical joint at 10 MPa working pressure. The compressive strength is higher than the tensile strength, and with slipper structures this is more important.

The maximum PV-rate of the PEEK 1 is 18 MPa m/s and 2.4 MPa m/s for PEEK 2. When these are compared to the values in Table 1, it is noticed that the maximum values of the materials are low. Although the pressure level is only 10 MPa, also the PV-rates with hydrostatic balance are higher than the PEEK manufactures recommend. This means that the PV-rate is one of the factors that limit the pressure level of the water hydraulic axial piston pump.

The surface finish of the sliding surface of the slipper is not critical because PEEK will polish during operation. Carbon fiber or glass fiber reinforcements can cause scratching to the swashplate and their use has to be fully thought through.

The swashplate and the pistons of the pump are usually made from some stainless steel, for example AISI 431 or AISI 316. Stainless steels are commonly used in water hydraulic components because of their high resistance to corrosion and high strength. A slipper made totally in stainless steel is not recommended because of the poor lubricating properties of the water, which does not allow a steel-steel sliding pair. The pistons and the swashplate are made from stainless steel in all commercial pumps at the moment. In calculations the properties of AISI 431 are used for the material of the stainless steel part of the slipper, the piston and swashplate.

3.6 Pressure-Velocity (PV) rate of the slipper

Plastics have special properties which make them unsuited for examination of wear in the same way as for metals. Usually, the wear of plastics is described with PV-rate. PV-rate is based on the idea that the wear rate is a function of the energy used on the sliding surface.

It is important to note that polymers have maximum values of the PV-rate, which could be a restrictive factor of slipper design in water hydraulic components. The PV-rate of the slipper is an important parameter and it is discussed separately, although the PV-rate of the slipper is closely related to the dimensions of the slipper and the properties of the pump. Pressure means the surface pressure of the sliding surface of the slipper and velocity means the sliding velocity of the sliding surface of the slipper. Equation 29 shows how the PV-rate is calculated.

$$PV_{slipper} = 2\pi R_{rot} n \frac{F_{piston}}{A_{slipper}} \tag{29}$$

The angle of the swashplate is assumed to be zero degrees and F_{piston} is used for surface pressure calculation. The PV-rate is proportional to the surface pressure and to the velocity of the slipper. So if the pressure or the rotation speed is doubled, also the PV-rate will be doubled. The rotation speed of the pump is often 1500 rpm and pressure level is some desirable value, so possible changes affecting the PV-rate are dimensions, the diameter of the rotation circle, diameter of the piston, and the inner and outer diameters of the sliding surface.

It is notable how the surface pressure is calculated. Figure 5 shows the PV-rates with hydrostatic balance and without it. The ratio of the inner and outer radius is constant. The rotation speed of the swashplate is 1500 rpm and the piston diameter is 16.29 mm in all the curves in this chapter.

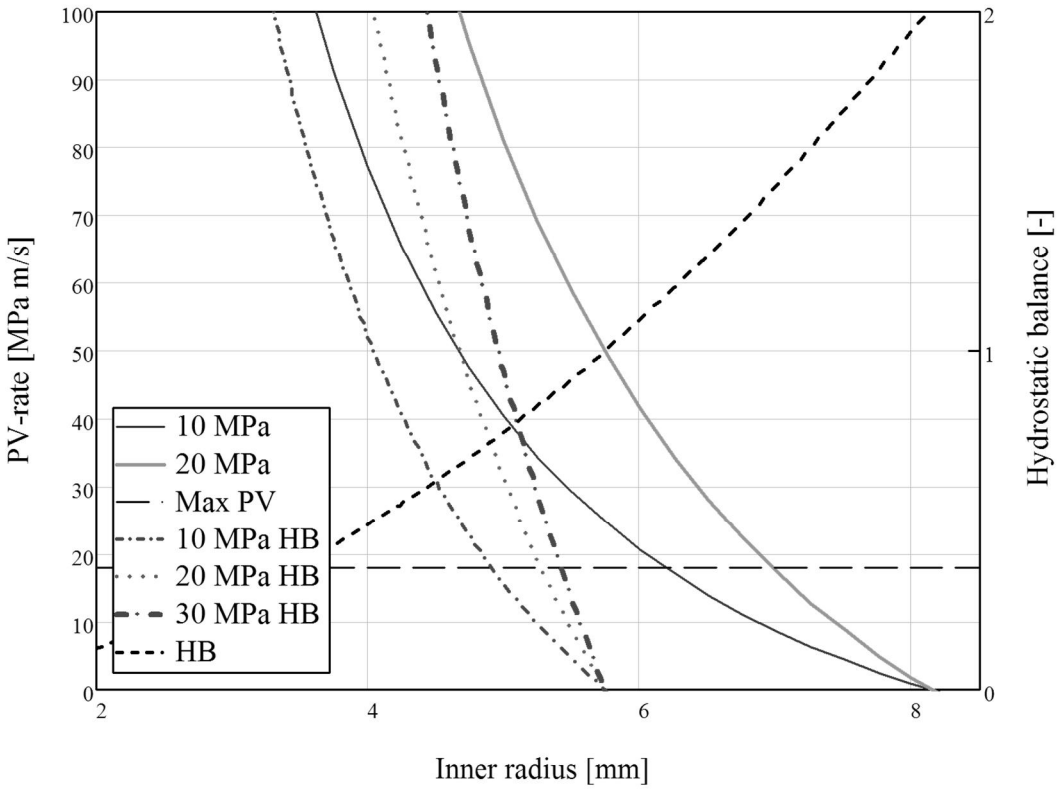

Figure 5. PV-rates of the slipper with hydrostatic balance and without it.

Figure 5 shows that when the ratio between the inner and the outer radius of the sliding surface is kept constant the PV-rate reduces if the inner radius is increased. Figure 5 also shows that the hydrostatic balanced surface pressure is better to use because in that way the zero value of the PV-rate and the line between overclamped and underclamped behaviour are the same. Without taking the hydrostatic balance into account, the inner radius has values which are not possible to realize because the hydrostatic balance is higher than one. In that case, the leakage flow is increased too high. With the hydrostatic balance the curves show more realistic PV-rate values. However, it is notable that the hydrostatic balance is only an approximation because the deformations change the pressure profile under the sliding surface.

It is remarkable that with higher pressure levels, the sensitivity of the slipper PV-rate is higher. Figure 5 shows that at a pressure level of 30 MPa the change of the PV-rate is much higher than at a pressure level of 10 MPa.

It is noticeable that if the outer radius of the sliding surface is constant and the inner radius is made bigger, the PV rate is reduced because the hydrostatically compensated part of the piston forces increases. That happens, although the area of the sliding surface reduces.

Figure 6 shows how the PV-rate and the area of the sliding surface changes as a function of the inner radius. The ratio between inner and outer radius of the sliding surface is constant 0.53, which is the optimum ratio according to the pumping power loss [Hamrock 1994]. In this case the losses from the viscous dissipation are assumed to be neglected, which is near the truth. The maximum PV-rate (18 MPa m/s) of the material is also marked in Figure 6.

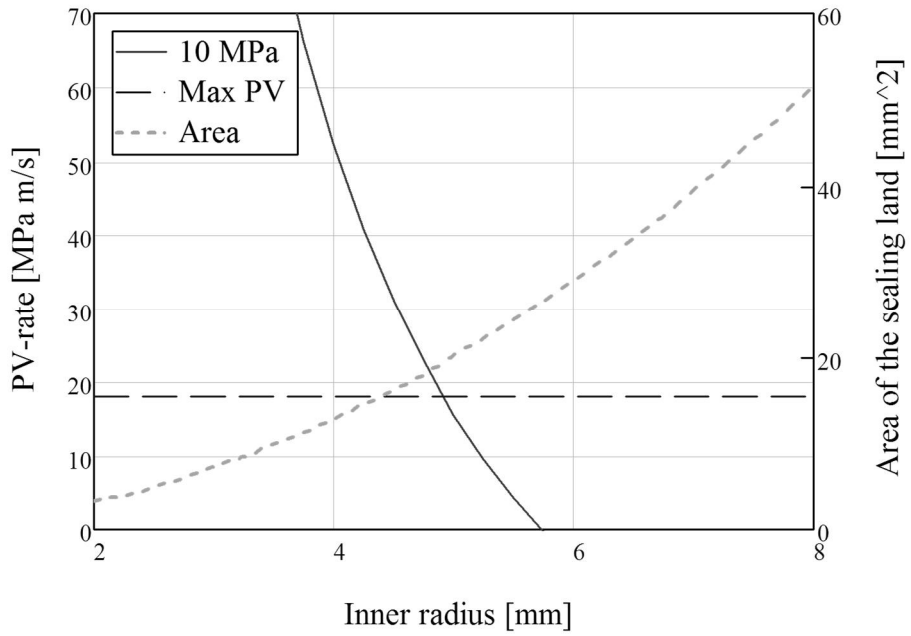

Figure 6. PV-rate and the area of the sliding surface of the slipper.

Figure 6 shows that if the area of the slipper doubles the PV-rate of the slipper does not reduce to half because also the piston forces a change due to hydrostatic balance. The sensitivity of the PV-rate is dependent on the pressure level.

Figure 7 shows the PV-rates and hydrostatic balance of the slipper with the different pressure levels and different inner radius of the sliding surface.

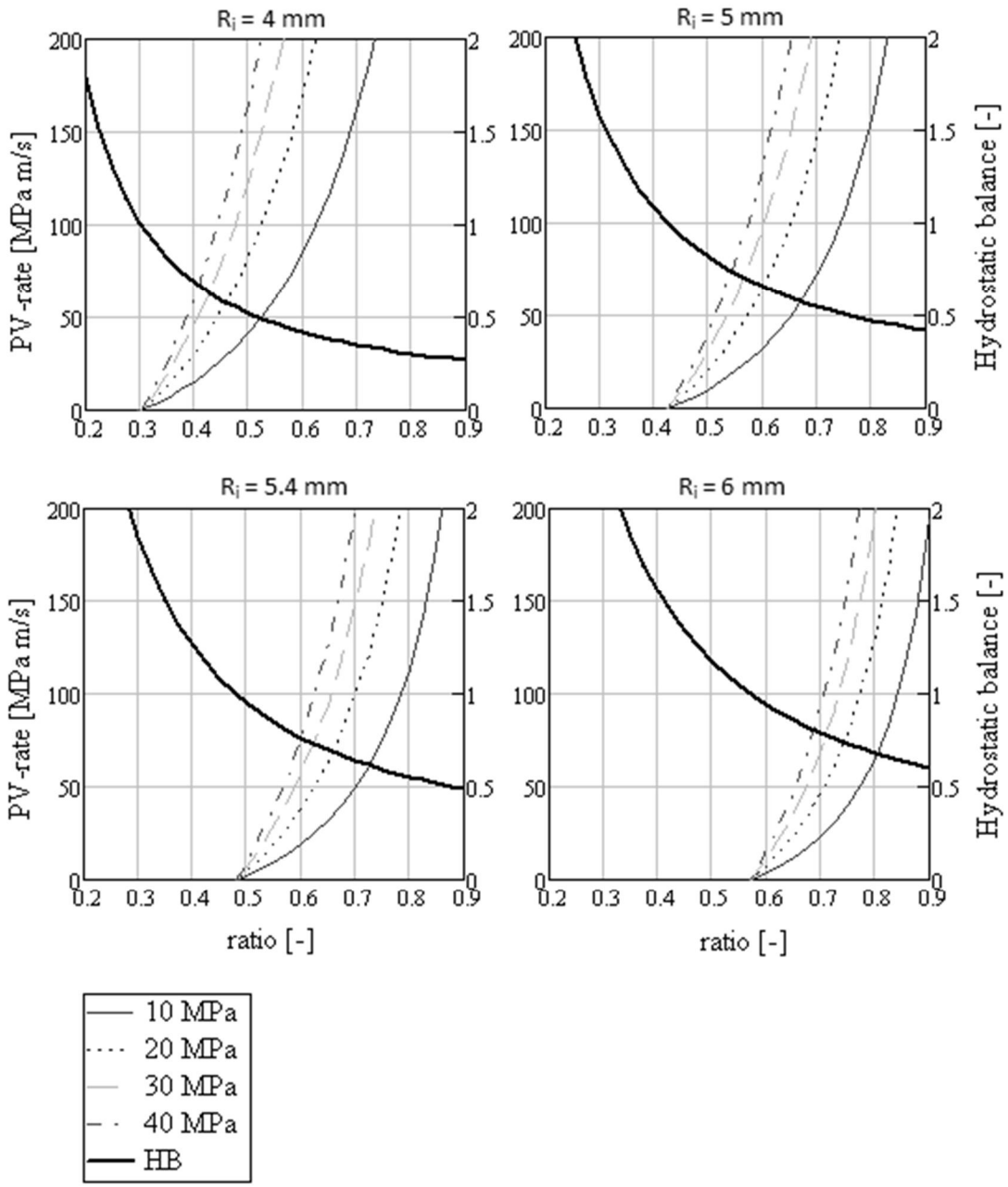

Figure 7. PV-rates and hydrostatic balance of the slipper with different pressure levels and different inner radius of the sliding surface.

The point which the PV-rate curves are started is the point where the lifting force equals the piston force. At that point the hydrostatic balance is 1. Figure 7 shows that the diameter of the inner radius is very significant. With a correctly designed slipper it is possible to achieve high pressure levels with low PV-rates. In that case the inner diameter of 5.4 mm gives very good results. With a ratio of 0.53, the PV-rates are acceptable also at a pressure level of 40 MPa. With a ratio of 0.53 the outer radius of the sliding surface is 10.19 mm.

Figure 8 shows the changes if the piston diameter is increased from 16.29 mm to 20.00 mm.

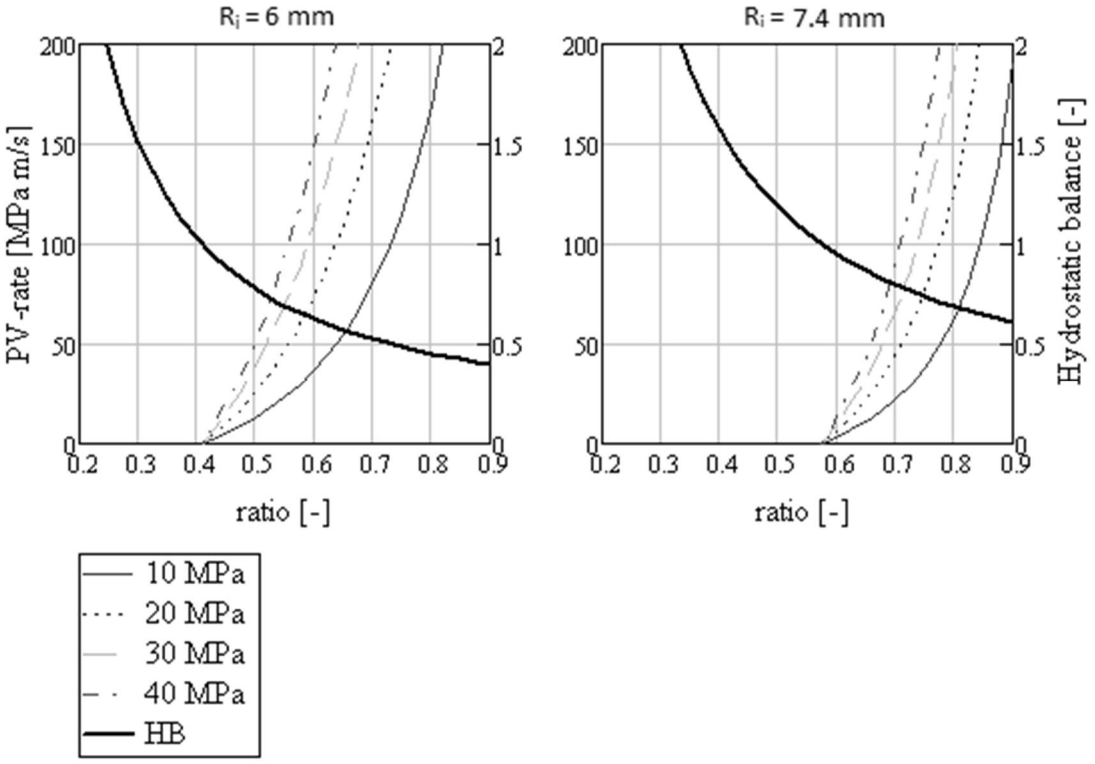

Figure 8. PV-rates and hydrostatic balance of the slipper. Piston diameter is 20.00 mm.

Figure 7 and Figure 8 show that if the inner radius of the sliding surface is the same but the piston diameter is increased, the low PV-rates move to lower ratio values. That is quite obvious because the bigger outer radius of the sliding surface also increases to lifting force. It is interesting that acceptable PV-rates are still achieved. Figure 8 shows also that with bigger inner radius it is possible to achieve the same behaviour as earlier. In fact, the whole system is just scaled up. There is no big difference in the sensitivity of the ratio between piston sizes.

Figure 9 shows the effect of the piston diameter on the PV-rate of the slipper.

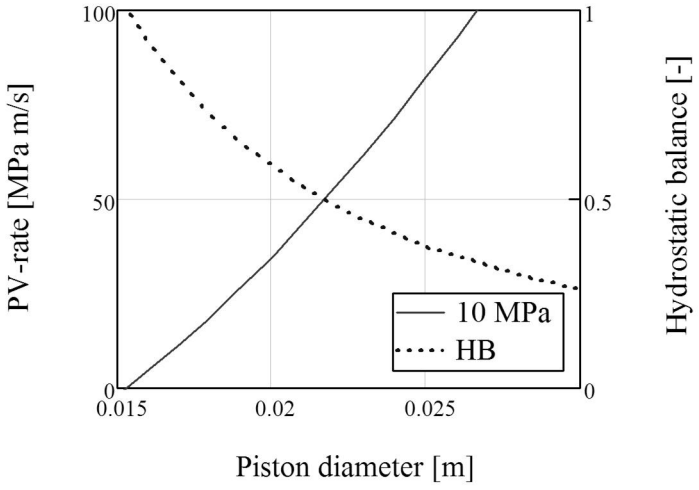

Figure 9. Effect of the piston diameter on the PV-rate of the slipper.

Figure 9 shows the PV-rate if the piston diameter is changed. The inner and the outer radius of the sliding surface are constant. Figure 6 shows the same as Figure 7 and Figure 8; only the point of view is different. All the dimensions should be fixed exactly in the design to obtain acceptable results.

3.7 Slipper deformations

The equations presented in the previous chapters work fine in theory, but in the real world there are phenomena like deformations which change the slipper properties. Slipper deformations are an important part of the research of the lubrication conditions between slipper and swashplate. Deformation of the slipper is related to the pressure level, material, structure and the dimensions of the slipper.

Slipper deformations affect the pressure profile, load carrying capacity and leakage flow rate of the bearing, which means that in slipper research and design it is very important to know what kinds of changes will happen. Different slipper deformation modes are shown in Figure 10.

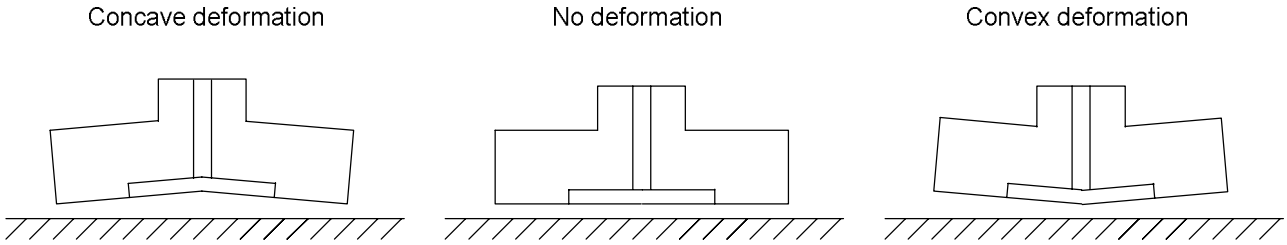

Figure 10. Slipper deformation modes.

There are two basic deformation modes, as Figure 10 shows. In concave deformation the inner edge of the sliding surface is opened just as in convex deformation the outer edge of the sliding surface is opened. The theoretical calculations for these deformation types are presented in reference [Manring 2002]. Deformation is described with dimensionless value of slope with the parameters shown in Figure 11.

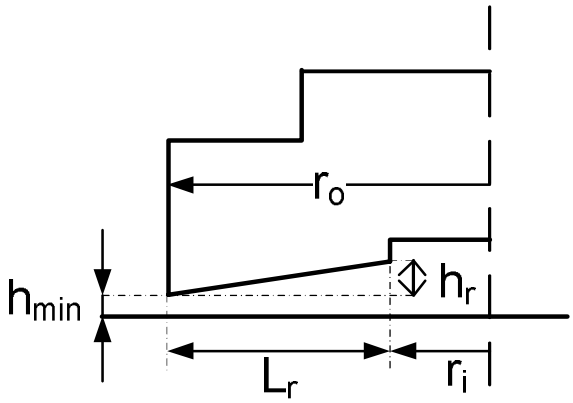

Figure 11. Parameters of the deformation calculations.

Equation 30 and Equation 31 describe how the slope of the deformation is calculated. The equations are defined in the same dimensionless way as in [Manring 2002].

$$\delta = \frac{h_r}{L_r} \tag{30}$$

$$\hat{\delta} = \delta \frac{r_o}{h_{\min}} \tag{31}$$

Dimensionless gap height is

$$\hat{h} = \frac{h}{h_{\min}} \tag{32}$$

Fluid film thickness for concave deformations can be shown [Manring 2002]

$$\hat{h} = 1 + \hat{\delta}\left(1 - \hat{r}\right) \tag{33}$$

where

$$\hat{r} = \frac{r}{r_o} \tag{34}$$

For concave deformation the pressure profile between the used slipper and swashplate is as Figure 12 shows. In this case slipper D, shown in Figure 3, is used.

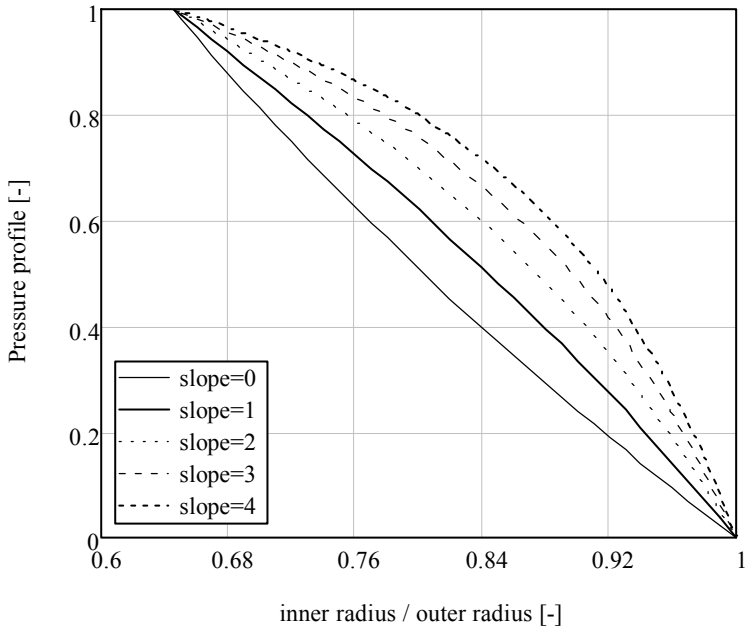

Figure 12. Pressure profile between slipper and swashplate with concave deformations.

Figure 12 is plotted with five different values for slope of deformation. For concave deformations the slope of deformation is always positive. It could be supposed that because of pressure profile changes also the hydrostatic balance varies a lot with the function of slipper deformation.

To obtain the pressure profile, the same procedure as shown in Chapter 3.4, starting from Equation 20, is made with radius dependent gap height. The gap height is radius dependent because of the deformation of the slipper.

$$\frac{\partial p}{\partial r} h^3 + \frac{\partial}{\partial r}\left(r h^3 \frac{\partial p}{\partial r} \right) = 0 \tag{35}$$

Although the velocities are zero, the gap height is not time dependent and it is the same in all angular positions, and the pressure does not vary in the angular direction; thus Equation 35 is complex. Now Equation 33 is used in Equation 35.

$$\frac{\partial p}{\partial r}\left(h_{\min} + h_{\min}\,\hat{\delta}(1-\hat{r}) \right)^3 + \frac{\partial}{\partial r}\left(r\left(h_{\min} + h_{\min}\,\hat{\delta}(1-\hat{r}) \right)^3 \frac{\partial p}{\partial r} \right) = 0 \tag{36}$$

Many assumptions have been made, but still Equation 36 is very complex to solve. So if deformation and gap height changes as a result are taken into account, numerical method should be used to solve the pressure profile.

If slipper and swashplate are not parallel, gap height could be calculated as a function of radius and angle, as Equation 37 shows [Pelosi 2008].

$$h(r,\theta) = r\sin\theta \frac{\sqrt{\frac{1}{3}}}{r_o}\left(h_2 - h_3\right) + r\cos\theta \frac{1}{3r_o}\left(2h_1 - h_2 - h_3\right) + \frac{1}{3}\left(h_1 + h_2 + h_3\right) + \Delta h \tag{37}$$

If the slipper and swashplate are parallel, the first two terms in Equation 37 are zero and that equation reduces to

$$h = \frac{1}{3}\left(h_1 + h_2 + h_3\right) + \Delta h \quad \rightarrow \quad h = h_{\min} + \Delta h \tag{38}$$

In fact, Equation 33 and Equation 38 are the same. In Equation 38 the term Δh includes the deformation of the slipper.

To get a realistic idea of the impact of the deformation, slipper flow and load carrying capacity are shown in Figure 13 and Figure 14. The slipper D dimensions shown in Figure 3 are used.

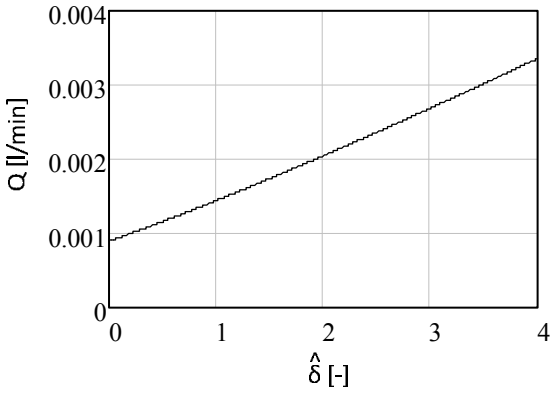

Figure 13. Slipper flow with different concave deformations.

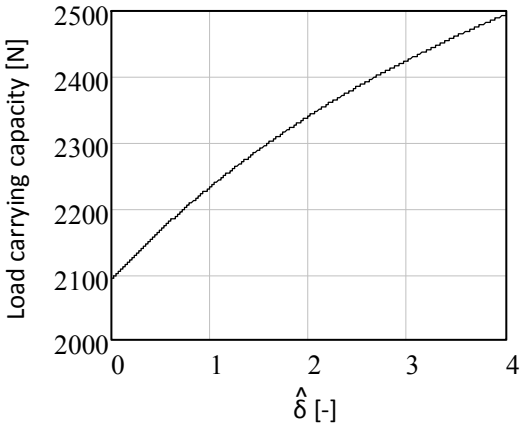

Figure 14. Slipper load carrying capacity with different concave deformations.

Figure 13 and Figure 14 are plotted with slipper D pressure of 10 MPa and the minimum film thickness is assumed to be 1 µm. Without deformation the results in Figure 13 and Figure 14 are the same as the basic equations concerning hydrostatic slipper gives. It can be noticed with this numerical example that the effect of deformations on slipper behaviour is significant.

FEM-analysis of the slipper deformations is presented in Chapter 5. The sliding surface deformations and deformations of the inner radius of the slipper are studied.

3.8 Power loss of the slipper

There is a global trend to reduce losses in all areas. So also in water hydraulics there is a demand for efficiency in all the systems, components and structures inside the component. All the solutions should be as good as possible measured as overall costs. A significant part of the volumetric losses of the axial piston pump comes from the slipper-swashplate contact, and optimization of that contact is important.

One important property of the slipper is leakage flow. Because the leakage is the function of the ratio of the inner and the outer radius, as Equation 28 shows, the amount of leakage does not change if the ratio is constant. This means that the scaling of the piston-slipper assembly is not a problem. This does not take deformations into account.

The power losses of the slipper-swashplate contact consist of two parts: viscous dissipation and pumping loss. Viscous dissipation is a product of the angular velocity and the frictional torque. Pumping loss is slipper flow multiplied by pressure in the slipper pocket. The losses in equation form are shown in [Hamrock 1994] and Equation 39.

$$H = H_v + H_p = \frac{\pi\eta\omega^2}{2h}(r_o{}^4 - r_i^4) + \frac{\pi h^3 p_{slipper}^2}{6\eta \ln\left(\frac{r_o}{r_i}\right)} \tag{39}$$

It is noteworthy that H_v is inversely proportional to h and H_p is proportional to h^3, whereas H_v is proportional to η and H_p is inversely proportional to η. The water properties affect both of the parameters h and η and this way lead to losses.

Equation 39 shows the losses, and because the gap height is of interest in water hydraulic slipper bearings, the equation differentiates with respect to h and equates to zero.

$$h = \sqrt[4]{\frac{\pi^2\eta^2\omega^2(r_o^8 - r_i^8) + 2\pi^2\eta^2\omega^2(r_i^6 r_o^2 - r_i^2 r_o^6)}{4w^2 \ln\left(\frac{r_o}{r_i}\right)}} \tag{40}$$

Equation 40 gives the optimum gap height according to the power losses. Load capacity w is shown in Equation 9.

Often the bearing velocities are low and the viscous dissipation is neglected. In that case the optimum ratio regarding the power loss between the inner radius of the sliding surface of the slipper and the outer radius of the sliding surface of the slipper is 0.53. In water lubricated slipper-swashplate contact the velocity is not totally neglected and the optimum ratio can be calculated by differentiating Equation 39 with respect to inner radius and equating to zero the equations as in 41.

$$-r_i^2 - 4r_i^{10} + r_o^2 - 4r_i^2 \ln\left(\frac{r_o}{r_i}\right) + 4r_i^4 r_o^6 - 12r_i^6 r_o^4 + 12r_i^8 r_o^2 = 0 \tag{41}$$

In Equation 41 the optimum ratio regarding the power loss between the inner radius and the outer radius of the sliding surface of the slipper is 0.53, which can also be found in Figure 15.

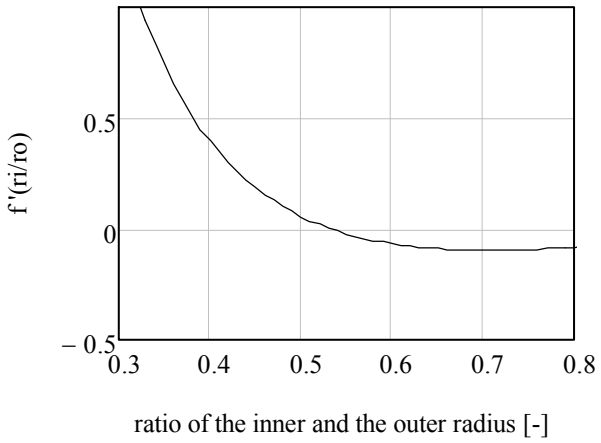

Figure 15. Zero position of the power losses.

When the viscous dissipation is taken into account the change of the optimum ratio is minimal and the right value is still 0.53 with two decimals.

Figure 16 shows the viscous dissipation of the slipper as a function of the gap height.

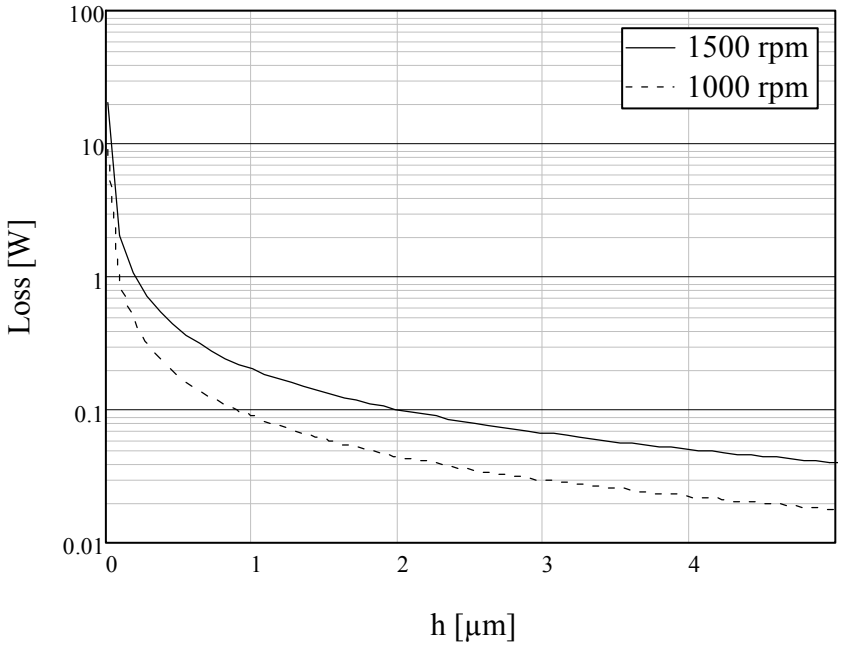

Figure 16. Viscous loss of the slipper B.

Viscous dissipation is rather low, under 1 W, in all the gap height values which are bigger than 0.2 μm. The rotation speed of the swashplate affects the loss. The viscous loss is bigger with higher rotation speed, as Figure 16 and also Equation 39 show. Viscous dissipation is not pressure dependent.

The pumping loss with different pressure levels is shown in Figure 17.

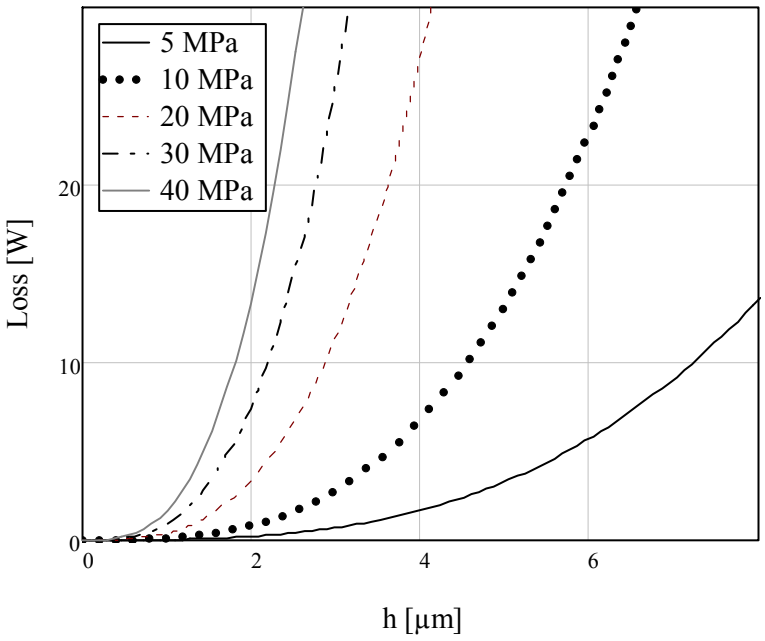

Figure 17. Pumping loss of the slipper.

Figure 17 shows that pumping losses are highly dependent on the pressure level of the pump. Also the gap height is very significant, which can be deduced from Equation 39. Because of the low viscosity of water, the losses are very high with a high gap height and high pressure level. However, water film is very thin, which make the losses acceptable.

With 1500 rpm, 30 MPa pressure and 1 µm gap height the viscous dissipation is 0.2 W and the pumping loss is 0.9 W. This example demonstrates that the loss from viscous dissipation is not totally negligible compared to the pumping loss in the water hydraulic slipper as the optimum ratio of the inner and outer radius of the sliding surface is 0.53 in spite of the viscous dissipation.

The problem is that the power loss calculation assumes the pressure profile without deformation. If the slipper is manufactured so that the optimum is achieved according to these equations, the situation in real life is different. Pressure level and deformation should be taken account in the design phase. In that way it is possible to achieve the real optimum. Numerical methods, like FEM and FSI, are helpful tools in working out the design parameters.

3.9 Discussion

Water lubrication is reasonable in water hydraulic axial piston pumps but water is a challenging medium because the water film is thin and water has a low viscosity-pressure coefficient. Water as a pressure medium causes limitations to the materials and industrial plastics are widely used. Industrial plastics are a reasonable solution in axial piston pumps. However, plastics are more elastic materials than stainless steel, which has to be taken into account. A steel core or collar for the slipper is needed because of the pressure cycle. The steel core or collar changes the tension to compression which PEEK material can tolerate better.

Although the idea of the hydrostatic bearing is very simple, the realization in water hydraulic pumps is challenging. In slipper design all the presented theoretical aspects affect the design of the hydrostatic bearing. It would be easy to design and manufacture a very good slipper for the water hydraulic pump if the

deformations were not taken into account. It is possible to match the water properties, material, PV-rate, forces and optimum power loss. Again, if we left out PV-rate, the design process of the slipper would be straightforward. The challenge is that all things have to be taken into account and the demands are partially in conflict.

Many forces affect the slipper but the pressure force is the most important. Because of the industrial plastics used in water hydraulic axial piston pumps, the pressure force should always compensate to achieve reasonable pressure levels. Slipper force depends on pressure level, the dimensions of the slipper and the piston and also the deformation of the sliding surface.

It is shown that it is possible to follow the maximum PV-rate of the material. However, that means that the sizing of the slipper is designed near the limit. The problem is that the deformations can prevent that. If there are deformations which are remarkable compared to the water film thickness, the properties of the slipper will change. Slipper deformations affect the pressure profile, load carrying capacity and leakage flow rate of the bearing. The water properties cause a thin film, so we come back to the water properties once again. Because all the studies and equations assume a parallel gap, better theoretical study is needed to get realistic results. Deformations play a key role and they are more deeply studied in Chapter 5.

Material selection and dimensioning of the piston-slipper assembly are very important, because these are things which determine the properties of the slipper. But it is obvious that the designer needs to know all aspects to make the design correctly.

The power losses of the slipper-swashplate contact consist of two parts: viscous dissipation and pumping loss. Usually the viscous dissipation is assumed to be neglected but the numerical example shows that the loss should be taken into account in water hydraulics slipper design because the water film thickness is low. However, the ratio of the minimum losses is still 0.53.

4 EMPIRICAL COMPARISON OF SLIPPER STRUCTURES IN WATER HYDRAULIC AXIAL PISTON PUMP

Empirical study of the lubrication situation between slipper and swashplate is challenging, because the water properties and plastics cause errors with the results. Contact between slipper and swashplate and also the relatively high deformation of PEEK affect the measurement results. However, it is more important to study changes in the circumstances and these can clearly be seen from the measurements.

4.1 Test set-up

Tests in a realistic environment are needed to verify the results from theoretical and numerical studies. The structure of the test rig in this study allows changing the angle of the swashplate during measurements, unlike the situation in other test rigs in research of the film between swashplate and slipper pad. That is important because changes of the swashplate angle (or pressure level) are the most important things to study in the empirical tests. The schematic figure of the experimental test rig that is used in the measurements is shown in Figure 18.

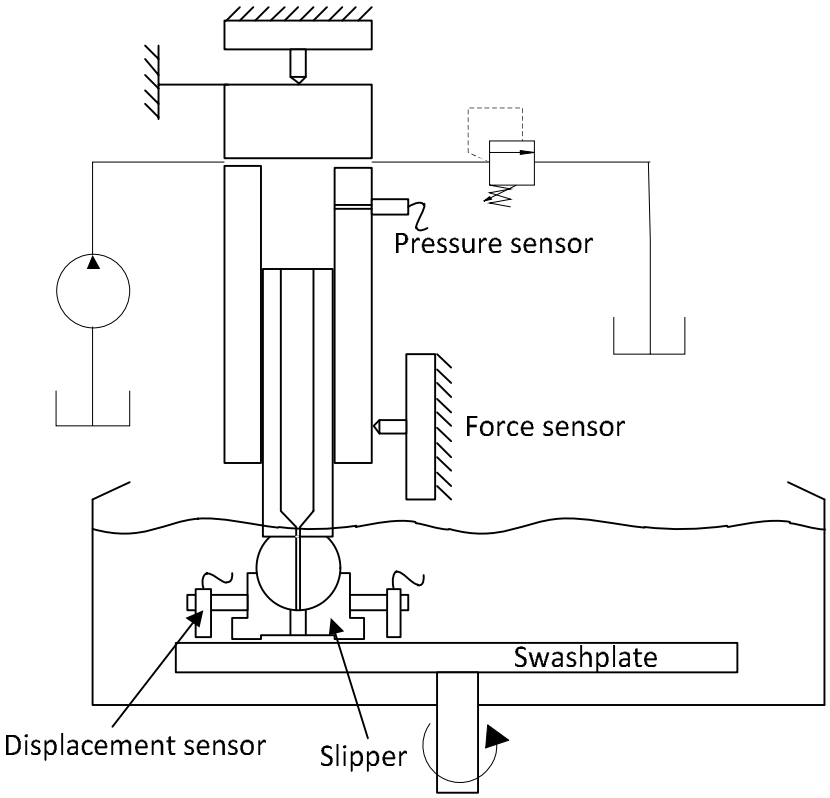

Figure 18. Structure of the test rig.

The special cylinder block includes one cylinder where the coated piston moves. The cylinder includes a PEEK-bushing that is reamed. The construction is exactly the same as in some commercial water hydraulic

pumps. Two different sizes of cylinder blocks are made because there is a need to use two different sizes of pistons. The slipper pad and swashplate are submerged all the time in the water tank surrounding the test system. During the measurements there is a plastic film above the water tank to avoid contamination and splashes.

There are two different possible cylinder positions in the test system. On the first position the turning axle of the swashplate goes through to a spherical joint of the piston and the piston does not move while the swashplate angle is changing. On the other position the distance between the turning axle of the swashplate and the piston is maximum; and the piston movement is also maximum if the swashplate angle is changed. All the results in this thesis are measured in the latter position.

The movements of the swashplate are realized with oil hydraulic actuators. The angle of the swashplate is controlled by a hydraulic cylinder. The movement range of the swashplate angle is ±20 degrees. The rotation of the swashplate is realized with a hydraulic motor. Both actuators are controlled with a regel-valve. The control system is built with Simulink (Simulink is a commercial tool for modeling, simulating and analyzing multidomain dynamic systems) and used in real time via dSPACE (dSPACE is a real-time control unit).

Figure 19 shows the measuring situation and coordinate system of the test rig. The radius of the rotation circle is 40 mm. Three eddy current sensors are equally spaced on the collar around the slipper pad. The distance between the centre point of the slipper and the eddy current sensor is 27 mm. The gap heights are measured outside of the slipper pad, which makes changes of the water film and deformations of the slipper clearer to see because of the geometric conditions. The measurements are made with three eddy current sensors with 1 mm measuring ranges (S1, S2, S3). The resolution of the sensors is 0.05 µm and static repeatability 0.1 µm. The surface roughness of the swashplate is measured to be between Ra = 0.22-0.24 µm.

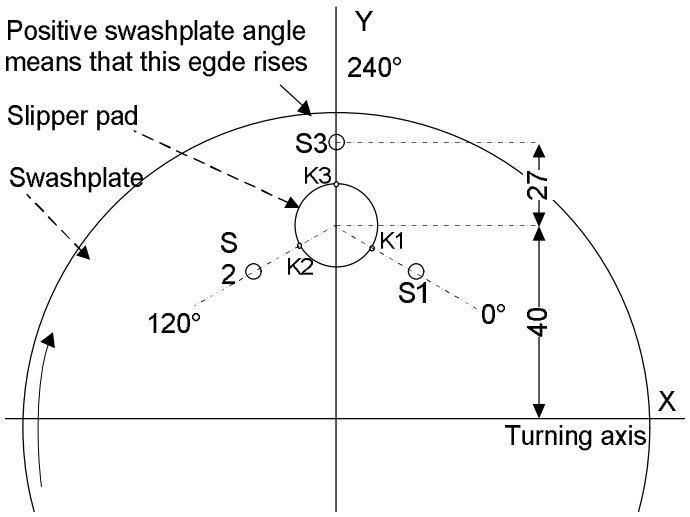

Figure 19. Dimensions and coordinate system of the test system.

The measured values are converted to the clearances between slipper pad and swashplate at points K1, K2, K3. With these points the minimum gap height and location of the minimum gap can be calculated. The point of maximum gap is located 180 degrees clock wise from the minimum point.

The test system is lubricated with tap water. The filtration ratio of the water is 10 µm. The water temperature is about 30°C, and in that temperature the kinematic viscosity of water is $0.8 \cdot 10^{-6}$ m^2/s.

4.1.1 Sensors

To obtain useful information about the lubrication circumstances and the forces acting on the piston, the test rig is equipped with the set of sensors shown in Figure 20. The locations of the sensors are indicated with numbers referring to Table 3, which shows the types, ranges and resolutions of the sensors.

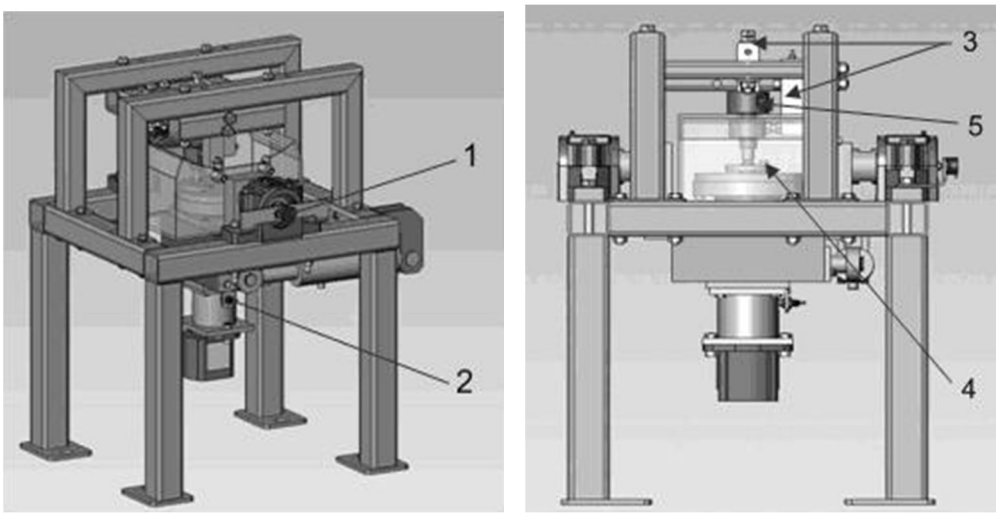

Figure 20. Sensor locations at the test system.

Number	Sensor	Capacity / Range	Resolution
1	Potentiometer	308°	0.03°
2	Inductive sensor	5 kHz	-
3	Load cell	500 kg	±0.02 % FSO
4	Eddy current sensor	1 mm	0.005 % FSO
5	Pressure sensor	25 MPa	

Table 3. Sensors of the test system.

The angle of the swashplate is measured by a potentiometer calibrated so that the horizontal swashplate corresponds to zero angle. The rotation speed of the swashplate is measured with an inductive sensor. Water pressure inside the cylinder is measured with a pressure sensor. The forces acting on the cylinder are measured with three beam type force sensors. Each sensor measures forces acting in one coordinate axis. Force sensors slightly affect each other, but this is taken into account. For measurements of static swashplate angle, the force sensor to the Y-axis is removed. The film thickness is measured with an eddy current sensor, a type of sensor which has successfully been used to measure film thickness in difficult conditions. The eddy current sensor is calibrated with the swashplate material, in this case stainless steel.

4.2 Behaviour of the gap height

The following figures show the gap between slipper pad and swashplate at the three clearance points (K1, K2, K3), at the centre of the slipper (Av) and also the minimum value (Min). Figure 21 shows the reference measurements with 0 degree swashplate angle. The angular locations of the minimum and maximum values of the clearance during measurements are also plotted.

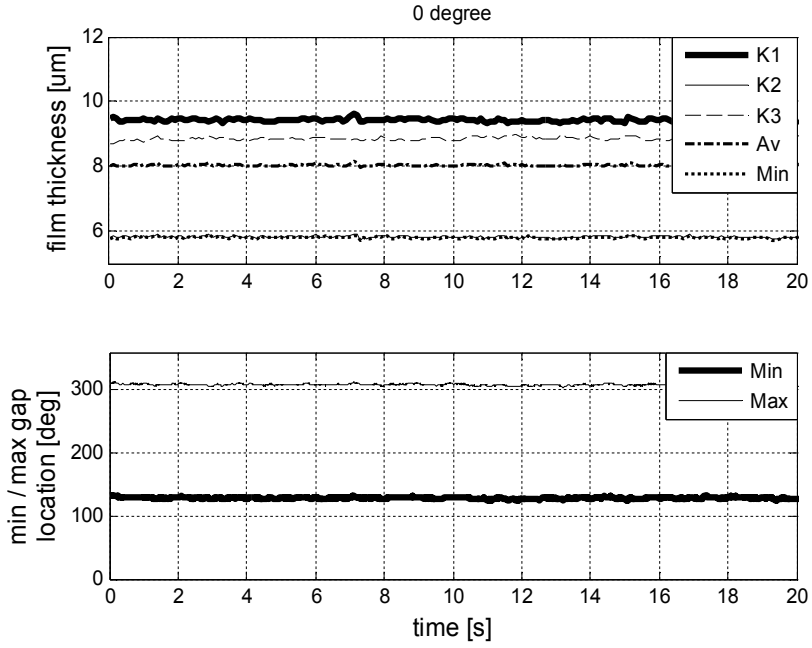

Figure 21. Gap heights of the slipper pad points with 1000 rpm, 0 degree swashplate angle and 10 MPa pressure difference.

According to references [Donders 1997] and [Wieczoreck 2000] gap height is highest at the inner edge and smallest at the outer edge. The slipper is tilted backwards, which means that gap height on the leading edge is higher than on the trailing edge. The measurements in this case show a different kind of orientation, as Figure 21 shows. It should be remembered that in a real situation the cylinder block is the rotating object. There are also some deformations at the slipper pad and zero position is not exactly the same as measured in 5 N load in dry circumstances. That is quite obvious because the average gap height is remarkably high in all measurements. Because of all these question marks and because the measured values are close to each other, minimal error can change the results significantly. That is why the absolute values of the locations of the minimum and maximum clearances are not exactly right. However, it is possible to compare locations between measurements. Figure 21 shows that the minimum clearance is located at about 129 degrees and maximum clearance located at 309 degrees (see Figure 19).

Orientation of the slipper pad is measured with four different constant swashplate angles: 0, 5, 10 and 15 degrees. Figure 22 shows the orientation of the slipper pad with 5, 10 and 15 degree swashplate angle. Both measurements conditions are made in the following order: first adjustment of the swashplate angle, then application of load pressure and finally setting the rotation speed.

A comparison between Figure 21 and the curves in Figure 22 show that there is no big difference in gap heights between different swashplate angles. The gap height changes are within 2 µm and on average gap height changes only under 1 µm. It should also be remembered that deformations affect the measurement

result of the gap height. Also locations of the minimum and maximum points are almost the same; the difference is only a few degrees. That is obvious because contact between the swashplate and slipper pad can carry only perpendicular load. Change at this perpendicular force is quite small. For example, with slipper B at 10 MPa, the force change between 0 and 10 degree angle is only 1.5 %.

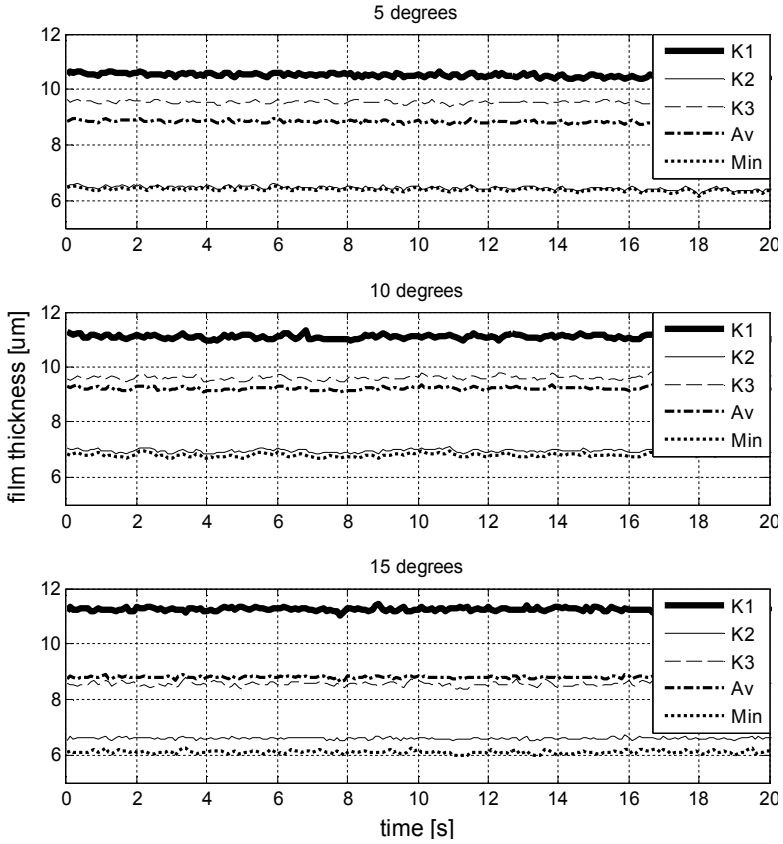

Figure 22. Gap heights of the slipper pad points at 1000 rpm rotation speed, 5, 10 and 15 degree swashplate angle and 10 MPa pressure difference.

The situation is not exactly the same if the 10 degree swashplate angle is achieved during operation, as Figure 23 and Figure 24 show. Figure 23 and Figure 24 show the gap heights during swashplate turning with 0.2 MPa and 10 MPa. Changes in the gap heights are very smooth during the turning process. At both 0.2 MPa and 10 MPa pressure levels, the orientation of the slipper pad is not exactly the same before and after the steps. The figures also show that during step 0° to 10° the average gap height reduces. During the step from 10° to 0° the gap height rises but overall changes are quite small.

It should be noticed that the structure of the spherical joint is important for sliding conditions. This is because friction of the spherical joint orientation of the slipper pad depends on the turning direction and speed of the swashplate. In actual pumps the phenomenon is not significant because of the low pressure area. It could be assumed that during the suction stroke orientation of the slipper pad is returned to the normal sliding position.

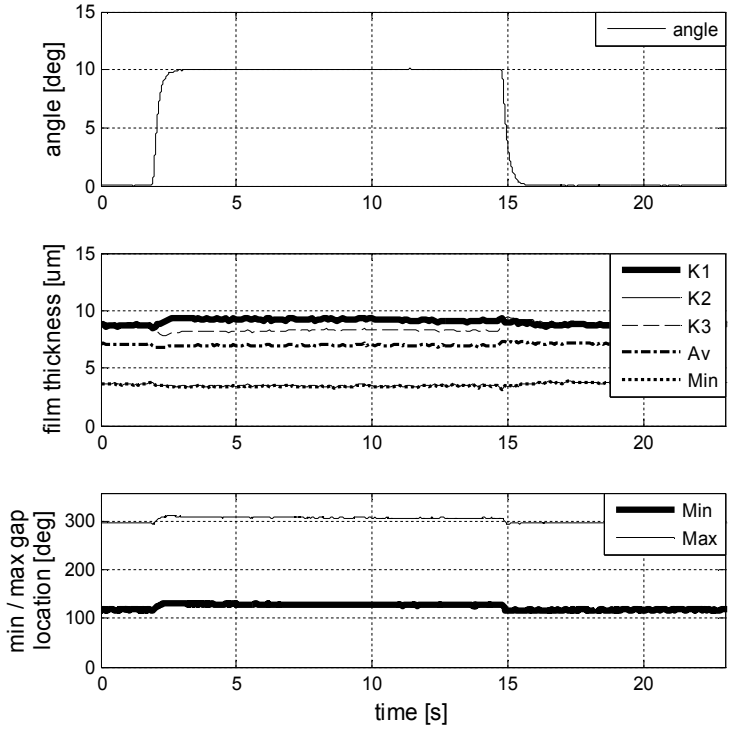

Figure 23. Gap heights during swashplate turning at 0.2 MPa load pressure and 1000 rpm rotation speed.

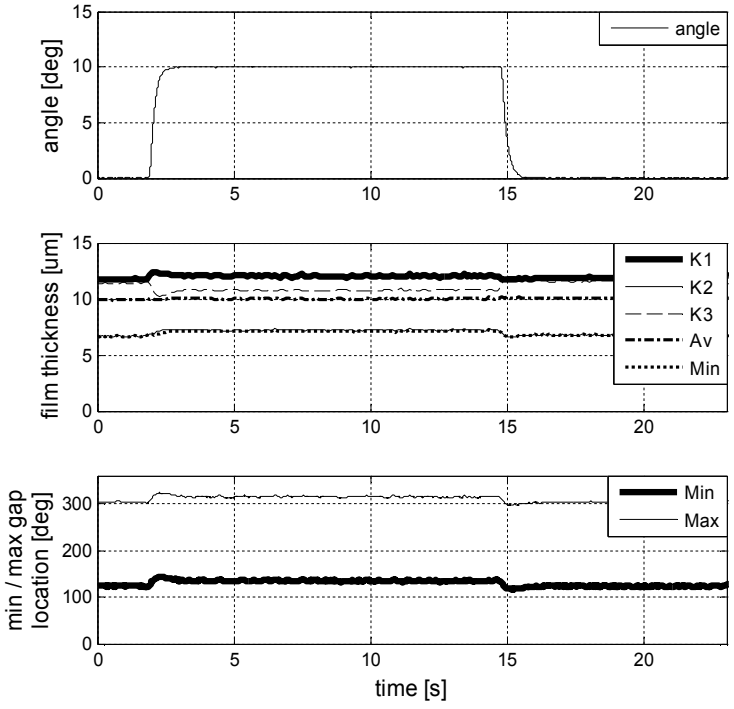

Figure 24. Gap heights during swashplate turning at 10 MPa load pressure and 1000 rpm rotation speed.

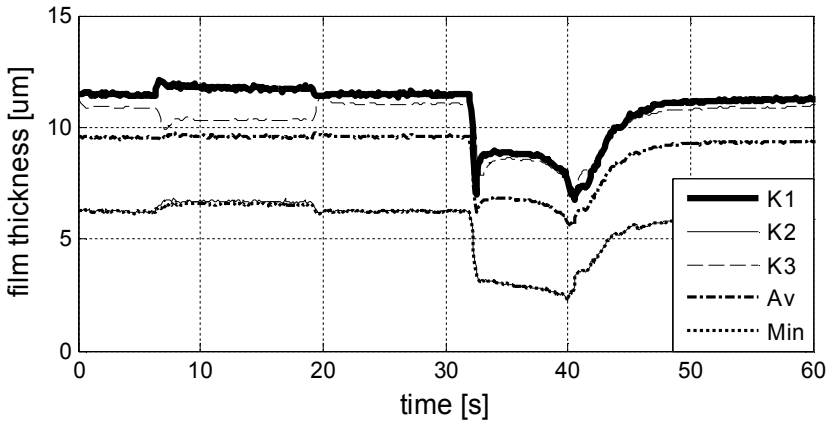

Figure 25. Gap heights during swashplate turning and pressure changes at 1000 rpm rotation speed.

Figure 25 shows changes during swashplate changes (from 10 degrees to 0 degrees and back to 10 degrees) and after that during pressure changes from 10 MPa to 0.5 MPa and back to 10 MPa. It can be seen that the effect of pressure level is more significant than the effect of the swashplate turning or effect of the swashplate angle.

The gap height measurements can be concluded so that the results of the gap heights are useful during swashplate turning. It can be seen that nothing remarkable happens during swashplate turning, which is positive and means that it is possible to realize the variable displacement pump. Pressure level has a remarkable effect on the absolute values of the gap height. That is why the absolute values cannot be trusted, and the need for deformation calculations becomes very obvious.

4.3 Leakages of the slippers

The leakage measurements of the slipper are mainly used to verify that the measuring situations are all correct, because if the leakage is visible, there is something wrong. Leakages in the static situation (without swashplate rotation) are very low with slippers B and D. The leakage is only a few drops during 10 minute measurements at a pressure level of 2, 7 and 12 MPa. That is quite obvious because the hydrostatic balance is under 1, which means that sliding surface is pushed against the swashplate and actually there is no gap between the slipper and the swashplate.

The measured leakage of the piston-slipper (slipper B) assembly is approximately 0.2 l/min with 1000 rpm swashplate rotation. The measured leakage can be compared to values computed assuming parallel gap flow [Ivantysyn 2001]. With the present slipper dimensions and 10 MPa pressure difference, a leakage flow of 0.2 L/min corresponds to an average gap height of 7 μm. That is, however, too high because part of the leakage is coming between the piston and cylinder. But if the leakage between the slipper and swashplate is about half of the measured values, that tells that the gap is not parallel and the leakage is higher than the parallel gap height expected. That backs up the assumption that deformations affect the behaviour of the slipper.

Leakages of the spherical joint between slipper and piston are also very low; actually the leakage is zero. In this case the situation is the same also during swashplate rotation because the motion in the spherical joint is low. That result is expected because usually the leakage between slipper and piston is not taken into account in research.

Although slippers with hydrostatic balance over 1 are not studied in this paper, some measurements are made with slipper F and the piston with the control orifice. Because the hydrostatic balance of the slipper is over 1.0, the leakage is very high. The leakage is dependent on the supply pressure. In that case, the leakage is several litres per minute at a pressure level of 10 MPa.

4.4 Friction of the slippers

The friction coefficient of slipper B and slipper D is measured. Several measurements are made with three different pressure levels, 2 MPa, 7.5 MPa and 13 MPa. The pressure force of the slipper is calculated based on the piston area, the pressure of the system and the hydrostatic balance of the slipper. Because the swashplate angle is zero, the pressure force is equal to normal force. The lateral force of the piston is measured with a force sensor (Y-axis force sensor is removed to get more accurate results). The friction coefficient could be calculated from the normal and lateral force. All the measurements are combined to the range of the friction coefficient. That is because the friction coefficient changes at different pressure levels are not evident in either slipper B or slipper D. The friction coefficient range of both slippers versus the sliding speed of the slipper is shown in Figure 26.

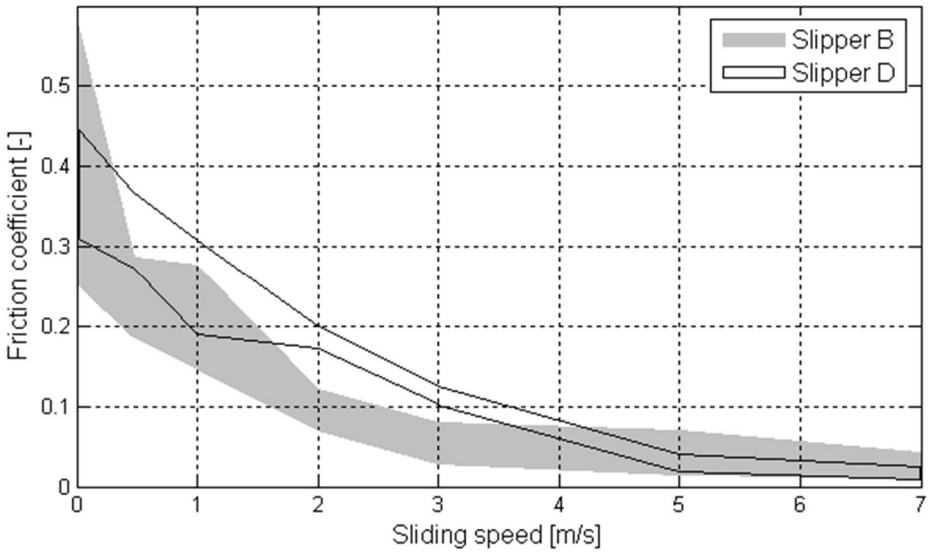

Figure 26. Measured range of friction values of slippers B and D.

Figure 26 shows that trend of the friction coefficient acts as expected. The friction coefficient reduced when the sliding speed increased. Slipper B has high values of friction coefficient with very low sliding speed values and also the variety of the values is high. The reason is that pressure is first adjusted and after that the rotating of the swashplate is started. Because of the low hydrostatic balance of slipper B a high range of friction values is measured. The slipper D friction coefficient is higher between 0.5 m/s to 4 m/s because the friction coefficient of the PEEK 2 is higher. Sliding speeds over 4 m/s friction coefficient are clearly below 0.1 in all measurements with both of the slippers.

Friction force is also measured in both slippers B and D during swashplate change at a pressure level of 10 MPa and a rotation speed of 1000 rpm. The force sensor gives the force change to the X-direction. It should be remembered that also the pushing force of the slipper changes when the swashplate angle changes, as Equation 11 shows. Friction acts smoothly during turning and there are no friction peaks during turning. Friction value change is very little and in practise negligible. It is understandable that change is very small

because the circumstances do not change significantly with different swashplate angle values. It can also be noticed that the situation is good during turning as well.

Some measurements are also made with slipper F and piston with control orifice. Because the hydrostatic balance of the slipper is over 1.0, it is obvious that the friction force is very low in that case, which is also noticed in measurement. All in all changes of the rotation speed of the swashplate, the angle of the swashplate and the supply pressure are not significant concerning the friction of the underclamped slipper. Underclamped slippers are not studied in this paper.

4.5 Slipper behaviour with different PV-rates

To verify the theoretical ideas about the effect of the PV-rate, experimental tests have been done. The effect of the PV-rate is difficult to measure. That is why the friction and the wear rate are used to compare different PV-rates. Figure 27 shows the friction between the slipper and swashplate as a function of the PV-rate. All the curves are approximations based on at least three different measurements.

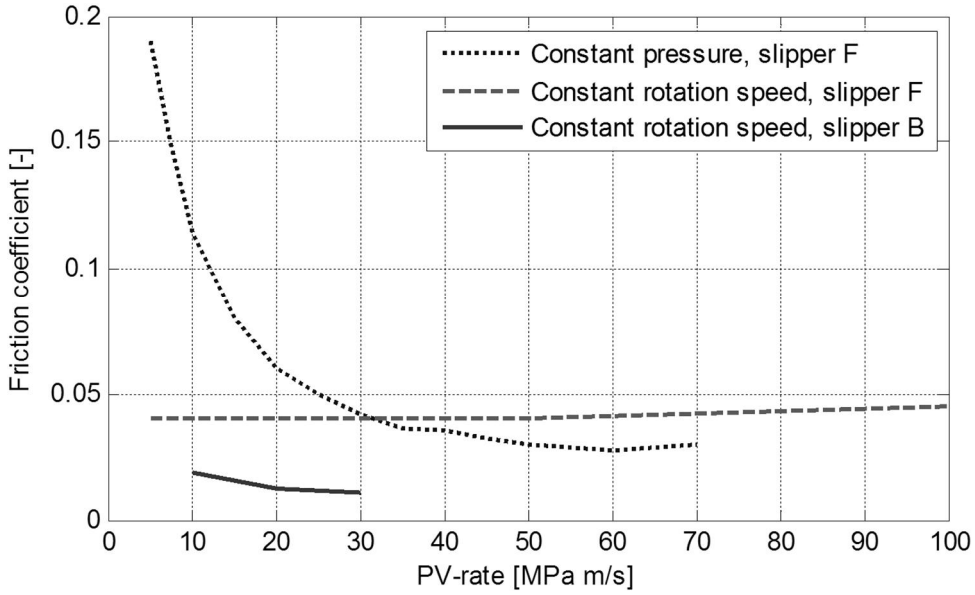

Figure 27. Friction as a function of the PV-rate of the slipper with constant pressure level and with constant rotation speed of the swashplate.

Figure 27 shows that the higher the PV-rate is the lower the friction between the slipper and the swashplate is if the pressure is constant and the rotation speed is changed. Although the PV-rate rises, the behaviour is better than with lower PV-rates. The impact of the rotation speed is more important than the impact of the PV-rate. The rotation speed should be over 500 rpm in all cases to obtain smooth operation. Of course, the same PV-rates are achieved with the constant rotation speed of the swashplate and friction coefficient is also measured that way by changing the pressure of the system. In that case, the friction increases slightly as the PV-rate increases.

The behaviour of slipper B is quite similar. This slipper is hydrostatically compensated, which restricted the PV-rate to 30 MPa m/s in the test system. However, also that is over the maximum PV-rate of the material. Low friction values are expected and the friction is lower than with slipper F because of better lubrication.

With the constant pressure measurements with slipper F, a PV-rate of 30 MPa m/s is achieved with a rotation speed of 700 rpm. With constant rotation speed measurements, a PV-rate of 30 MPa m/s is achieved at a pressure level of 3 MPa. At the point of 1000 rpm and 4 MPa, friction should be the same because both values are identical. However, there is a small difference, which mainly comes from measurement error.

In real pumps the situation can be controlled because the rotation speed of the cylinder barrel is generated before the pressure level rises.

4.6 Wear rate of the slippers

The wear rates of slipper B and F are measured with water lubrication. Slipper F is run with constant rotation speed (1000 rpm) and constant pressure. The pressure level is 2.1 MPa and 5.4 MPa. The PV-rates of the slipper are 20 MPa m/s and 50 MPa m/s. Both tests took ten hours. Slipper B was tested with 20 MPa m/s PV-rate and that test took ten hours. So the tests are short compared to real use. The mass of the slippers is measured with an accuracy of one milligram.

With 20 MPa m/s PV-rate, there is no wear; the mass of the slippers is exactly the same before and after the tests. It is surprising that also with a PV-rate of 50 MPa m/s the wear rate is negligible, and actually the mass of slipper F is exactly the same as before the test. That is interesting because 50 MPa m/s represents even 2.8 times a higher value than the informed value. If the whole sliding surface wears away, the change of mass is 0.1 g, which tells that already 5 % wear is very easy to see with 5 mg mass change. Although the test is short, it shows that it is possible to achieve higher PV-rates than recommended.

However, the test shows that the slippers become polished during operation because of the mechanical contact. Because of that the surface finish of the slipper is not critical.

The wear rate of slipper F is also studied with a control orifice and because the hydrostatic balance of the slipper is over 1.0, it is obvious that there is no wear.

4.7 Discussion

Measurements are needed to verify theoretical ideas, and in this case accurate results are difficult to measure because PEEK is elastic and deformations occur. That is a problem because also the position of the eddy current sensor might change. That can clearly be seen in the gap height measurement because the higher pressure level strongly increases the measured gap height. However, it is possible to compare measurements. Gap height and frictional forces are measured during swashplate angle changes. The gap height measurements showed that the operation of the slipper is very smooth during swashplate angle changes. There was nothing found in gap height measurements that would prevent swashplate angle changes during operation.

Friction measurement of the slipper showed that with at least 4 m/s sliding speed area both slippers worked fine in static and also in changing situations. Friction values are low and peaks do not occur during angle changing. PEEK has the maximum PV-rate but in water hydraulic components it is easy to exceed. PV-rate measurements with high PV-rate values have been done and with all measured slipper the friction values are low despite being over the limit values. Also the wear rate is negligible in all measurements. Although the PV-rate limits are quite low, higher values can be used if the rotation speed is high enough.

5 DEFORMATIONS OF SLIPPER STRUCTURES

In this chapter, the deformations of slipper structures and fluid structure interaction are studied with numerical analysis. Also the stress components of the slipper are considered. Figure 28 shows the motivation of that chapter.

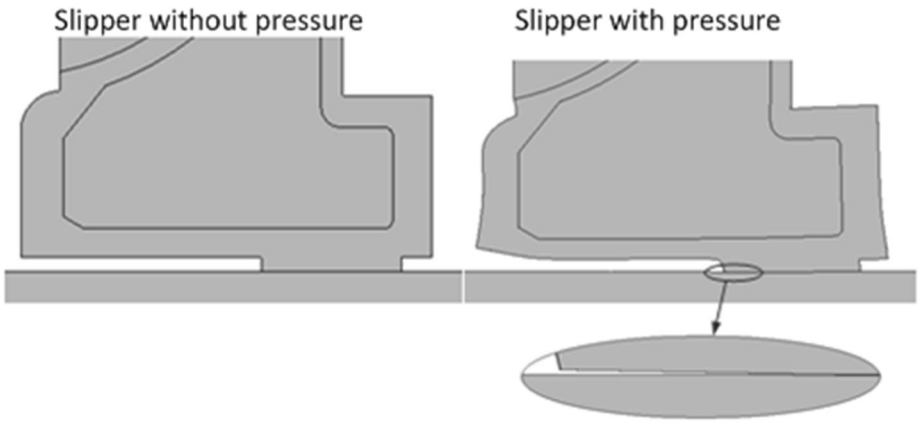

Figure 28. Slipper deformations at 100 times magnification.

Figure 28 shows an example how the working pressure of the pump can change the geometry of the slipper. It is easy to notice and understand that the changes of the dimensions of the slipper and also the sliding surface deformations really should be taken into account in slipper research.

5.1 Deformations of dimensions of the slipper

In this chapter the changes of the vertical deformation and the inner radius of the slipper are studied. Slippers are compared based on different materials, pressure level and structure. The measured vertical deformation of slippers B and D in a static situation is shown in Figure 29.

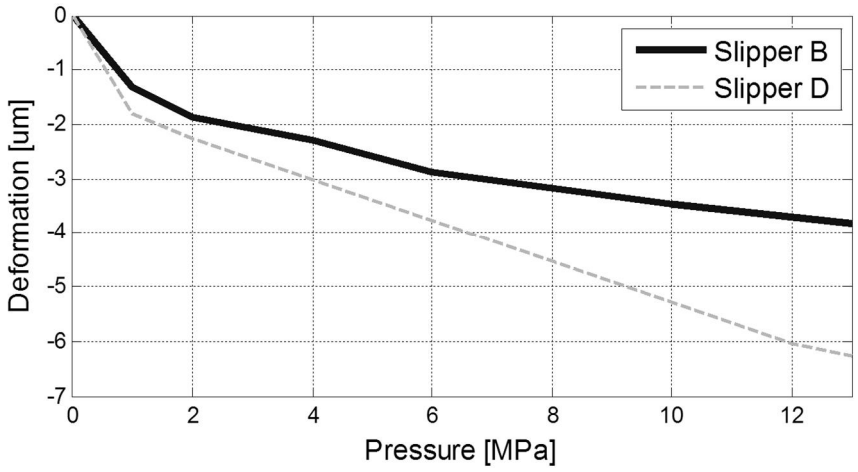

Figure 29. Measured vertical deformation of slipper B and slipper D as a function of pressure level.

Figure 29 shows that the vertical distance between the centre point of the slipper and the swashplate is reduced when the pressure rises. The change mainly occurs because of the material deformations. The change is the fastest from 0 to 2 MPa and after that the change is slower. The faster change at low pressures is mostly derived from the surface roughness of the components. The change in slipper B is smaller than with slipper D in spite of the PEEK-part of the slipper B being thicker and slipper D having only PEEK coating. The difference is caused by the properties of the PEEKs. The PEEK 2 of slipper D is more elastic than PEEK 1 in slipper B. Because the parts of the pumps are designed only for 14 MPa pressure level, the measurements are made only to 12 MPa and the behaviour with higher pressure levels is approximated with numerical calculations.

The piston-slipper assembly is modelled in FEM-software and because of the circular symmetry only a 20 degree sector of the assembly is studied. 3D tetrahedral solid elements are used for meshing. The model is loaded with working pressure and fixed with an outer piston shell which allows only vertical movement and with a lower surface of 10 mm thick stainless steel made swashplate. The contact between the piston and part 2 of the slipper (Figure 3) is defined as no penetration with all the slippers as well as the contact between part 2 and the swashplate. The contact between part 2 and part 1 of the slipper is defined as no penetration with slipper B and as bonded with slippers A, C, D and E.

PEEK is defined as a linear elastic material in the calculations. That assumption can be made if the maximum stress is below yield stress. If the maximum stress is slightly below yield stress the material should be defined as linear viscoelasticity, and if the stress is higher than yield stress the most advanced material model is needed. The maximum yield stress values for tension and compression of PEEK 1 and PEEK 2 are shown in Table 2.

Figure 30 shows the vertical displacement of slipper D, and Figure 31 shows the vertical displacement of slipper B.

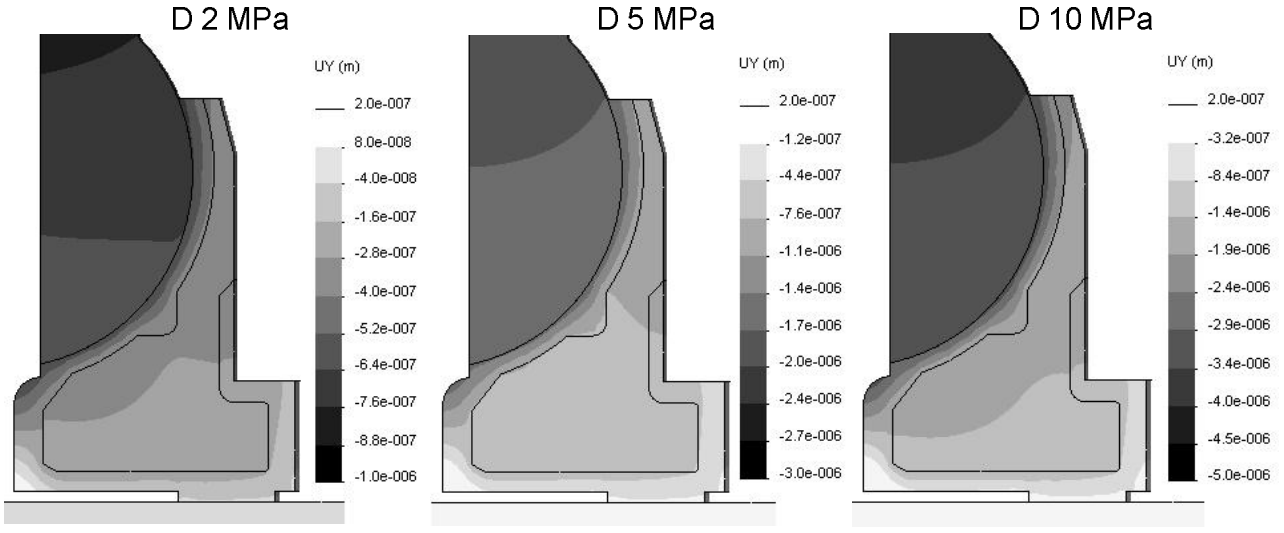

Figure 30. Vertical displacement of slipper D at pressure levels of 2 MPa, 5 MPa and 10 MPa.

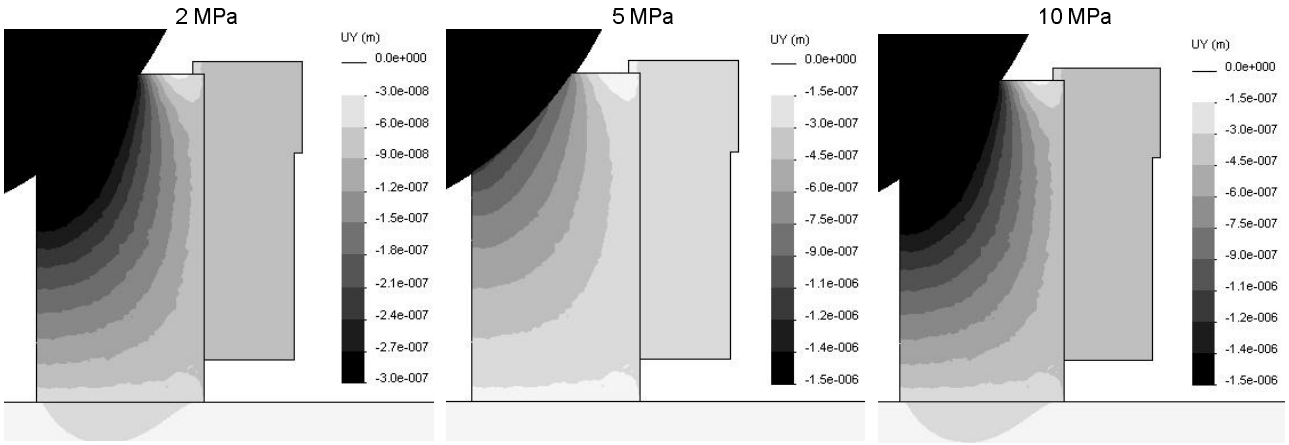

Figure 31. Vertical displacement of slipper B at pressure levels of 2 MPa, 5 MPa and 10 MPa.

Figure 30 and Figure 31 show that vertical compression depends on the pressure level. Both the measurements and the calculations show that the vertical deformation of slipper D is bigger than with slipper B. With slipper D the deformation is smaller than with the measured values at all pressure levels but the trend is similar. The change is almost linear. The calculated values of the vertical displacement are 0.3 µm, 0.7 µm and 1.4 µm. The calculated values are clearly smaller than the measured values.

Figure 31 shows that with the calculated values, vertical compression is smaller than with the measured values at all pressure levels. The calculated values of slipper B are < 0.1 µm, 0.2 µm and 0.4 µm at the location where the measurement collar is placed.

One reason for the smaller change is that the surface roughness of the components is not taken into account in the calculations. The surface roughness of the components causes most of the vertical deformation at a pressure level under 2 MPa. Without deformation from 0 MPa to 2MPa, deformations are closer to the calculated values, but still the measured values are bigger. Also the PEEK properties used in the calculation are literature values and are not derived from material property tests of the samples used in the deformation measurements. In addition, the measuring collar is around the slipper and because of this the horizontal displacement is bigger with the steel part of the slipper and this tilts the collar down.

In the following figures, there is also the pressure under the sliding surface, which is the realistic situation. Pressure is assumed to be circular symmetrical over the sliding surface, linearly decreased from the inner edge to the outer edge. Figure 32 shows the vertical deformations of slippers C, D and E with 2 MPa, 10 MPa, 20 MPa and 40 MPa. Figure 33 shows the vertical deformations of slippers A and B with 2 MPa, 10 MPa, 20 MPa and 40 MPa.

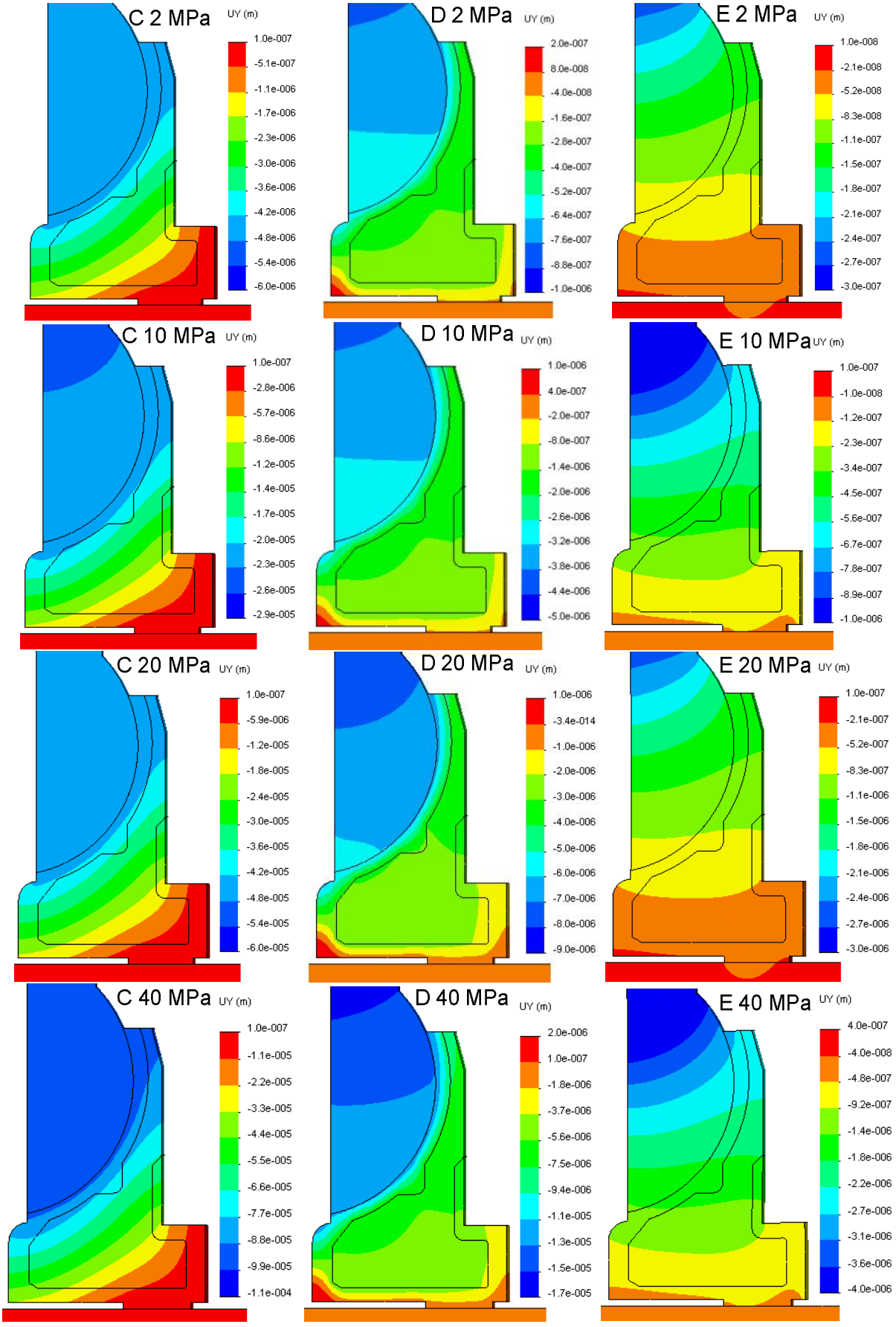

Figure 32. Vertical deformation of slipper C, D and E at pressure levels of 2, 10, 20 and 40 MPa.

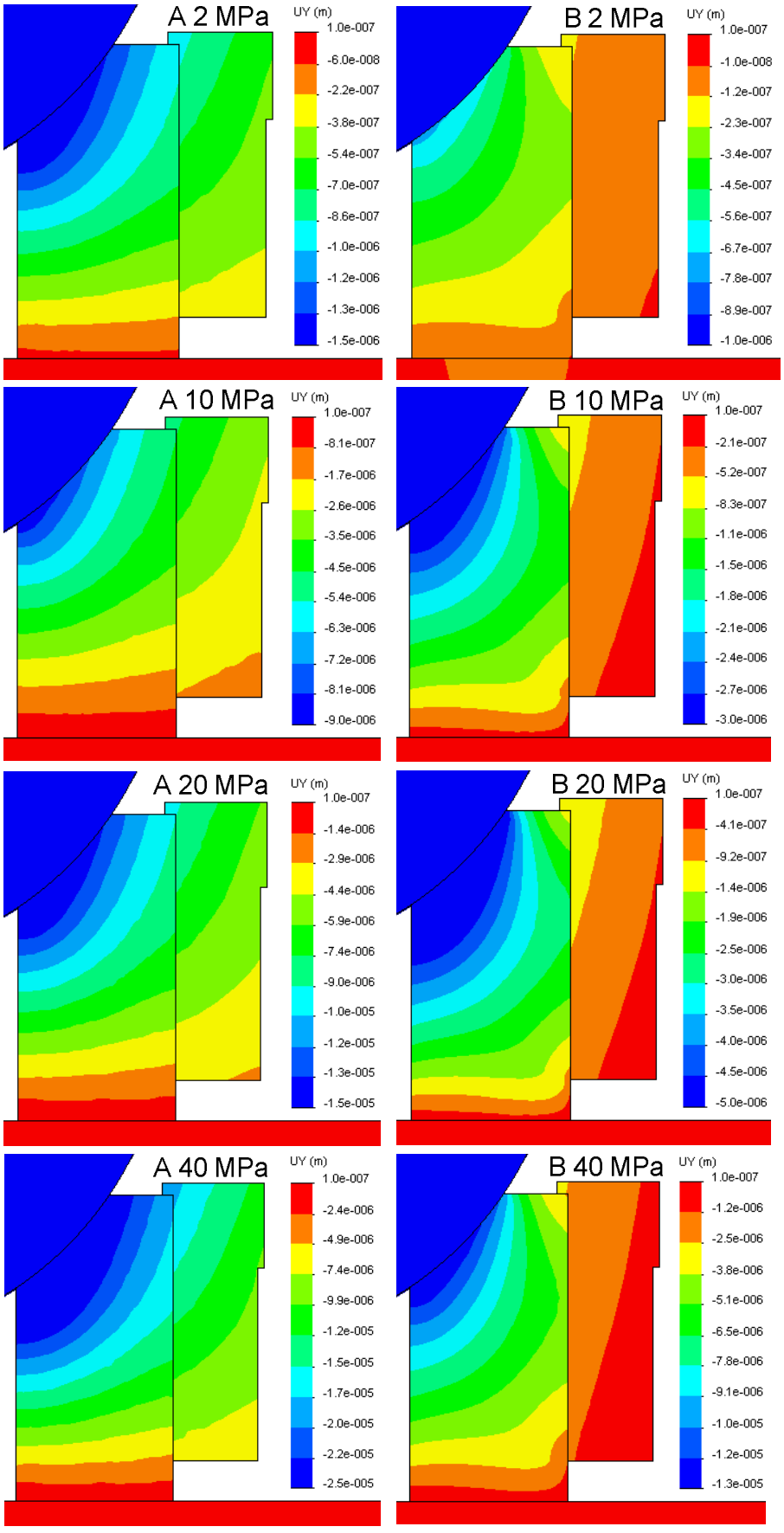

Figure 33. Vertical deformation of slipper A and B at pressure levels of 2, 10, 20 and 40 MPa.

Figure 32 and Figure 33 show the vertical deformations of the slippers and the deformation values of the centre of the slipper cross-section are collected in Table 4.

Pressure	Slipper A	Slipper B	Slipper C	Slipper D	Slipper E
2 MPa	0.54	0.23	2.3	0.27	0.05
10 MPa	2.6	1.2	12	1.3	0.23
20 MPa	5.1	2.5	24	2.6	0.52
40 MPa	9.9	5.1	44	5.6	0.92

Table 4. Vertical deformation [μm] of the different slippers.

The deformations of slipper C are about eight times bigger than in slipper D. The deformations in slipper E, which is made from stainless steel, are five to six times smaller than for slipper D. That is a very big difference, although there is a thick layer of PEEK. The differences between the material properties of stainless steel and PEEK are easy to see. It is very appropriate to use a stainless steel heart in this type of slipper, also with the point of vertical deformations, because the impact is very clear. The same ratio is also found between the overall displacements of the slipper, because vertical displacement has the biggest impact. Figure 32 and Table 4 show that the deformation increases almost linearly when the pressure level rises, which is obvious because the material models are linear elastic. The behaviour is the same with all the slippers.

Figure 33 shows the vertical deformation of slippers A and B. The deformations of slipper A are about twice as big as those of slipper B. The difference between a fully PEEK-made slipper and one with a steel collar is not as big as between slipper C and slipper D. That is because the properties of the PEEK are different and the material of part 1 of the slipper is not so significant as in that type of structure. However, the effect of the steel collar is obvious.

The deformation of slipper D is the same with and without pressure under the sliding surface, as Figure 30 and Figure 32 show. With a different type of slipper structure, such as slipper B, the pressure under the sliding surface changes the behaviour of the slipper. The shape and magnitude of the deformation change, as Figure 31 and Figure 33 show.

If the measured deformations are compared to the slipper calculations with pressure under the sliding surface, the differences in the values of the vertical deformation are shown in Figure 34.

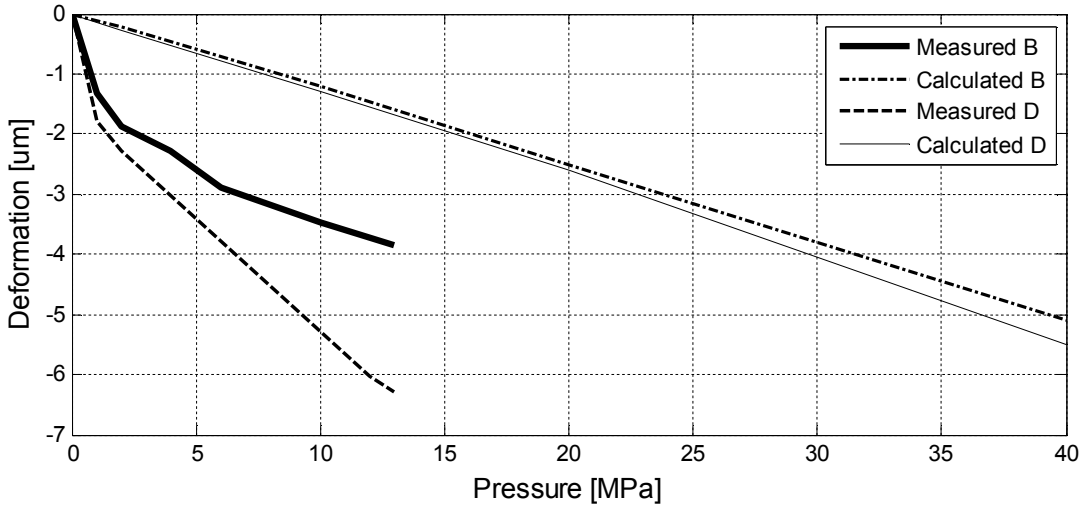

Figure 34. Measured and calculated deformations of slipper B and slipper D as a function of pressure level.

Figure 34 shows that after the low pressure area the slope of the measured deformation curve of slipper B closes up to the slope of the calculated curve. With slipper D the deformation is higher through the whole measuring range. That is notable, because strong deformation after the low pressure area is difficult to explain. However, it could be expected that the slope should close up to the calculated slope. If that does not happen the properties of the PEEK are noticeably different to the datasheet values.

The change of slipper inner radius is studied with all the slippers. At a pressure level of 10 MPa the radius increases 3.1 µm in slipper C made with PEEK 2. The change in slipper D is 0.1 µm and 0.03 µm with slipper E. All in all, the inner radius changes are very small in that type of slipper structure. The deformation of slipper A is 13.1 µm and slipper B is 4.5 µm, which is larger than the deformation of slipper D because of the different kind of structure.

At a pressure level of 40 MPa the radius increases by 49 µm with slipper C made with PEEK 2. The change in slipper D is 6.9 µm and 0.6 µm with slipper E. The deformation of slipper A is 54 µm and in slipper B it is 18 µm, which is larger than the deformation of slipper D because of the different kind of structure. All the changes with 40 MPa, except slippers A and C made totally in PEEK, are so small that deformations do not need to be taken into account during the design process when dimensioning the pocket radius.

5.2 Deformations of sliding surface

Sliding surface deformations are the most interesting part of the deformation study, because the effects are assumed to be significant. Concave deformations change the pressure profile and that increases the hydrostatic balance and load carrying capacity of the slipper. Convex deformation also changes the pressure profile, but that change decreases the hydrostatic balance and load carrying capacity. Both deformation types increase the leakage flow of the slipper, which is shown in [Manring 2002].

Figure 35 shows the deformations of the sliding surface of the slipper D with three different pressure levels.

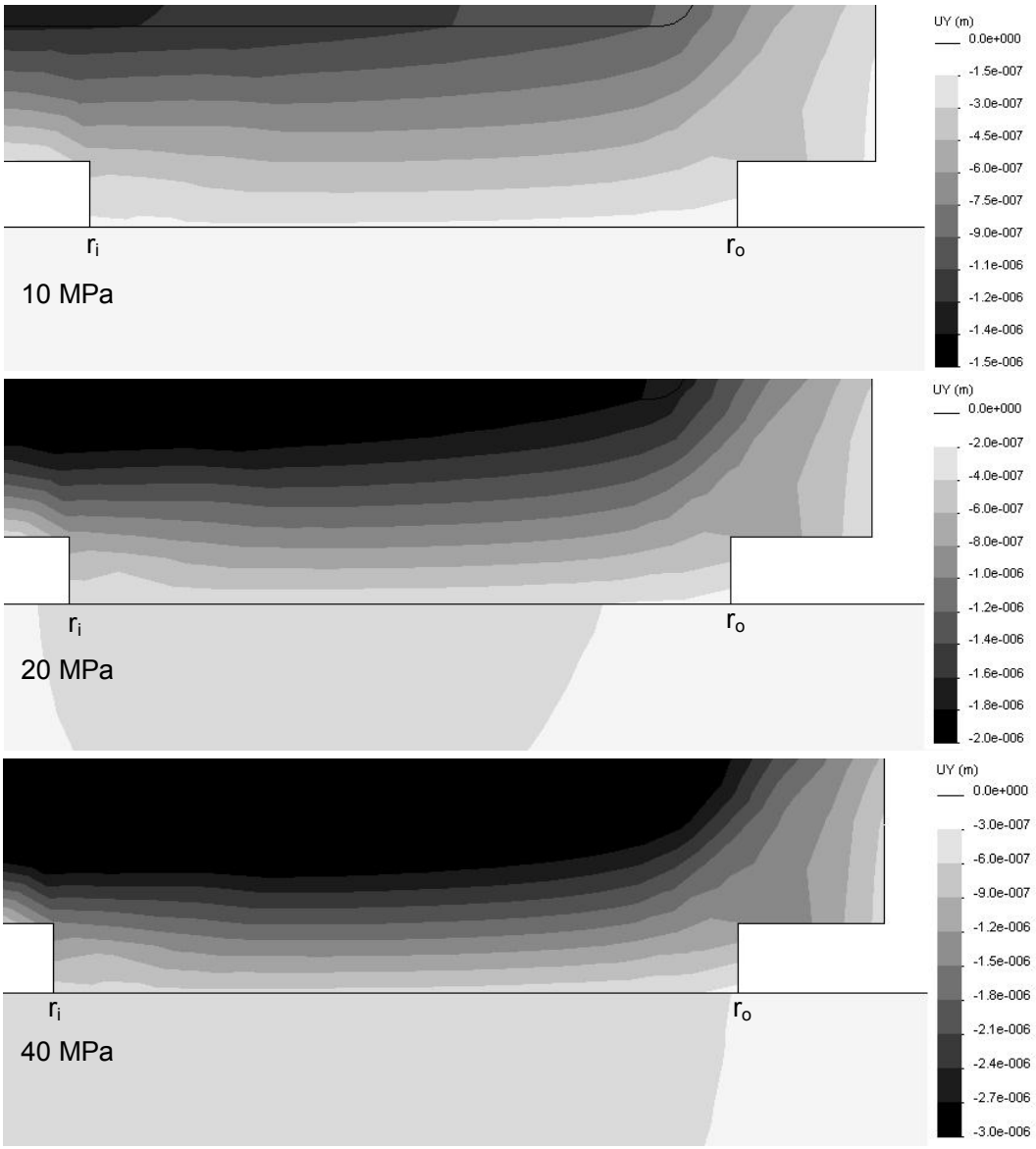

Figure 35. Deformation of the sliding surface of slipper D.

Figure 36 shows the deformations of the sliding surface of slipper B.

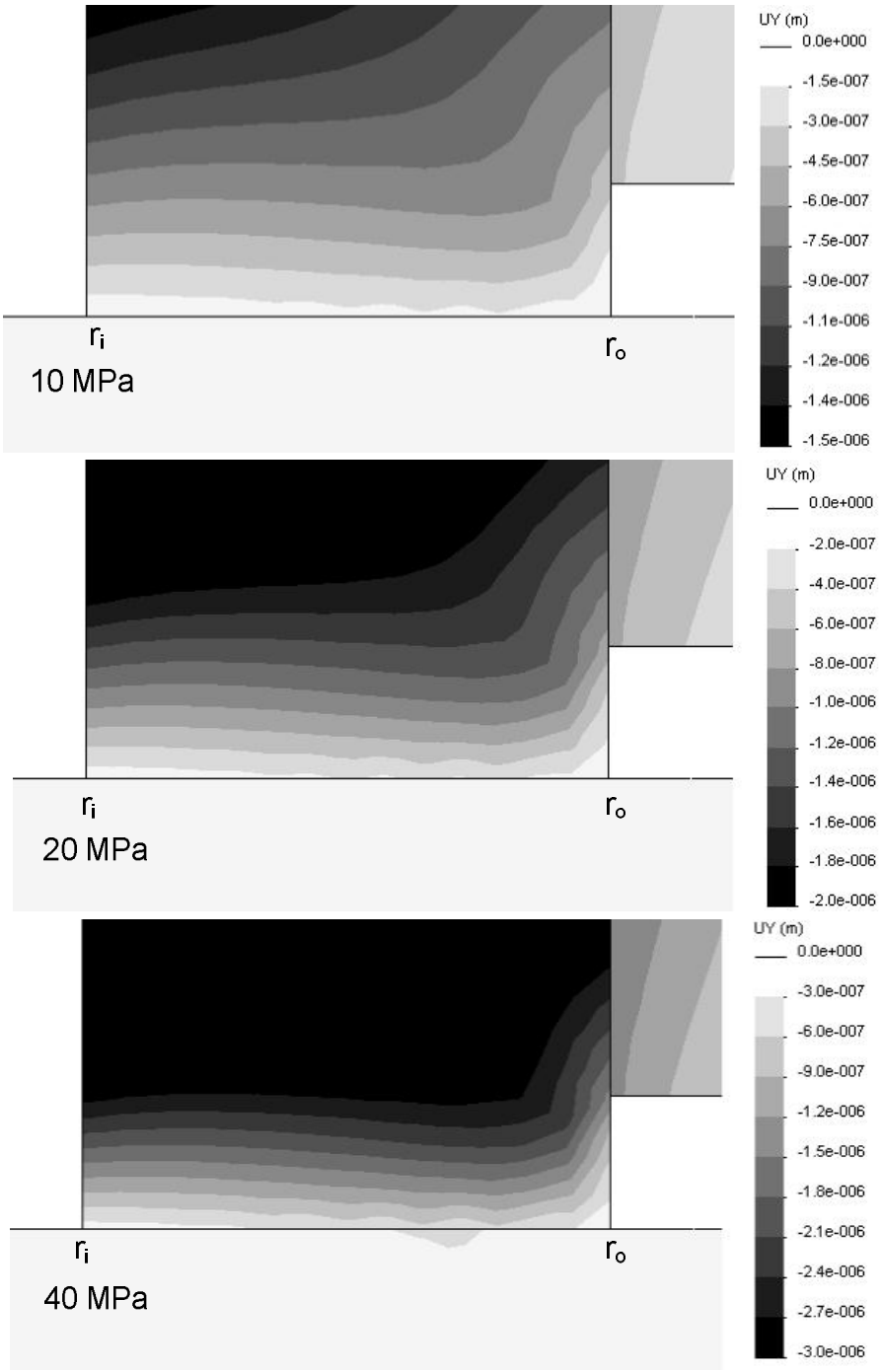

Figure 36. Deformation of the sliding surface of slipper B.

Figure 35 and Figure 36 show that all the displacements of the sliding surface are negative and the deformation is slightly concave with all the calculated pressure levels. Actually, the lowest point of the sliding surface is between the centre point and the outer edge of the sliding surface with slipper B and between the inner edge and the centre point of the sliding surface with slipper D. That means that the deformations are both convex and concave. Concave deformation occurs because of the high pressure in the pocket and under the sliding surface near the inner edge. Convex deformations occur because the pressure pushes the sliding surface outward and the PEEK-part squeezes the area between the steel part and the swashplate.

Absolute deformation is very small, but comparing to the film thickness the slope of the deformation is significant with high pressure levels.

5.3 Stress components in the PEEK-part

Because materials have a maximum stress durability, the stress components of the slipper structures are studied. The stress components of the slippers are calculated with numerical methods. Figure 37 and Figure 38 show the stress components of slipper B. The pressure levels are 20 MPa and 40 MPa.

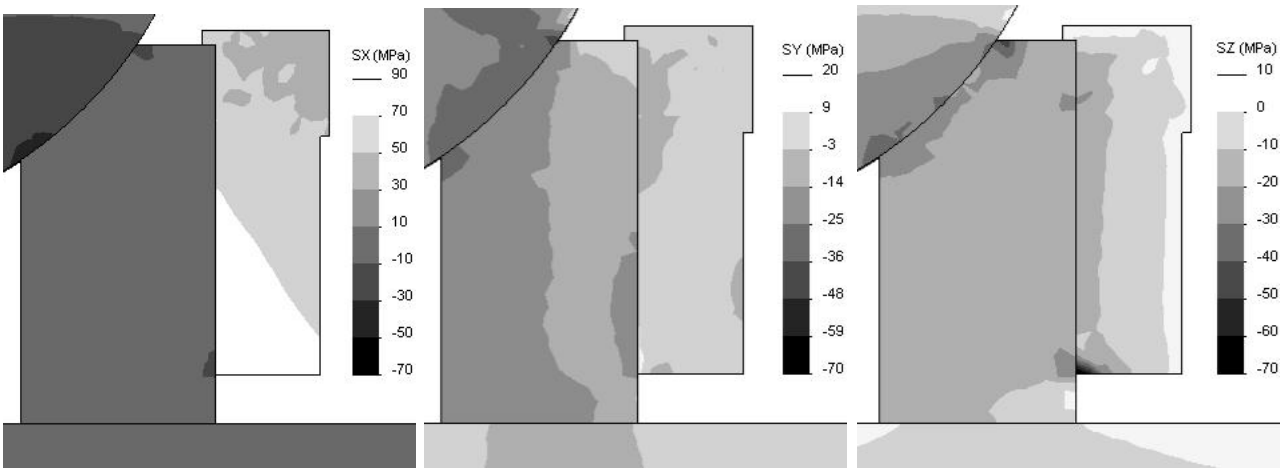

Figure 37. Stress components of slipper B with 20 MPa.

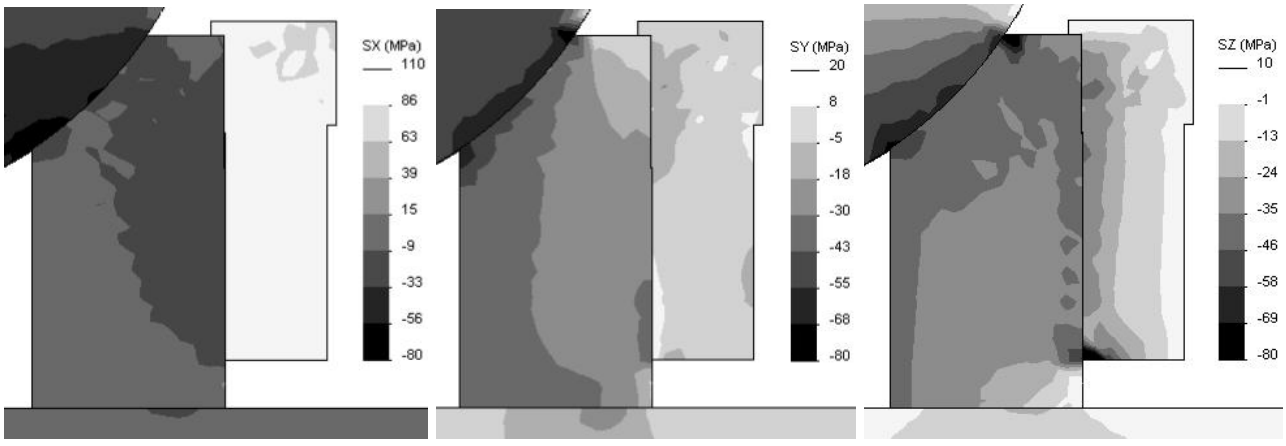

Figure 38. Stress components of slipper B with 40 MPa.

The sign of the value shows the direction of the stress (+ tension / - compression). Figure 37 shows that the PEEK-part is under compression but the steel ring round the PEEK-part is under tension. The maximum compression stresses inside the PEEK-part are about 15 MPa, 60 MPa and 65 MPa (x, y, z) at a pressure level of 20 MPa, as Figure 37 shows. Figure 38 shows that at a pressure level of 40 MPa, the maximum compression stresses inside the PEEK-part are about 30 MPa, 80 MPa and 110 MPa (x, y, z).

The yield strength of PEEK 1 (119 MPa for tension and 152 MPa for compression) is high enough for slipper use with both pressure levels. At a pressure level of 40 MPa the total stress is quite high (under 139 MPa, because the points of the maximum stress components are different) and near to the compression yield

strength. However, compression yield strength is not exceeded and there are only some high stress points in the spherical joint, which makes it possible to use a linear elastic model. Figures show that high stresses are in the contact zone between the piston and slipper. Stress values elsewhere in the slipper are much lower. The maximum contact pressure of the slipper B is about 105 MPa in the spherical joint and 31 MPa between the slipper and swashplate at 40 MPa working pressure.

Figure 39 and Figure 40 show the stress components of slipper D. Pressure levels are 20 MPa and 40 MPa.

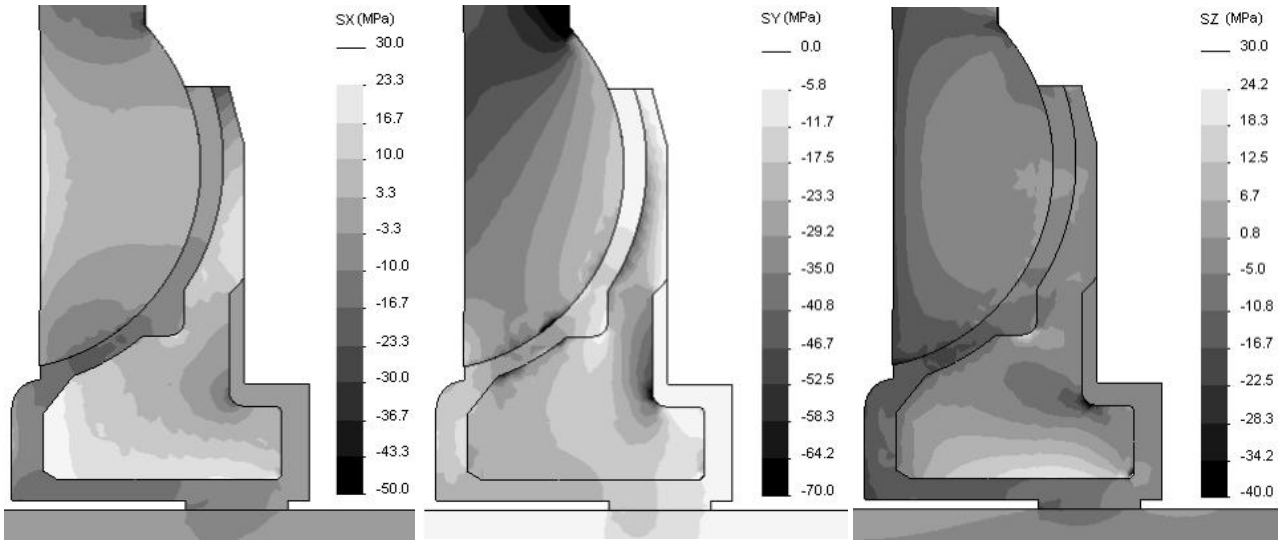

Figure 39. Stress components of slipper D with 20 MPa.

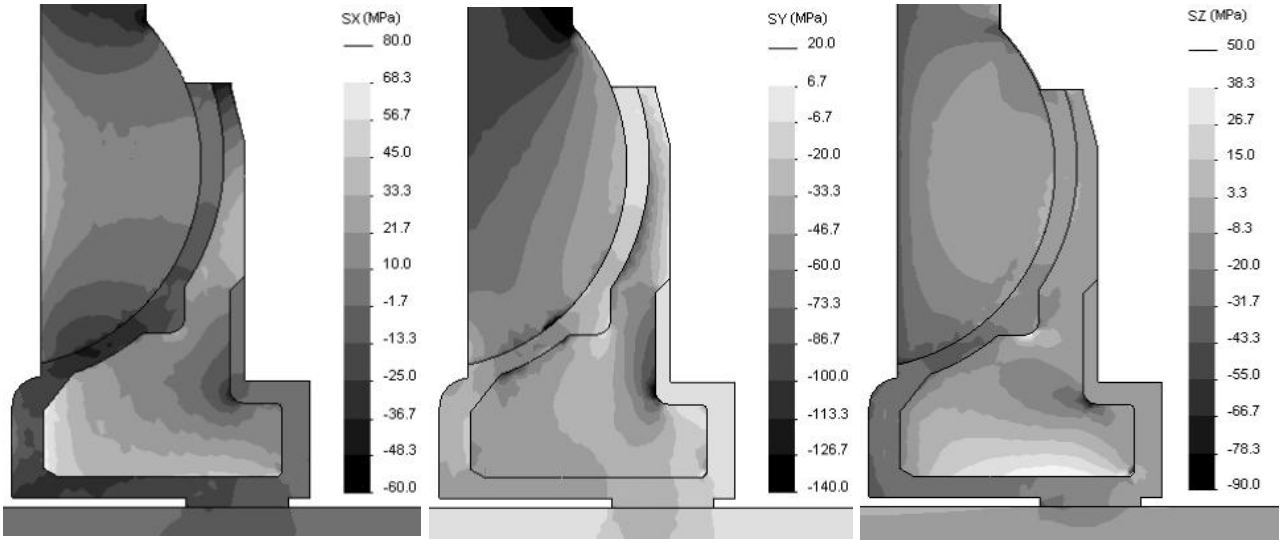

Figure 40. Stress components of slipper D with 40 MPa.

Figure 39 shows that maximum compression stresses inside the PEEK-part are about 20 MPa, 33 MPa and 25 MPa (x, y, z) at a pressure level of 20 MPa. Figure 40 shows that at a pressure level of 40 MPa the maximum compression stresses inside the PEEK-part are about 35 MPa, 73 MPa and 60 MPa (x, y, z). The maximum stresses in x and y directions are in the piston connection and z direction on the inner edge of the sliding surface. The structure of the slipper affects so that there is a big difference in the z direction

stress between slipper B and slipper D. The steel structure of slipper D carries more load in y and z directions than slipper B.

The yield strength of PEEK 2 (97 MPa for tension and 118 MPa for compression) is high enough for slipper use at a pressure level of 20 MPa. At a pressure level of 40 MPa the stresses are quite high, but the total stress (101 MPa) is under the compression yield strength of the material. The maximum contact pressure of slipper D is about 159 MPa in the spherical joint and 44 MPa between the slipper and swashplate at 40 MPa working pressure. The contact pressure at one point of the spherical joint is so high that is not acceptable for PEEK 2 and the spherical joint should be studied further at a pressure level of 40 MPa.

5.4 Pressure profile under sliding surface

It is noted that deformations in the sliding surface are significant in water lubrication. It is possible to find the pressure profile in a situation of real deformation with numeric calculation if fluid dynamics and fluid-structure interaction are taken into account. Ansys Workbench 13.0 software package is used for CFD and FSI calculations. The mechanics are modelled with Ansys Design Modeler and fluid flow can be modelled with Ansys FLUENT or Ansys CFX. Ansys FLUENT and Ansys CFX are computational fluid dynamics (CFD) software packages used to simulate fluid flow problems. Both use the finite volume method to solve the governing equations for a fluid. The method is commonly known and the same method is also used in water hydraulic research to study the characteristics of water hydraulic seat valve structures by Leino [Leino 2008]. Also other research in the hydraulics area is shown, and accurate CFD calculations can give the right results.

In this case 2-way FSI is needed. CFD alone is not enough, because deformations of the slipper sliding surface are the reason for a different pressure profile compared to the basic equations. The idea of the 2-way FSI between CFD and structural analysis is shown in Figure 41.

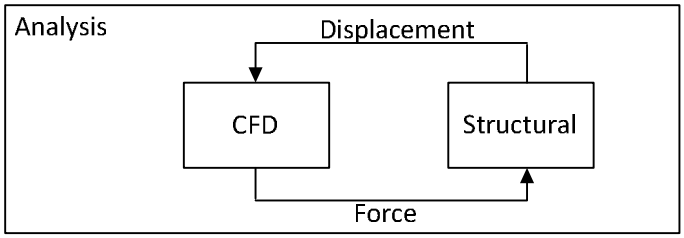

Figure 41. The principle of 2-way fluid-structure interaction.

Fluid-structure interaction analysis is a multiphysics problem, where the interaction between two different analyses is taken into account. In the analysis the results of structural analysis in the mechanical application is transferred to CFD analysis as a displacement. Similarly, the results of the CFD analysis are passed back to the mechanical application as a load. The analysis will continue until overall equilibrium is reached between a mechanical and CFD solution. [Anon 2009]

5.4.1 No deformation case

To verify the CFD environments, the system is first modelled without deformation. In FLUENT the model is modelled in 2D, but the symmetry of the slipper has to be taken into account to obtain the right pressure profile. The CFX fluid model is modelled in 3D with a narrow sector. With a constant gap height the

pressure profile under the sliding surface can be calculated, as shown in Equation 26. That equation and the CFD results with constant gap height are plotted in Figure 42 with the dimensions of slipper A and B.

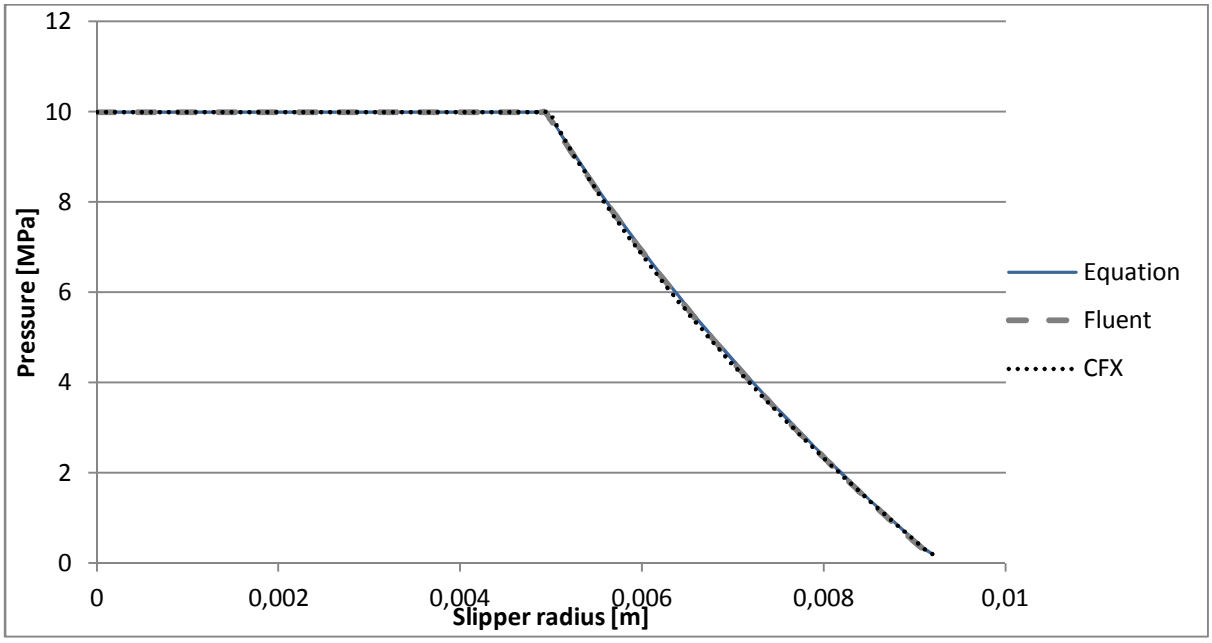

Figure 42. Pressure under the sliding surface according to Equation 26 and with CFD calculations.

Figure 42 shows that the correspondence between analytical and numerical solution is very good. Error between pressure profiles is negligible with both FLUENT and CFX.

Leakage flow with constant gap height can be calculated as Equation 28 shows. With 1.5 µm gap height, the leakage flows are presented in Table 5.

	Equation	FLUENT	CFX
Leakage flow [m^3/s]	2.798e-8	2.822e-8	2.848e-8
Difference [%]	-	0.7	1.8

Table 5. Parallel gap leakage flows of slipper B.

Table 5 shows that the difference between leakage values is only a few percent. That shows that with a basic situation CFD gives the right results. The water properties, dimensions of the slipper and pressures are the same in all cases. In FLUENT gap height is divided on 15 parts to obtain accurate results and in CFX 20 parts are used.

In the real situation the deformations of the slipper have to take into account. The next chapter show the CFD procedure with slippers B and D. CFX is used for CFD, because the two-way interaction between solid and fluid part is easier to implement.

5.4.2 Modelled geometry and calculation mesh

The accuracy of the numerical result depends on the calculation mesh. In the previous case without deformation the pressure is relatively easy to obtain equivalent to the values of the basic theory, but leakage flow is sensitive to the size of the calculation mesh. The size of the calculation volume is made smaller to obtain the leakage flow near the right value. Under the sliding surface the calculation volume is

smaller than in the pressure pocket. In all solutions, inlet and outlet pressure is set as the boundary conditions. Each solution is started by calculating the initial condition, using the outlet pressure as an initial value.

The geometry of the slippers is kept as simple as possible. Part of the pressure pocket, the PEEK part and the whole gap area are modelled. With both slippers, slipper B and slipper D, a 20 degrees sector of the slipper is modelled to allow thicker calculation mesh. 3D quadrilateral solid elements are used for meshing. Figure 43 shows the geometry.

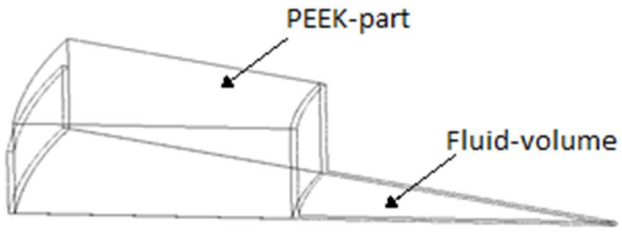

Figure 43. Geometry in the numerical pressure profile calculations.

Because the pressure in the slipper pocket is constant, only a narrow part of the fluid volume near the PEEK-part is modelled, as Figure 43 shows. The same principle is used also at the other end of the gap. The swashplate is modelled as a wall and the upper face and the part of the outer face of the slipper is fixed.

The accuracy of the numerical calculation is dependent on the calculation mesh. The gap between the slipper and swashplate is very narrow, which makes it a challenge to get the mesh accurate enough. The gap area is meshed more accurately than the other parts of fluid volume. Different mesh accuracies are tested and the leakage flows of the slipper are compared. In that way it is decided how accurate enough the mesh needs to be. The PEEK part of the slipper is more sparsely meshed than the fluid volume. Detailed parameters of the CFX calculation are shown in Appendix A.

5.4.3 Properties of the deformed sliding surface

The pressure profile under the sliding surface is calculated at pressure levels of 2.5, 5, 10, 20, 30 and 40 MPa. The changes in the pressure profile occur because of the deformation of the PEEK-made sliding surface. An example of the result of the FSI calculation is shown in Figure 44.

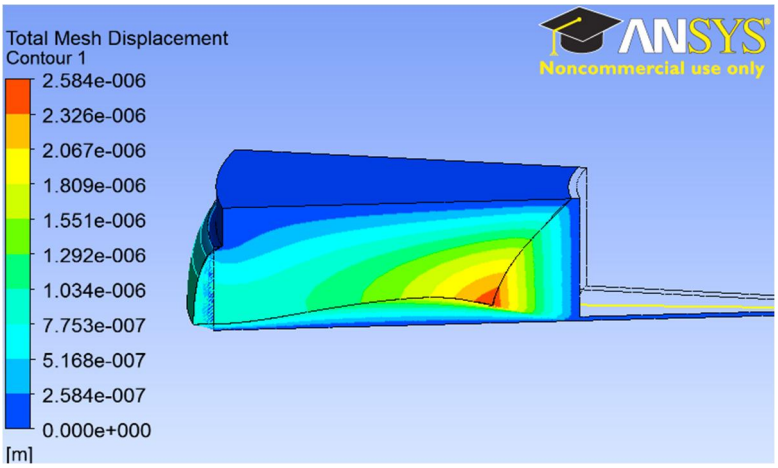

Figure 44. Slipper total mesh displacement at a pressure level of 20 MPa in FSI calculation. Magnified deformation view.

Figure 44 shows a magnified view of the slipper total deformation. The deformation is highest on the inner edge of the sliding surface. It is easy to notice that the deformation is neither convex nor concave and it is not possible to assume a constant gap height.

Figure 45 shows the pressure profile under the sliding surface of slipper B with different pressure levels.

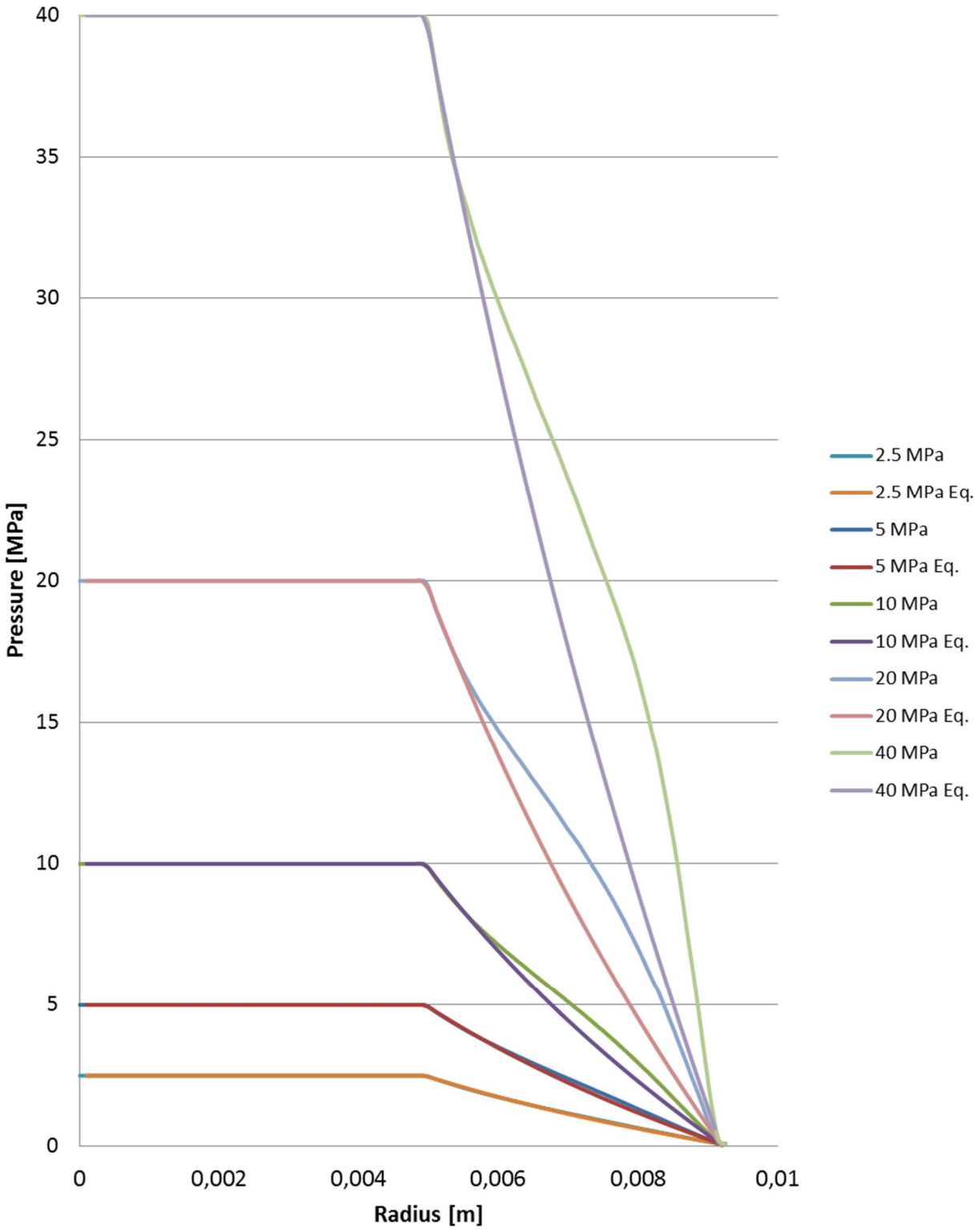

Figure 45. Pressure profile under the sliding surface of slipper B at pressure levels of 2.5, 5, 10, 20, 30 and 40 MPa with gap height of 1 µm. Also the pressure profile with basic equations is presented.

Figure 45 shows that the pressure profiles change at all pressure levels. The shape of the curves is similar; near the inner edge the pressure profile acts like the basic equation assumes and the difference is biggest after the centre point of the sliding surface. 1 μm gap height is used as an example because measured gap height changes during swashplate turning and the references [Li 1991] and [Donders 1997] show that 1 μm gap height is realistic. The difference between basic equation and CFD-based pressure profile rises when the pressure level rises. That can be seen also in Figure 46.

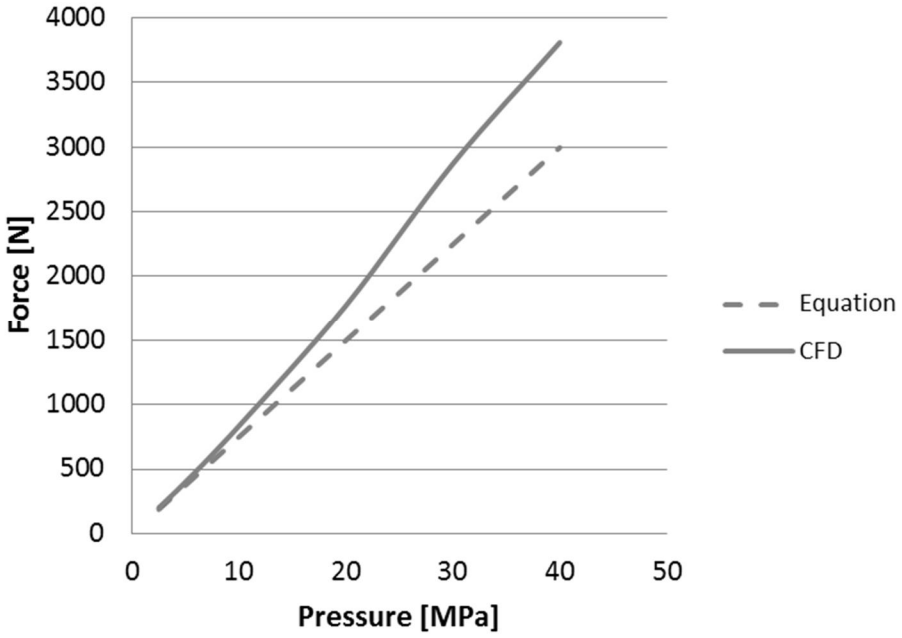

Figure 46. Force of slipper B sliding surface with and without deformation.

Figure 46 shows that at a pressure level of 10 MPa, slipper B sliding surface force is 11.4 % bigger than the basic equation assumes. The difference rises, as Figure 46 shows, and at a pressure level of 40 MPa the difference is 27.1 %.

A polynomial curve can be fitted on the pressure curves. These polynomial curves are used in the simulation model. The force of the sliding surface determines when the curve is integrated from the inner radius to the outer radius. The results are the same as those from the CFD-calculations. An example is shown in Chapter 6.1.

Leakage flow as a function of the pressure level is the other interesting feature derived from the pressure profiles. The shape of the leakage curve from CFD results is second order polynomial, but the difference from the basic equation curve is huge. Figure 47 shows how the leakage increases compared to the basic equation results as a function of pressure level. The calculation points are 2.5, 5, 10, 20, 30 and 40 MPa.

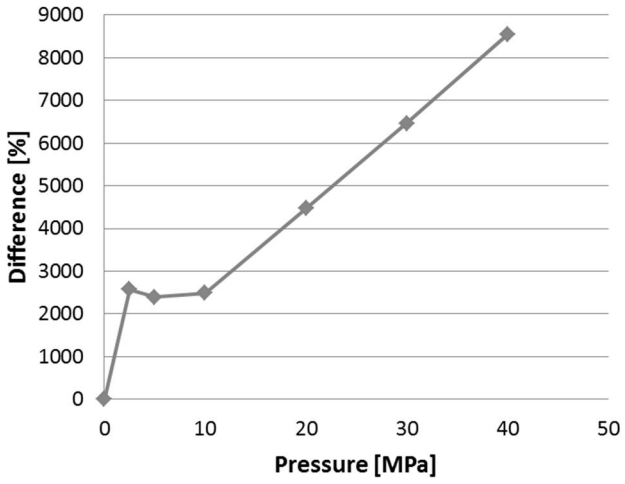

Figure 47. Percentual difference of leakage between basic equation and FSI calculation with 1 μm gap height.

Figure 47 show that the bigger the pressure level is, the higher is the difference between the basic equation and the numerical solution. At a pressure level of 40 MPa the error of the basic equation is almost 9000 %. This means that the leakage is ninety times bigger than the basic equation expected. It should be noticed that the gap height is self-adjusting, so the FSI calculation results, which assume that the gap height is 1 μm plus the effect of the deformation, are too high. Ninety times bigger leakage values is same than leakage trough parallel gap height of 4.7 μm. The difference is quite linear from 10 MPa to 40 MPa. It was also revealed that the bigger the gap height is, the smaller is the percentual difference between numerical and basic equation solution. That is quite obvious because with bigger gap height deformations are relatively smaller. Compared to the measurement results at 10 MPa, the leakage from FSI calculation is still lower than measured one. That is because in the measurements slipper and swashplate are not parallel as in FSI calculations.

The previous figures are for 1 μm gap height. The following two figures show what happens if the gap height is not constant. Figure 48 shows how the force of the slipper sliding surface acts as a function of the gap height.

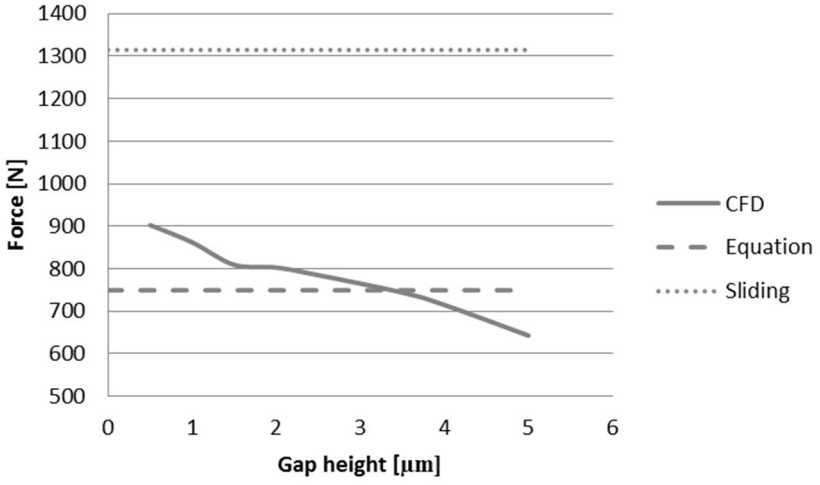

Figure 48. Slipper sliding surface force as a function of gap height at a pressure level of 10 MPa.

As Equation 26 shows, the force is not gap height dependent. However, if the deformations are taken into account, force is not constant, as Figure 48 shows. With realistic gap heights the force is higher than the basic equation expected. Figure 48 also shows that in case of slipper B the load of the sliding surface at a pressure level of 10 MPa.

Figure 49 shows the slipper leakage flow with basic equation and FSI calculation with deformation.

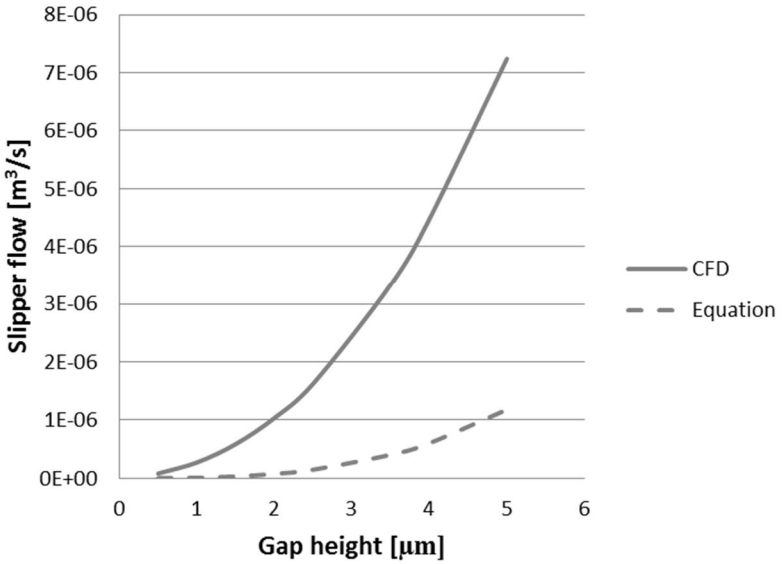

Figure 49. Slipper leakage as a function of gap height according to Equation 28 and CFD-calculations at a pressure level of 10 MPa.

Figure 49 shows that the absolute difference between the CFD-calculations with deformation and the basic equation (Equation 28) become remarkable when the gap height increases. However the percentual difference is biggest with small gap heights. Deformations change the pressure profile and the leakage flow increases.

To compare the results between FEM and FSI calculations, a change of inner radius is shown in Figure 50.

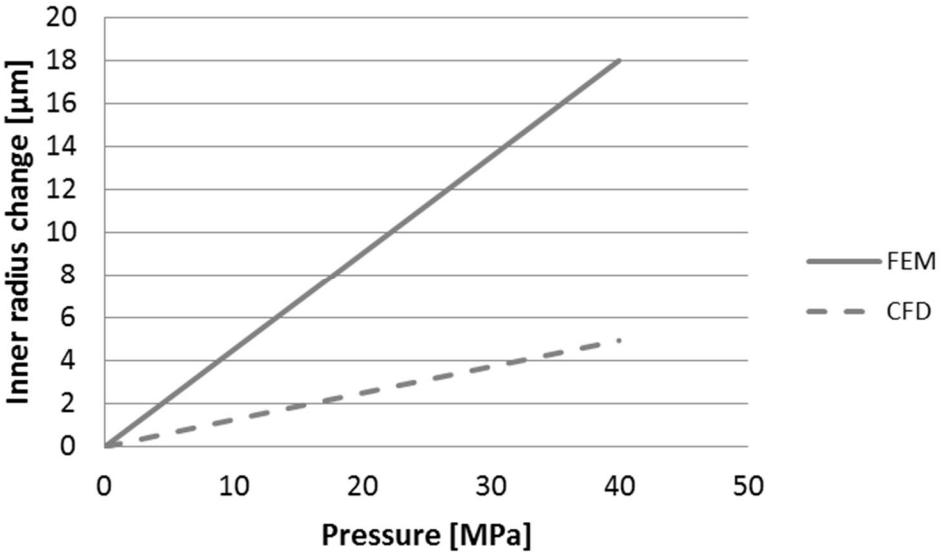

Figure 50. Change of slipper inner radius with and without FSI calculation.

Figure 50 shows that FEM gives too high deformation values. To take the fluid-structure interaction into account the inner radius change is smaller, about one fourth at a pressure level of 40 MPa. That is because of the different kind of deformation of the sliding surface.

Figure 51 shows the pressure profile under the sliding surface of slipper D with different pressure levels.

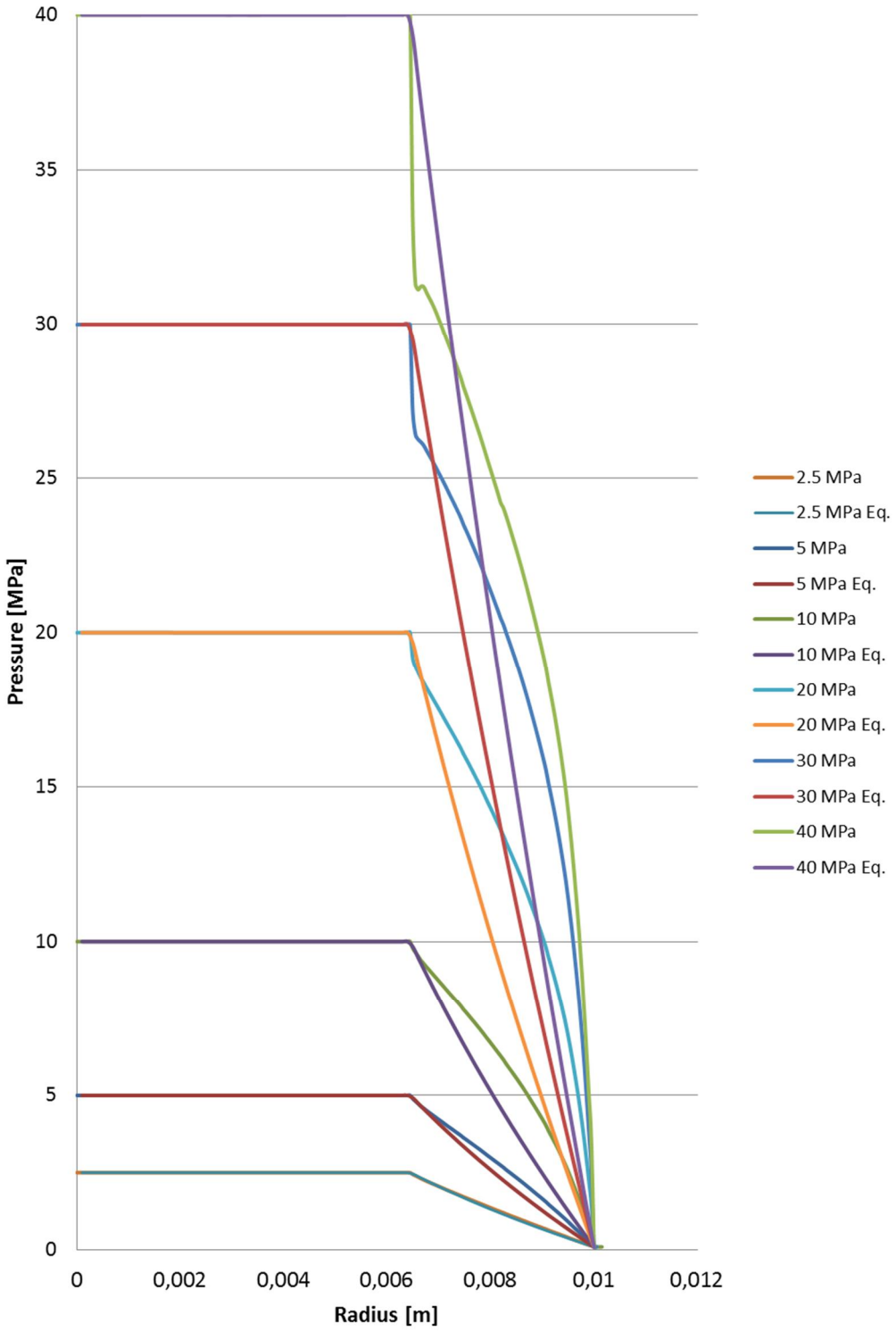

Figure 51. Pressure profile under the sliding surface of slipper D at pressure levels of 2.5, 5, 10, 20, 30 and 40 MPa with gap height of 1 µm. Also the pressure profile with basic equations is presented.

Figure 51 shows that the pressure profile of slipper D changes more when the pressure level rises. To compare Figure 45 and Figure 51, it is obvious that slipper structure and the different PEEK properties change the pressure profile. With slipper D the change near the inner edge of the sliding surface is totally different than with slipper B at a high pressure level. Pressure goes down very fast because the inner edge of the sliding surface bends downward and makes an orifice. That happened already at a pressure level of 20 MPa. In spite of the collapse, the force is much higher than the basic equation expected, because pressure is higher in all the area after that.

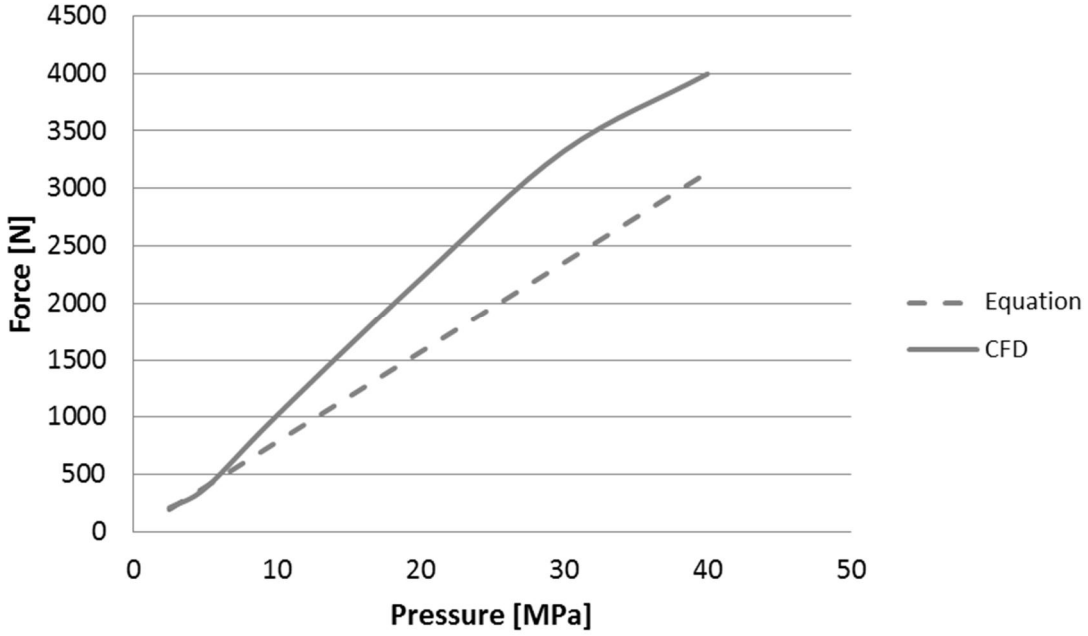

Figure 52. Force of slipper D sliding surface with and without deformation.

Figure 52 shows that at a pressure level of 10 MPa, the sliding surface force of slipper D is 29.4 % bigger than the basic equation assumes. The difference rises, as Figure 52 shows, and at a pressure level of 30 MPa the difference is 41.2 %. At pressure levels over 30 MPa the pressure profile goes down strongly at the inner edge of the sliding surface and the percentual change reduces. At a pressure level of 40 MPa the precentual difference is 27.3 %.

According to the FSI calculation, the leakage flow of slipper D is significantly higher when the deformations are taken into account. The shape of the curve is similar to that with slipper B. The percentual difference is almost constant at pressure levels between 2.5 MPa and 10 MPa. Between 10 MPa and 40 MPa the percentual difference rises. The magnitude of the difference is about three times higher than with slipper B at all pressure levels.

It is an interesting question as to how big the role of the material is. The PEEK materials of the slippers are reversed and the results are shown in Figure 53 and Figure 54.

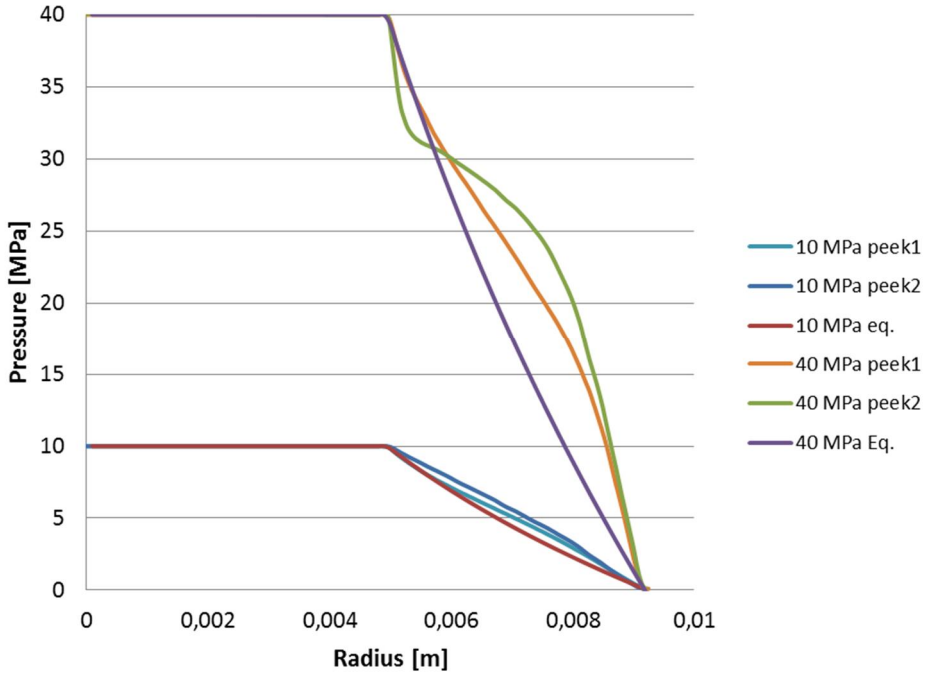

Figure 53. Impact of the material for the pressure profile of slipper B at pressure levels of 10 MPa and 40 MPa.

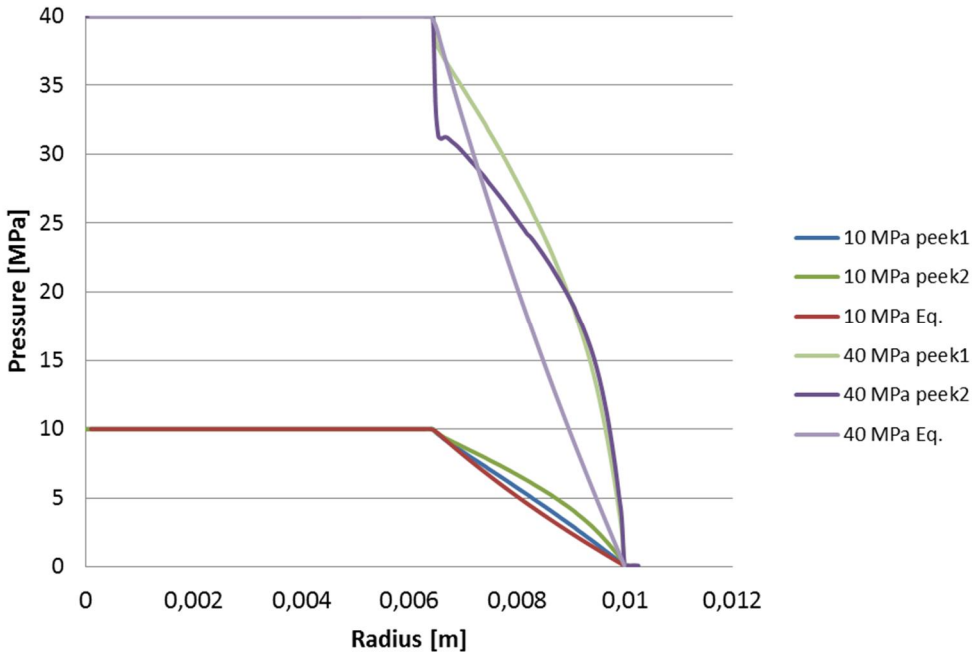

Figure 54. Impact of the material for the pressure profile of slipper D at pressure levels of 10 MPa and 40 MPa.

Figure 53 and Figure 54 show that the deformations of PEEK 2 are higher in both cases. With slipper B, the sliding surface force increases remarkably with PEEK 2 at a pressure level of 10 MPa. The sliding surface force is 902.2 N with PEEK 2 and 835.1 N with PEEK 1, and without deformation the force is 749.3 N. At a pressure level of 40 MPa the deformations are so big that the results of the FSI calculation are not even

reliable. Also with slipper D, the deformations with PEEK 1 are smaller and the behavior is more stable at both pressure levels.

5.5 Discussion

It is has been noticed and shown in numerical calculations that deformations are very important to take into account. That also confirmed the observation that pressure level affects a lot for the measurement results of the gap height because of slipper deformations. Most significant are the deformations of the sliding surface, because the pressure profile and hydrostatic balance will change. If the slipper is designed near to the limit, the slipper can lift from swashplate. On the other hand, too safe design causes low hydrostatic balance and high PV-rate of the slipper. There are some structural possibilities to try to avoid deformations. Manufacturers have used stainless steel inside or around the slipper. That makes the slipper remarkably stiffer than a fully PEEK-made slipper, as shown in Figure 32 and Figure 33.

Figure 32 shows that the vertical deformations in slipper C, which is totally PEEK-made, are about eight times bigger in the centre of the slipper cross-section than in slipper D. Deformations in slipper E, which is made from stainless steel, are about five times smaller than for slipper D. That is a very high difference, although there is only a thick layer of PEEK. Figure 33 shows the vertical deformation of slippers A and B. The vertical deformation of slipper A is about twice as big as the deformation of slipper B. The difference between a fully PEEK-made slipper and slipper with steel collar is not as big as between slippers C and D. That is because the properties of the PEEK and the structure of the slipper are different. In both cases the differences between properties of the stainless steel and PEEK are easy to see.

The deformation of the inner radius of slipper B is larger than the deformation of the inner radius of slipper D because of the different kind of structure. When fluid-structure interaction is taken into account the inner radius changes are smaller than FEM calculations show. This shows that a more accurate examination changes the results significantly. For the studied structures the changes at a pressure level of 40 MPa are so small that deformations do not need to be taken into account during the design process when dimensioning the pressure pocket radius.

Stress analysis shows that in both slippers the stress components in the sliding surface are acceptable also at a pressure level of 40 MPa. In slipper B compressive yield strength is not exceeded, but in the spherical joint of slipper D the contact pressure is too high. All in all, the spherical joint is the structure that should be scaled up to achieve higher pressure levels.

Sliding surface deformations are one of the key factors in pump design. The deformations are so big that the pressure profiles are totally different from those expected from the basic equations. The leakage flow is also different from that expected. The difference of the force of the sliding surface between the basic equation and FSI calculation rises when the pressure level rises. For example, with slipper B the sliding surface force is 11.4 % higher at a pressure level of 10 MPa, and 27.1 % higher at a pressure level of 40 MPa than was expected from the basic equation.

Nowadays, power loss is one significant basis for deciding the size of the slipper. However, the optimum ratio is calculated based on the basic equations, which give the wrong results. Because the pressure profile is different with different pressure levels, the slipper does not work in the best possible way in all situations. The sizing of the slipper is a compromise. Instead of optimum power loss, the slipper should be designed according to the maximum load of the slipper, so that deformations are taken into account. The

outer radius of the slipper should be made bigger, because in that way the PV-rate and the leakage decrease and the maximum load capability increases.

The material properties are most important in handling deformations because the difference between materials is remarkable. Both slipper types are possible to use at a high pressure level if the material is chosen carefully. Deformations of the material are difficult to avoid with a structural solution because usually the PEEK layer should be thick enough. It should be noticed that the structure can limit the material selection because of, for example, the manufacturing process.

It has been shown that FSI calculations are necessary to make the right decisions in slipper design. However, it is not necessary to calculate all the different situations because the behaviour of the slipper is logical. Slipper behaviour can be predicted accurately enough with the simulation model. This is studied in the next chapter.

6 SLIPPER ANALYSIS WITH SIMULATION MODEL

Theory, numerical analysis and measurement are connected in this chapter. The connection is made via a semi-empirical simulation model of the piston-slipper assembly. The basic idea of the simulation model is shown in Figure 55.

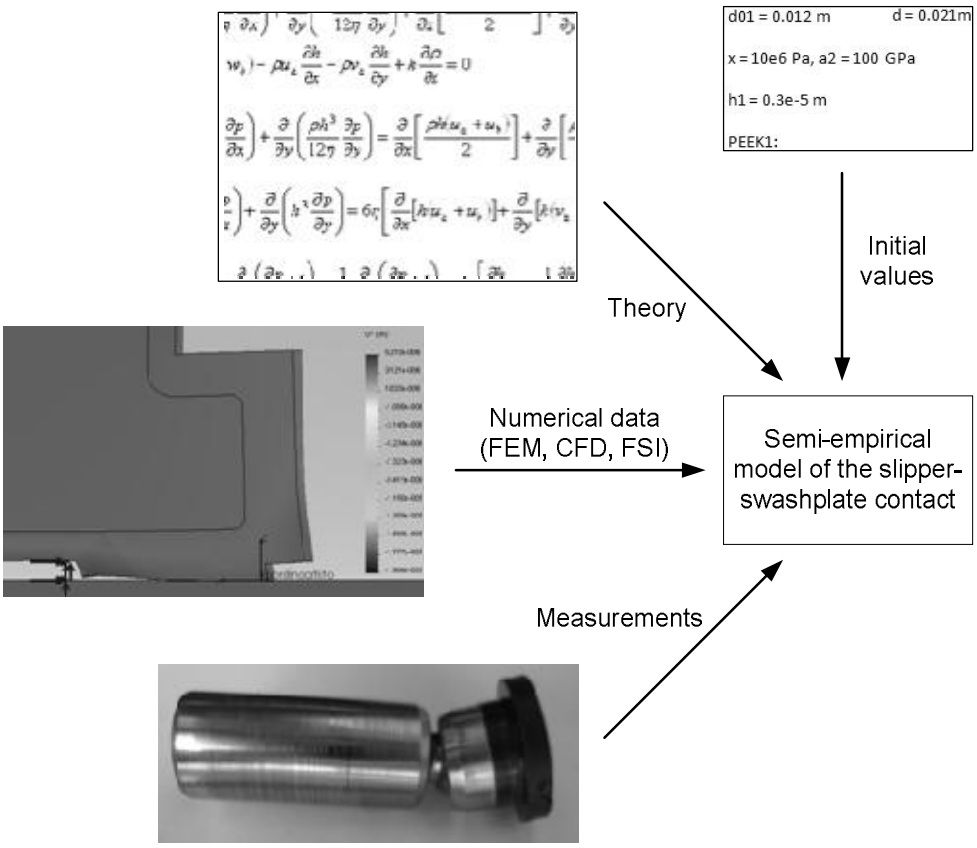

Figure 55. Inputs of the simulation model.

The one piston simulation model was built to investigate the parameters, situations and dimensions which are not, or cannot be, measured. The main focus is to take the elastic deformations into account in the calculation of the slipper properties. The result is a semi-empirical model which could be used to predict slipper behaviour in the water hydraulic axial piston pump. However, only one part of the pump, the piston-slipper assembly with swashplate contact, is modelled. There were some assumptions made when building the model.

- Constant pressure or the ideal pressure cycle is used.
- The properties of the materials are constant.
- The water properties are constant.
- The rotation speed of the swashplate is constant, 1500 rpm.
- Only the dimensions of the sliding surface and piston diameter can be changed.

- The slipper hold-down device is not taken into account.
- Friction on the spherical joint is negligible.
- The piston and slipper does not rotate on its own axis.
- The model works properly with only two types of slippers.

6.1 Semi-empirical simulation model of the slipper behaviour

There are constant parameters in the simulation model. The material and water properties and the rotation speed are given as initial values to the model. Also the piston and slipper dimensions are constant except for the sliding surface deformations, including the slipper inner and outer radius.

The key element of the simulation model of the slipper behaviour is the deformation of the sliding surface. Deformation is defined in the FSI calculations. The FSI also give the pressure profile under the sliding surface, which is used as an input of the simulation model. With a new pressure profile, the basic equations, shown in Chapter 3, can be modified to obtain more realistic results.

The simulation model is divided into several logical blocks. The structure of the simulation model is shown in Figure 56.

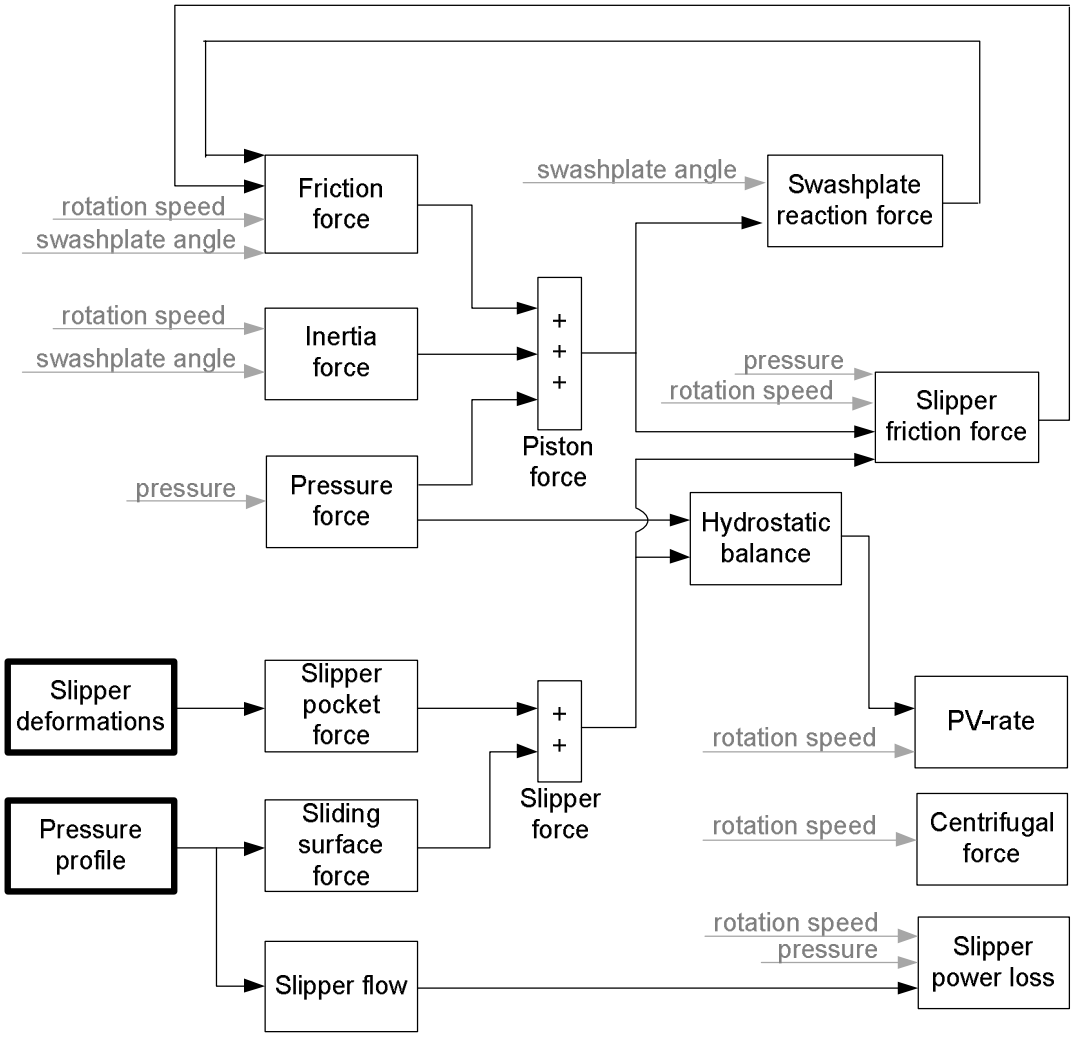

Figure 56. Structure of the simulation model. Grey arrows describe the operating parameters of the pump. The bolded boxes are inputs from the fluid-structure interaction calculations.

The piston force consists of three different forces, as Figure 56 shows. The pressure force is calculated according to the basic equation, Equation 2. The inertia force of the piston-slipper assembly can be defined with the mass of the parts and the acceleration of the assembly, as Equation 42 shows. The acceleration of the piston-slipper assembly can be calculated with the rotation speed of the swashplate and with the swashplate angle.

$$F_{inertia} = -(m_{piston} + m_{slipper})a \tag{42}$$

The friction force between the piston and cylinder is calculated with the help of the force perpendicular to the piston axis. The perpendicular force to the piston axis consists of the centrifugal force of the piston, the force from the swashplate and force from the slipper friction. To obtain the friction force the resultant force is multiplied with the friction coefficient. Most of the runs are made with zero angle, which means that the velocity and the friction force is zero.

The slipper force consists of two forces, as Figure 56 shows. The slipper pocket force is basically calculated with the pocket area and pocket pressure. In this simulation model the inner radius of the sliding surface is not a constant. Inner radius is defined as a function of the pressure level into the slipper pocket, as Equation 43 shows.

$$F_{slipper} = (K(p_{slipper})r_i)^2 \pi p_{slipper} \tag{43}$$

Gain K is from numerical calculation and it is different for different types of slippers.

Slipper deformations which are the input of the semi-empirical simulation model are defined in the FSI calculations. Deformation data is fed to the model with look-up tables. Figure 57 shows the curves based on the deformation data.

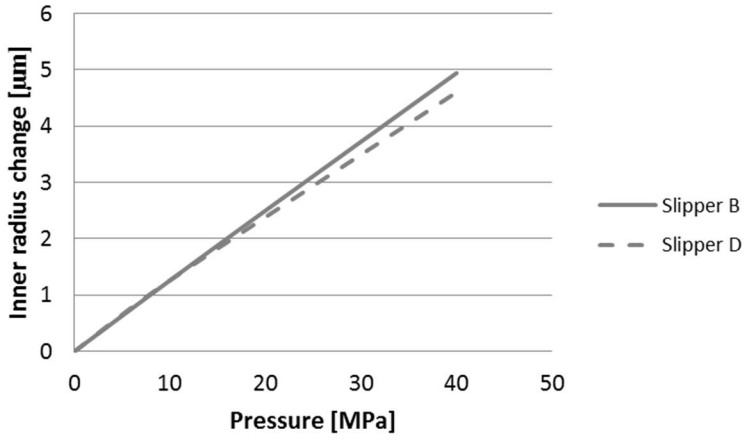

Figure 57. Change of the inner radius of slipper B and slipper D when the pocket pressure changes from 0 to 40 MPa.

Figure 57 shows that the inner radius changes are quite linear. All in all, changes are very small and the change of the inner radius is not important to take into account. As an example, the change of the pocket force of slipper B at a pressure level of 40 MPa is 6.1 N (3079.1 N -> 3085.2 N).

The slipper sliding surface force consists of hydrostatic and hydrodynamic force. Also the force caused by the contact between slipper and swashplate surfaces can be included. In this model only hydrostatic force is implemented. Hydrostatic force from the sliding surface can be calculated if the pressure profile under the sliding surface is known. With parallel plates the analytical solution is shown in Equations 22 to 26 and Equations 3 to 8. However, the assumption that the film thickness is the same in any radial position is not true. Chapter 3.7 shows that with slipper deformations the equations to solve pressure profile are very complex and a numerical solution is needed. The pressure profile under the sliding surface is calculated in CFD and it is one of the inputs of the simulation model. The pressure equations are shown in Chapter 5.4.3. Because the force is the desired quantity, the pressure profile multiplied with one rotation is integrated over the sliding surface, as Equation 44 shows.

$$F_{sealing} = \int_{r_i}^{r_o} p(r) 2\pi r \, dr \tag{44}$$

For example, integrating third order polynomial to describe pressure profile in slipper B at a pressure level of 10 MPa is shown in Figure 45.

$$F_{sealing} = \int_{0.00495}^{0.009175} (-68754851321004x^3 + 1450349941254.1x^2 - 12232745549.22x + 43205584)\, 2\pi x \, dx = 835.535N \tag{45}$$

The result of Equation 45 is the same as that given by CFD calculation. Because the pressure profile is different for each slipper and pressure level, all the integrated values are fed to the simulation model. The right value is chosen according to the initialization of the simulation model.

It is possible to obtain the slipper leakage flow by integrating velocity profile. However, the leakage flow can be obtained straight from the CFX and those values are used in the simulation model.

Hydrostatic balance from the new pressure profile can be derived in the same way as a ratio as in Equation 10. Piston force is now calculated in exactly the same way, but the slipper force is defined as shown in Equation 43 and Equation 44.

The friction between the slipper and swashplate are modeled in both the ways shown in Equation 12 and Equation 13. In the model it is possible to choose which friction equation is used. However, Equation 13 is used because the use of Equation 12 does not offer any additional value in this study. It is quite simple to obtain friction force near the truth because it can be verified with the measurement results. The friction coefficient in the simulation model is defined as 0.04. The friction measurements, shown in Figure 26, and also the PV-rate measurements in 27, show that with 1500 rpm (6.3 m/s) friction the coefficient is very low. Also the sources, for example [Terävä 1995], show that the friction coefficient value 0.04 is at the right magnitude.

The PV-rate is calculated in the simulation model as Equation 29 shows, but of course the hydrostatic balanced force is taken into account. The pressure profile under the sliding surface, the deformations and realistic piston forces are taken into account in the force calculation. The whole slipper sliding surface area is used, although the edges of the area are deformed. Changes at the inner and outer radius of the sliding surface are included in the PV-rate calculations.

The swashplate reaction is calculated by the force on the piston axis and the swashplate angle, as shown in Equation 11. In this model swashplate reaction force is used to calculate the friction force between piston and cylinder. On a bigger scale the swashplate reaction force is important in pump design. The centrifugal force of the slipper and the slipper power loss are also calculated in the simulation model.

The simulation model is based on the measurements, the results of the FSI and well known constant parameters, which make the results of the simulation model reliable in this specific case. Verification of the data is already made in the FSI calculations. A semi-empirical simulation model of the slipper behaviour is realized with Matlab/Simulink software. The parameters of the simulation model are shown in Appendix B and an overview of the Simulink model in Appendix C.

6.2 Effect of pressure level on the slipper behaviour

The pressure level of the system affects the slipper behaviour because deformation occurs. In the simulation model the pressure level changes can be simulated based on the data from FSI calculations. Figure 58 shows the hydrostatic balance of slipper B.

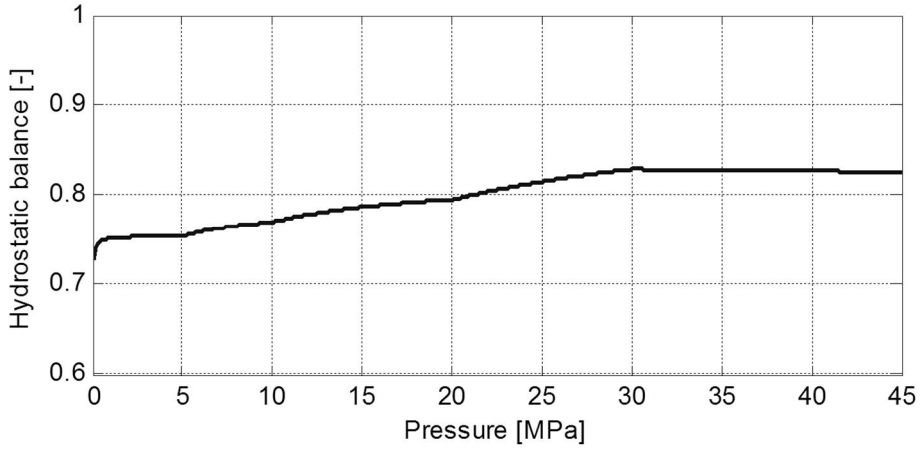

Figure 58. Hydrostatic balance of slipper B with swashplate at zero angle.

Figure 58 shows that the hydrostatic balance of slipper B increases as a function of the pressure level. In theory that helps to achieve the higher pressure levels because the bigger part of the force is compensated when the pressure rises. However, the change should be well known in the design process because the hydrostatic balance cannot be too high. In the case of slipper B, the pressure profile changes are acceptable and the maximum value of the hydrostatic balance is 0.83. Even a higher hydrostatic balance is acceptable, because that would help with the PV-rate, which rises quite high, as Figure 59 shows.

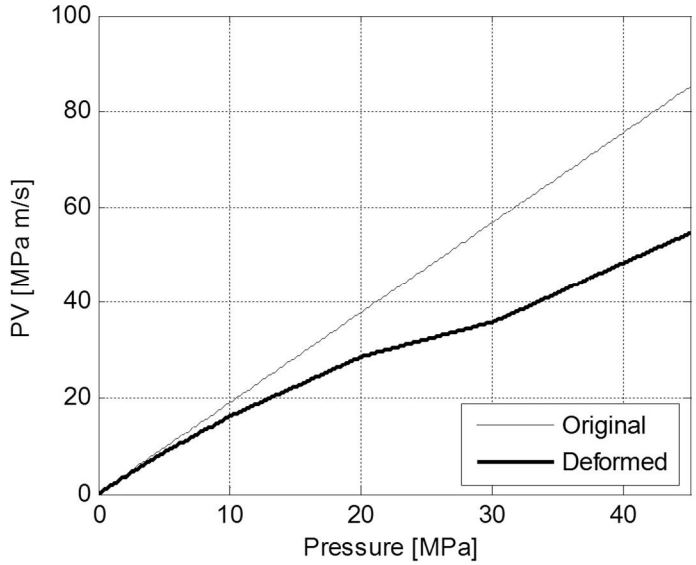

Figure 59. Pv-rate of the slipper B with zero angle of the swashplate.

Figure 59 shows how the PV-rate of the slippers changes. Deformations increase the lifting force, which causes the PV-rate of the slipper to be lower than the basic theory assumes. Equation 29 shows that if the pressure level is doubled, so also the PV-rate is doubled, which is the original curve in Figure 59. In any case, the PV-rate values are much higher than the maximum value of the PEEK 1.

Figure 60 and Figure 61 show the hydrostatic balance and the PV-rate of slipper D.

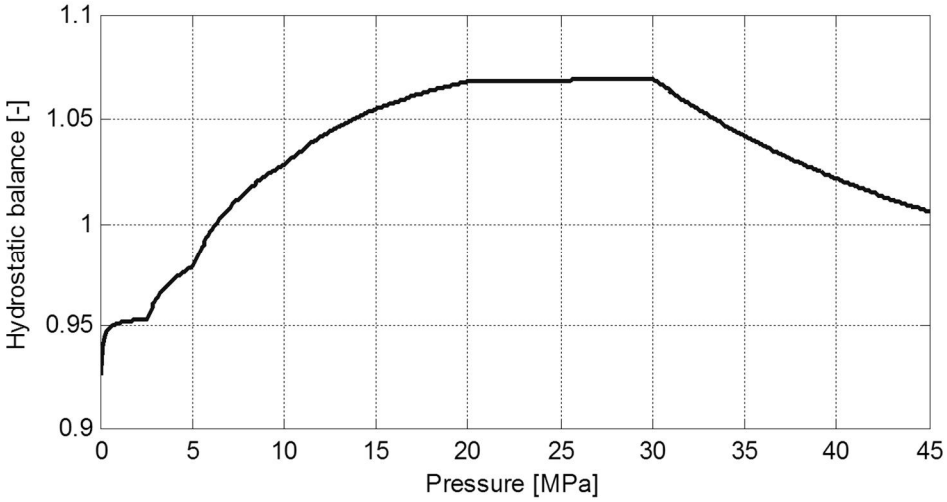

Figure 60. Hydrostatic balance of slipper D with zero angle of swashplate.

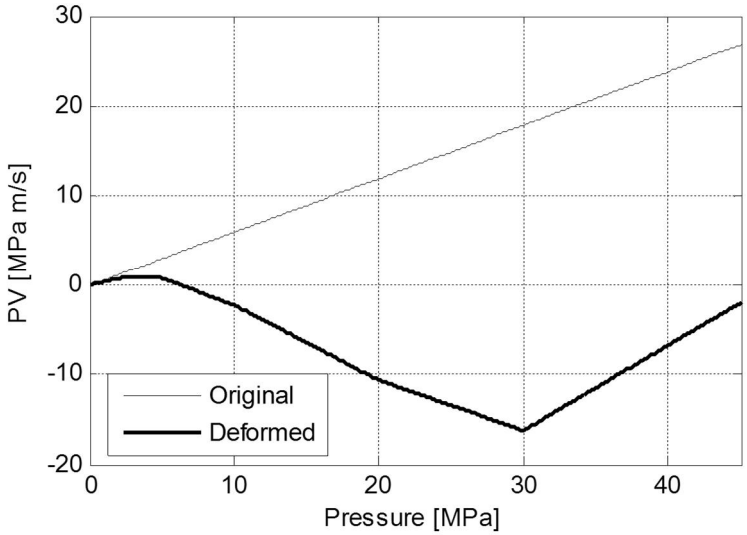

Figure 61. Pv-rate of slipper D with zero angle of swashplate.

Figure 60 and Figure 61 show the reason for the limited pressure level of slipper D. The hydrostatic balance of the slipper rises over the limit already at pressure level of 6.5 MPa. That is because the dimensions of the slipper determine that the starting point is high and the PEEK is elastic material. The PV-rate of the slipper D is negative while the hydrostatic balance is over one. However, slipper D can be used at a pressure level of 14 MPa, because the angle of the swashplate is not zero and there is a slipper hold-down mechanism in a real pump. It should be noticed that an error occurs also because in a real pump the pressure profile is not same in all angular positions during operation.

Leakages of the slippers are shown in Figure 62.

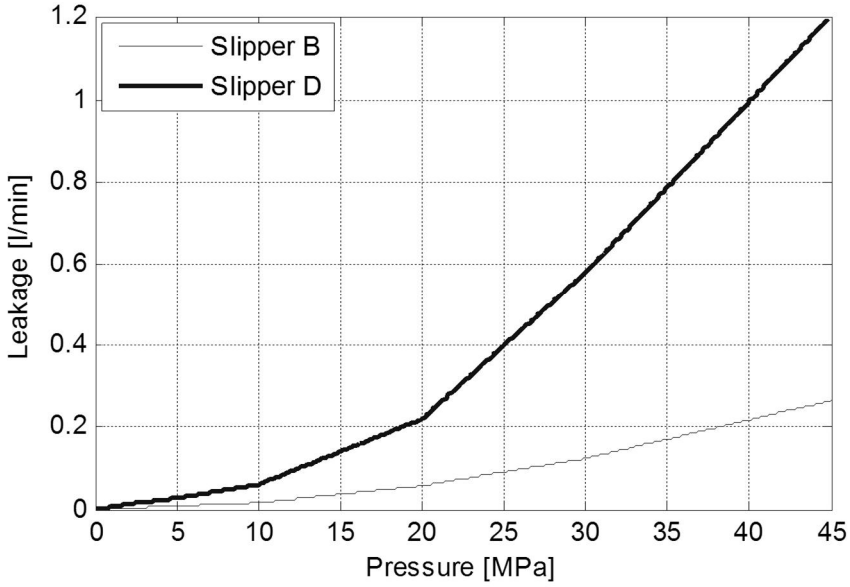

Figure 62. PV-rate of slipper B and slipper D with 1 μm gap height.

Figure 62 shows that the leakage is very high. The leakages in both slippers are noticeably higher than without deformation. The leakage of slipper D is higher than that of slipper B because the ratio between the inner and outer radius of the slipper is higher and the deformation of the sliding surface is bigger

because of the properties of the PEEK 2. Leakages at high pressure levels are very high and the volumetric efficiency of the pump reduces. As shown in Equation 28, the leakage is a function of the inner and outer radius of the sliding surface. The sizing of the slipper should look also at the leakage point of view. However, it should be noticed that in Figure 62 the gap height of 1 μm is used in FSI calculation.

6.3 Effect of swashplate angle changes on slipper behaviour

The effect of the swashplate angle changes are studied by turning the swashplate from 0 to 20 degrees and back to zero degrees as shown in Figure 63.

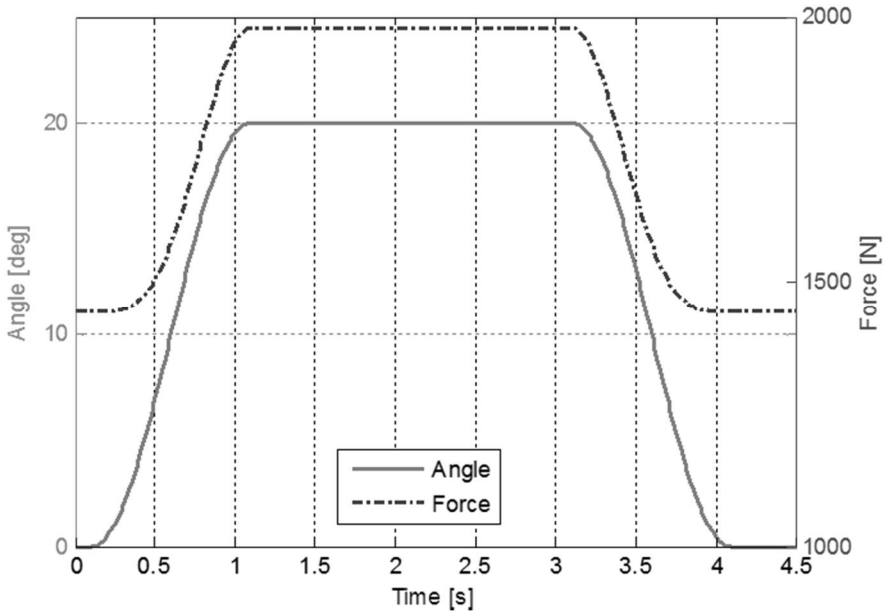

Figure 63. Swashplate angle and slipper force against the swashplate with slipper B at a pressure level of 40 MPa.

Figure 63 shows that the change in the slipper force is high. That is because the slipper force is always perpendicular to the swashplate and the slipper compensates the same absolute number force as zero degree. That is why the whole change can be seen in the force curve if the force against the slipper changes. The change of the angle should be remembered in the slipper design process because the force changes affect the hydrostatic balance and the PV-rate, as Figure 64 shows.

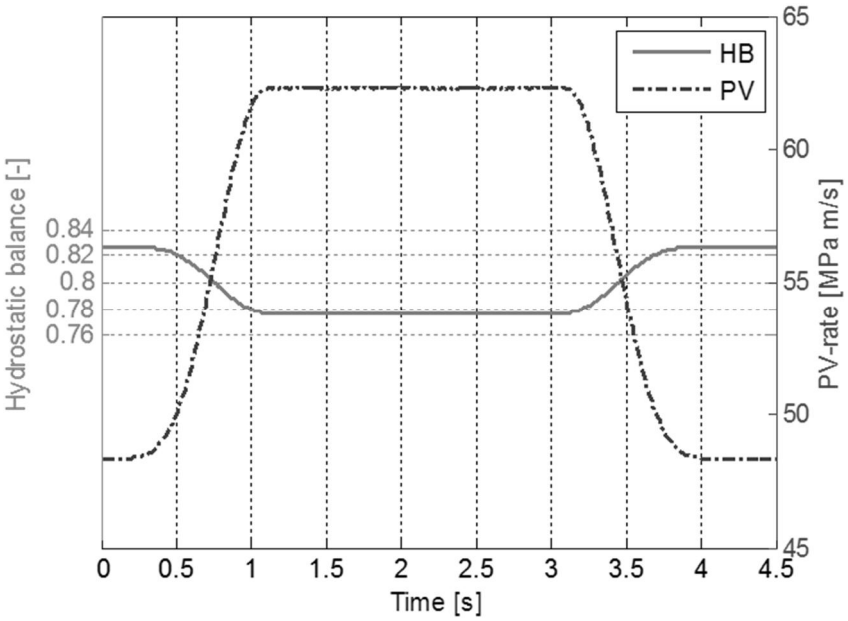

Figure 64. Hydrostatic balance and PV-rate of slipper B at a pressure level of 40 MPa.

Figure 64 shows that the hydrostatic balance of the slipper decreases when the angle of the swashplate rises. It is obvious that in this case the PV-rate of the slipper rises. The change in the PV-rate is high because the angle changing raises the pushing force, but the lifting force and other variables in Equation 29 are constant. An equally high PV-rate has been studied during measurements with the material of slipper B and the slipper works fine. It can be concluded that the higher the swashplate angle is, so the higher is the load of the slipper.

Next, the behaviour of slipper D during swashplate turning is presented in Figure 65 and Figure 66.

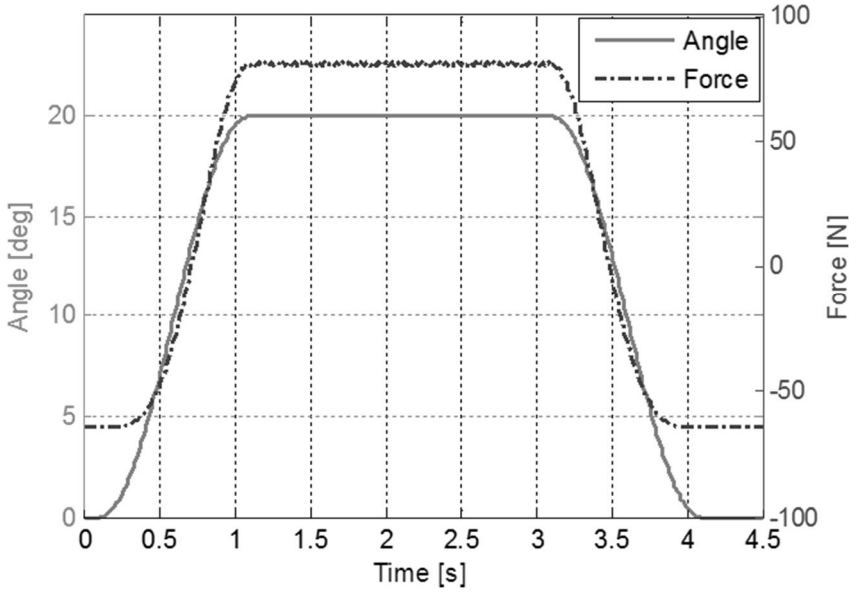

Figure 65. Swashplate angle and slipper force against the swashplate with slipper B at a pressure level of 40 MPa.

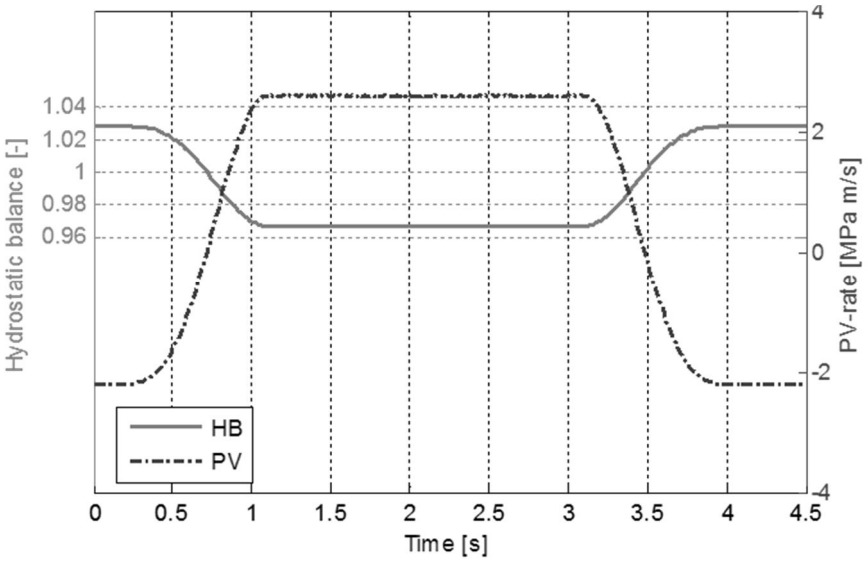

Figure 66. Hydrostatic balance and PV-rate of slipper D at a pressure level of 40 MPa.

Figure 65 and Figure 66 show that with slipper D, the behaviour of the slipper is on the limit all the time. With zero angle slipper D is over the limit and turning the swashplate makes the behaviour better. Figure 65 and Figure 66 show that the pressure level of 40 MPa is too high for slipper D. However, there is nothing that prevents swashplate turning if the pressure level is acceptable.

6.4 Discussion

The simulation model shows how the slippers act when the pressure level rises. It is possible to use slipper B at higher pressure levels. Slipper B is designed to be safe and the hydrostatic balance is quite low, which also means higher PV-rate values. The behaviour of slipper D changes significantly at high pressure level and the hydrostatic balance rises over the limit.

It is possible to realize the turning of the swashplate because the effect on the slipper behaviour can be controlled. However, the turning area and the changes of slipper behaviour should be taken into account in the slipper design process.

Pumping loss acts as Equation 39 shows. To minimize leakage, the ratio between inner and outer radius of the slipper should be as low as possible. In practise, it is obvious that it is not possible to increase the outer radius to an unlimited degree. However, for example with slipper B, it is possible to increase the outer radius. In that way it is possible to achieve many positive things: leakage flow decreases, the PV-rate decreases, hydrostatic balance and load capacity increase. The negative point is that the friction force increases. However, this should be accepted because otherwise leakages will rise too high.

The simulations show that there is high force after hydrostatic compensation pushing the slipper against the swashplate with slipper B. The force, which is not carried hydrostatically, should be carried in some other way. Hydrodynamic force is generated between nonparallel moving items. That carries part of the force, but the fluid film generation of water is low and another way to carry load is mechanical contact.

7 CONCLUSIONS

In this study different slippers and the characteristics of slipper-swashplate contact in water hydraulic axial piston pumps are investigated. Interest is focused on the changes between different pressure levels caused mainly by deformations. Also changes during swashplate turning are studied.

Water is a challenging medium in hydraulic components because the water film is thin and water has a low viscosity-pressure coefficient. Water as a pressure medium causes limitations to the materials, and industrial plastics are widely used in water hydraulic components. Because of that, deformations have a major role in slipper behaviour. Deformations of the slipper affect the pressure field under the sliding surface and that changes the hydrostatic balance of the slipper and the leakage flow of the slipper. Another consideration is that industrial plastics have a maximum PV-rate, which limits the load of the slipper.

With basic equations it is possible to size the slipper near the limit. All the different requirements can be fulfilled and the high pressure level or the adjustable swashplate angle is not a problem. The big challenge is that basic equations work only in ideal situations. In real situations there are many distractions, which make the basic equations inexact. The biggest error comes from sliding surface deformation.

The most important dimensions of the slipper are the inner and outer radius of the sliding surface because the behaviour of the slipper is mostly dependent on these. Although there are many different forces affecting the slipper, pressure dependent forces are dominant and the properties cannot be realized satisfactorily if the hydrostatic balance of the slipper is not in the right area.

The study of the PV-rate shows that the absolute size of the slipper or the piston is not significant. Instead, the ratios between the dimensions are very important because good behaviour can be achieved if the ratio between the dimensions is correct. A higher pressure level makes the PV-rate more sensitive in terms of the ratio. However, good behaviour can still be achieved. The experimental test shows that the maximum PV-rate of the material is not critical. Higher values can be used with normal rotation speed area.

Because plastic materials are used, deformations occur and the variety of the behaviour is significant. That makes measurement very challenging to make, but the changing situations can be analysed. Force and gap height measurements showed that the operation of the slipper is very smooth during swashplate turning. There was nothing found in gap height measurements that would prevent the swashplate turning during operation. The friction measurements of the slipper showed that with at least a 4 m/s sliding speed area both slipper structures worked fine in static and also in changing situations. The friction values are low and peaks do not occur during angle changing. PEEK has a maximum PV-rate, but in water hydraulic components it is easy to exceed it. PV-rate measurements with high PV-rate values have been done and with the measured slipper the friction values are low despite exceeding the limit values. Although the PV-rate limits are quite low, higher values can be used if the rotation speed is high enough.

A deeper study of the behaviour of the components is now needed and that can be achieved with numerical methods and simulation. Stress components of the spherical joint can easily be too high with a high pressure level. The way to avoid that is to scale up the spherical joint.

FSI calculations are used to obtain more information about the slipper-swashplate contact. The difference between the results of the basic equations and FSI are remarkable. If a higher pressure level or optimised pump characteristics are needed, FSI should be part of the design process of the slipper structure and characteristics. FSI calculations show that the pressure profile changes significantly and the higher the pressure is, the higher is the error between the basic equation and FSI calculations. Slipper leakage changes a lot when the deformations are taken into account.

The following restrictions and guidelines for slipper design should be highlighted, because these clearly came up during the study:

- Common rules for slippers cannot be found, for two reasons:
    - The structure of the slipper is very significant, because different combinations of stainless steel and industrial plastics cause different deformations.
    - There are various different kinds of industrial plastics on the market and their properties can vary significantly. The characteristics of the material affect the behaviour of the slipper.
- Slipper size is not significant and slipper dimensions can be scaled up or down. However, the ratio between the inner radius and outer radius of the slipper is important, because that affects all the main properties of the slipper. The change of the slipper inner radius as a function of pressure level is not significant and there is no need to take that into account in the design process.
- The significance of the deformations of the slipper is related to the lubrication film thickness. That is important in water hydraulic applications because the water film thickness is low and the used materials are easily deformable.
- The PV-rate has to be taken into account with industrial plastics; however, measurements show that maximum values can be exceeded. A higher pressure level makes the PV-rate more sensitive for the ratio between the inner and outer radius of the slipper.
- Swashplate angle turning can be effected with the studied slippers. The behaviour is smooth during changes in all measurements. That is also noticed from the theoretical point of view, because the force changes can be controlled.
- FSI calculations are necessary to make the right decisions in slipper design because slipper characteristics like hydrostatic balance cannot be sized near the limit if the deformations are not clarified accurately. However, all different situations are not needed for calculation because the behaviour of the slipper is logical.
- The pressure profile under the sliding surface changes remarkably as a function of pressure level. The changes occur because of the deformation of the sliding surface. Sliding surface force can rise by even one third, which has to be taken into account.

Some of the challenges in the future are to find the optimized structure of slipper water hydraulics. That means that a combination of stainless steel and industrial plastic is optimized to avoid deformations. The result should be more stable slipper characteristics in a wider pressure area.

The use of ceramics instead of industrial plastics would solve many problems but of course there are a lot of challenges as well. However, the ceramics should be taking into account to think about solutions for higher pressure levels.

REFERENCES

[Anon 2000] **Anon.** APP: High pressure water pumps for tap water or sea water applications, (Instructions). Hytar. 2000.

[Anon 2009] **Anon.** Mechanical (formerly Simulation). Tutorial, Release 12.1, Ansys, Inc. 2009.

[Anon 2010a] **Anon.** Material Properties Guide. Victrex. http://www.victrex.com (19.1.2010).

[Anon 2010b] **Anon.** Danfoss A/S homepage. http://www.danfoss.com/BusinessAreas/High-Pressure +Systems/Products/Pumps.htm (20.10.2010)

[Anon 2011] **Anon.** The Water Hydraulics Company homepage. http://www.waterhydraulics.co.uk/ new2/ pumps.php (4.5.2011).

[Backé 1999] **Backé, W.** Water- or oil-hydraulics in the future. 6th Scandinavian International Conference on Fluid Power, SICFP'99, Tampere, Finland, 1999.

[Bech 1999] **Bech, T., Olsen, S., Klit, P.** Design of Pumps for Water Hydraulic Systems. 6th Scandinavian International Conference on Fluid Power, SICFP'99, Tampere, Finland, 1999.

[Borghi 2009] **Borghi, M., Specchia, E., Zardin, B., Corradini, E.** The critical speed of slipper bearings in axial piston swash plate type pumps and motors. Proceedings of the ASME 2009 Dynamic systems and control conference, DSCC2009, Hollywood, California, USA. 2009.

[Brookes 1995] **Brookes, C. A., Fagan M. J., James R. D., Kerry P., McConnachie J.** The development of water hydraulic pumps using advanced engineering ceramics. 4th Scandinavian International Conference on Fluid Power, Tampere, Finland, 1995.

[Canbulut 2009] **Canbulut, F., Sinanoglu, C., Koç, E.** Experimental analysis of frictional power loss of hydrostatic slipper bearings. Industrial Lubrication and Tribology, Vol. 61 Iss: 3, pp.123 – 131, 2009.

[Carbone 2002] **Carbone, G., Soria, L.** Bearing load on circular slippers: hydrodynamic and hydrostatic aspects. 2nd International FPNI Ph.D. Symposium on Fluid Power, Modena, Italy, 2002.

[Donders 1997] **Donders, S., Backé, W.** Optimisation of high-pressure piston pumps for HFA-fluids. 5th Scandinavian International Conference on Fluid Power, SICFP'97, Sweden, 1997.

[Dong 2001] **Dong, W., Zhuangyun, L., Yuguan, Z.** Study of the key problems in a water hydraulic piston pump and its applications. Industrial Lubrication and Tribology, Volume 53, Number 5, pp. 211-216(6), 2001.

[Hamrock 1994] **Hamrock, B. J.** Fundamentals of fluid film lubrication. McGraw-Hill, Inc. 1994. p. 690. ISBN 0-07-025956-9.

[Harris 1996] **Harris, R. M., Edge, K. A., Tilley, D. G.** Predicting the behavior of Slipper Pads in Swashplate-Type Axial Piston Pumps. Journal of Dynamic Systems, Measurement and Control - Transactions of the ASME, Vol. 118(1), pp 41-47, 1996.

[Hooke 1988] **Hooke, C. J., Li, K. Y.** The lubrication of overclamped slippers in axial piston pumps - centrally loaded behaviour. Proceedings of the Institution of Mechanical Engineers, Vol. 202C, pp. 287–293, 1988.

[Huanlong 2006] **Huanlong, L., Jian, K., Guozhi, W., Lanying, Y.** Research on the lubrication characteristics of water hydraulic slipper friction pairs. Proceedings of the Institution of Mechanical Engineers Part C, Vol. 220. Number 10, pp. 1559-1568. 2006.

[Ivantysyn 2001] **Ivantysyn, J., Ivantysynova, M.** Hydrostatic Pumps and Motors, First English Edition, Akademia Books International, New Delhi, India, 2001. ISBN-81-85522-16-2.

[Jiao 2003] **Jiao, S., Zhou, H., Yang, H., Gong, G.** Investigation on materials for friction pairs in water hydraulic piston pump. The Eight Scandinavian International Conference on Fluid Power, SICFP'03, Tampere, Finland, 2003.

[Kazama 1993a] **Kazama, T., Yamaguchi, A.** Optimum design of bearing and seal parts for hydraulic equipment. Wear. Vol. 161, no. 1-2, pp.161-171, 1993.

[Kazama 1993b] **Kazama, T., Yamaguchi, A.** Application of a mixed lubrication model for hydrostatic thrust bearings of hydraulic equipment. Journal of Tribology. Vol. 115, no. 4, pp.686-691, 1993.

[Kazama 2005] **Kazama, T.** Numerical simulation of a slipper model for water hydraulic pumps/motors in mixed lubrication. Proceedings of the 6th JFPS International Symposium on Fluid Power, Tsukuba, Japan, 2005.

[Koc 1992] **Koc, E., Hooke, C. J., Li, K. Y.** Slipper Balance in Axial Piston Pumps and Motors. Trans. ASME, Journal of Tribology, 114, 766–772, 1992.

[Koc 1996] **Koc E., Hooke C. J.** Investigation into the effects of orifice size, offset and overclamp ratio on the lubrication of slipper bearings. Tribology International. Vol 29. No 4, pp.299-305, 1996.

[Koc 1997] **Koc E., Hooke C. J.** Considerations in the design of partially hydrostatic slipper bearings. Tribology International. Vol 30. No 11, pp.815-823, 1997.

[Kuikko 1997] **Kuikko T., Saari M.** Liukujärjestely. Patent FI964864. 1997. (in Finnish)

[Leino 2008] **Leino T.** On the flow and Cavitation Characteristics of Water Hydraulic Seat valve Structures. ISBN 978-952-15-1936-9. Tampere University of Technology, 2008.

[Li 1991] **Li, K. Y., Hooke, C. J.** A note on the lubrication of composite slippers in water-based axial piston pumps and motors. Wear, Vol. 147, no. 2, 1991.

[Manring 2002] **Manring, N. D., Johnson, R. E., Cherukuri, H. P.** The Impact of Linear Deformations on Stationary Hydrostatic Thrust Bearings. Journal of Tribology, Vol. 124 no. 4, pp. 874-877, 2002.

[Manring 2004] **Manring, N. D., Wray, C. L., Dong, Z.** Experimental Studies on the Performance of Slipper Bearings Within Axial-Piston Pumps. Journal of Tribology, Vol. 126 no. 3, pp. 511-518, 2004.

[Nie 2006] **Nie, S. L., Huang, G. H., Li, Y. P.** Tribological study on hydrostatic slipper bearing with annular orifice damper for water hydraulic axial piston motor. Tribology International, Vol. 39 no. 11, pp. 1342-1354, 2006.

[Olsen 2008] **Olsen, P., Hansen, O. T., Martensen, L.** Water hydraulic machine. Patent US 2008/0223207 A1.

[Pelosi 2008] **Pelosi, M., Ivantysynova, M.** A new fluid-structure interaction model for the slipper-swash plate interface. Proceedings of the 5th FPNI Ph.D. Symposium, Cracow, Poland, pp. 219 - 236. 2008.

[Pelosi 2009] **Pelosi, M., Ivantysynova, M.** A novel fluid-structure interaction model for lubricating gaps of piston machines. Proceedings of the Fifth Fluid Structure Interaction Conference, eds. C.A. Brebbia, WIT Press, Southampton, pp.13-24, 2009.

[Petrovic 2011] **Petrovic, R., Pezdirnik, J., Banaszek, A.** Mathematical Modeling and Experimental Research of Novel Sea Water Hydraulic Axial Piston Pump. The Twelfth Scandinavian International Conference on Fluid Power, SICFP'11, Tampere, Finland, 2011.

[Pohls 1999] **Pohls, O., Rantanen, O., Kuikko, T.** Sea water hydraulic axial piston machine. The Sixth Scandinavian International Conference on Fluid Power, SICFP'99, Tampere, Finland, 1999.

[Riley 1974] **Riley, K. F.** Mathematical methods for the physical sciences. Cambridge University Press 1974. ISBN 0 521 20390 2

[Rokala 2008a] **Rokala, M., Calonius, O., Pietola, M., Koskinen, K.T.** Test Equipment for Measuring Water Film Thickness between the Swashplate and the Slipper Pad in Water Hydraulic Axial Piston Pumps. 6. IFK2008 – Workshop 31 March, Dresden, Germany, 2008.

[Rokala 2008b] **Rokala, M., Calonius, O., Pietola, M., Koskinen, K.T.** Study of Lubrication Conditions in Slipper-Swashplate Contact in Water Hydraulic Axial Piston Pump Test Rig, JFPS2008, Toyama, Japan, 2008.

[Rokala 2010] **Rokala, M., Koskinen, K.T.** Comparison of slipper structures in water hydraulic axial piston pump. 6th FPNI-PhD Symposium, West Lafayette, USA, 2010.

[Rokala 2011] **Rokala, M., Koskinen K.T.** The Effect of PV-rate on PEEK-made Slipper Behaviour in Water Hydraulic Axial Piston Unit. The Twelfth Scandinavian International Conference on Fluid Power, SICFP'11, Tampere, Finland, 2011.

[Rydberg 2001] **Rydberg, K.-E.** Energy efficient water hydraulic systems. The Fifth International Conference on Fluid Power Transmission and Control, HangZhou, China, 2001.

[Rämö 1999] **Rämö, J., Hyvönen, M., Mäntylä, T., Koskinen, K.T., Vilenius, M.** Wear resistance of materials in water hydraulics. The Sixth Scandinavian International Conference on Fluid Power, Proceedings of the Conference, Tampere, Finland, 1999.

[Terävä 1995] **Terävä, J., Kuikko, T., Vilenius, M.** Development of sea water hydraulic power back. Proceedings of the Fourth Scandinavian International Conference on Fluid Power, Tampere, Finland, 1995.

[Trostmann 1996] **Trostmann, E.** Water hydraulic control technology. Marcel Dekker, Inc. 1996. ISBN 0-8247-9680-2.

[Urata 1999] **Urata, E.** Technological aspects of the new water hydraulics. 6th Scandinavian International Conference on Fluid Power, SICFP'99, Tampere, Finland, 1999.

[Usher 1998a] **Usher, S.** Improvements 10 years on – 2nd general water hydraulic pumps and motors. International Workshop on Water Hydraulic Systems and Applications, Lyngby, Denmark, 1998.

[Usher 1998b] **Usher, S., Markham T.** Improvements in and related to hydraulic pumps and motors. Patent WO 9839568 (A1). 1998.

[Wang 2002] **Wang, X., Yamaguchi, A.** Characteristics of hydrostatic bearing/seal parts for water hydraulic pumps and motors. Part 1: Experiment and theory, Tribology International, Vol. 35 no. 7, pp. 425-433, 2002.

[Wieczoreck 2000] **Wieczoreck, U., Ivantysynova, M.** CASPAR – a computer-aided design tool for axial piston machines, PTMC 2000, Bath, United Kingdom, 2000.

[Yang 2003] **Yang, H., Yang, J., Zhou, H.** Research on materials of piston and cylinder of water hydraulic pump. Industrial Lubrication and Tribology, Volume 55, Number 1, pp. 38-43, 2003.

[Yuge 2006] **Yuge, A., Hayashi, T., Nishida, H.** Performance of the Water Hydraulic Pump Using DLC Coatings, The 5th International Fluid Power Conference (IFK), Aachen, Germany, 2006.

[Zhou 1999] **Zhou, H., Yang, H.** Diagnosis of cavitation inception in water hydraulic piston pump. 6th Scandinavian International Conference on Fluid Power, SICFP'99, Tampere, Finland, 1999.

APPENDIX A: CFD model parameters

Table A1: Settings of Ansys CFX 13.0 Service Pack 2 used for FSI in Chapter 5.4.

Analysis type	
External Solver Coupling	
Option	ANSYS MultiField
Coupling Time Duration	Total time: 3[s]
Coupling Time Steps	Timesteps: 1[s]
Coupling Initial Time	Automatic
Analysis type	Steady State
Solver Control	
Advection Scheme	High Resolution
Convergence control	
Min. Iterations	1
Max. Iterations	100
Convergence Criteria	
Residual Type	RMS
Residual Target	0.0005
Coupling Step Control	Max. 10, Min. 1
Solution Sequence Control	
Solve ANSYS Fields	Before CFX Fields
Coupling Data Transfer Control	Under Relaxn. Fac. 0.75 Convergence target 0.0001
Default Domain	
Domain Type	Fluid Domain
Fluid 1	
Option	Material library
Material	Water
Morphology	Continuous Fluid
Reference Pressure	1 [atm]
Buoyancy Model	Non Buoyant
Domain Motion	Stationary
Mesh Deformation	Regions of Motion Specified
Heat Transfer	None
Turbulence	None (Laminar)
Combustion	None
Thermal Radiation	None
Material:Water	
Material Description	Water (liquid)
Molar Mass	18.02 [kg kmol^-1]

Density	997.0 [kg m^3]
Dynamic Viscosity	8.899e-4 [kg m^-1 s-1]
Thermal Conductivity	0.6069 8W m^-1 K^-1]
Global Initialization	
Cartesian Velocity Components	U: 0 [m s^-1], V: 0 [m s^-1], W: 0 [m s^-1]
Static Pressure	Automatic
Pressure Input	
Boundary Type	Inlet
Flow Regime	Subsonic
Mesh Motion	Stationary
Mass and Momentum	Static Pressure: 10 [MPa]
Flow Direction	Zero Gradient
Pressure Output	
Boundary Type	Opening
Flow Regime	Subsonic
Mesh Motion	Stationary
Mass and Momentum	Opening Pres. and Dirn: 0.1 [MPa]
Flow Direction	Normal to Boundary Condition
Interface	
Boundary Type	Wall
Mesh Motion	
Option	ANSYS MultiField
Receive from ANSYS	Total Mesh Displacement
ANSYS Interface	FSIN_1
Send to ANSYS	Total Force
Mass and Momentum	No Slip Wall
Domain Interface Side 1/ Side 2	
Boundary Type	Interface
Mesh Motion	Conservative Interface Flux
Mass and Momentum	Conservative Interface Flux
Interface Models	Rotational Periodicity
Axis Definition	Coordinate Axis
Rotation Axis	Global X
Mesh Connection Method	Automatic
ANSYS Mechanical	
Solver Type	Program Controlled
Large Deflection	Off
Calculate Stress	Yes
Calculate Strain	Yes
Calculate Results At	All Time Points
Material	PEEK_1
Nonlinear Effects	Yes
Thermal Strain Effects	Yes

```
================================================================================
OUTER LOOP ITERATION =    1                    CPU SECONDS = 8.299E+00
--------------------------------------------------------------------------------
| SOLVING : Mesh Displacement                                                  |
--------------------------------------------------------------------------------
|       Equation       | Rate | RMS Res | Max Res |  Linear Solution |
+----------------------+------+---------+---------+------------------+
| X-Disp               | 0.00 | 2.4E-01 | 9.9E-01 |       2.0E-03  OK|
| Y-Disp               | 0.00 | 1.2E-01 | 9.8E-01 |       1.2E-03  OK|
| Z-Disp               | 0.00 | 2.5E-02 | 3.3E-01 |  8.4  1.2E-03  OK|
+----------------------+------+---------+---------+------------------+
| X-Disp               | 0.01 | 1.3E-03 | 2.2E-02 |       9.1E-02  OK|
| Y-Disp               | 0.01 | 7.1E-04 | 2.5E-02 |       4.5E-02  OK|
| Z-Disp               | 0.01 | 1.5E-04 | 8.7E-03 | 23.3  4.6E-02  OK|
+----------------------+------+---------+---------+------------------+
| X-Disp               | 0.09 | 1.2E-04 | 9.4E-04 |       9.6E-02  OK|
| Y-Disp               | 0.06 | 4.6E-05 | 1.0E-03 |       5.4E-02  OK|
| Z-Disp               | 0.07 | 9.4E-06 | 3.5E-04 | 30.7  5.6E-02  OK|
+----------------------+------+---------+---------+------------------+
+------------------------------------------------------------------------------+
|                          Mesh Statistics                                     |
+----------------------+---------------+--------------+--------------+
| Domain Name          | Orthog. Angle | Exp. Factor  | Aspect Ratio |
+----------------------+---------------+--------------+--------------+
|                      | Minimum [deg] |   Maximum    |    Maximum   |
+----------------------+---------------+--------------+--------------+
| Default Domain       |       70.3 OK |         22  ! |         35 OK |
+----------------------+---------------+--------------+--------------+
|                      |  %!  %ok  %OK | %!  %ok  %OK | %!  %ok  %OK |
+----------------------+---------------+--------------+--------------+
| Default Domain       |   0    0  100 | <1    0  100 |  0    0  100 |
+----------------------+---------------+--------------+--------------+
--------------------------------------------------------------------------------
|       Equation       | Rate | RMS Res | Max Res |  Linear Solution |
+----------------------+------+---------+---------+------------------+
| U-Mom                | 0.00 | 2.1E-02 | 6.5E-01 |       5.5E-01  ok|
| V-Mom                | 0.00 | 1.5E+01 | 2.4E+02 |       9.9E-04  OK|
| W-Mom                | 0.00 | 1.8E+00 | 4.4E+01 |       4.3E-03  OK|
| P-Mass               | 0.00 | 1.1E-03 | 1.7E-02 |  9.2  1.0E-02  OK|
+----------------------+------+---------+---------+------------------+
```

Figure A1. Information about Ansys CFX first iteration loop.

APPENDIX B: Simulation parameters

```
% Slipper type
type=2;                                 % Slipper type:
                                        % 1= PEEK with steel collar (Slipper B)
                                        % 2= PEEK with steel core (Slipper D)

% Common parameters
rpm = 1500;                             % Rotation speed [r/min]
P_system = 100e5;                       % Pressure into the cylinder [Pa]
r_rot = 0.04;                           % Rotation circle [m]
h_G = 1e-6;                             % Gap height [m]

% Material properties
if type == 1
    Max_PV = 18;                        % Maximum PV-rate of slipper material
                                          [MPa m/s]
else
    Max_PV = 2.4;                        % Maximum PV-rate of slipper material
                                          [MPa m/s]
end


% Water properties
myy = 0.8e-3;                           % Dynamic viscosity [Pa*s]

% Structure
if type == 1
    % Piston
    piston_m = 0.108;                   % Mass (piston, slipper, collar,
                                           eddy current sensor) [kg]
    piston_r = 0.008145;                % Piston radius [m]
    piston_A = pi*piston_r^2;           % Piston area [m^2]
    friction_cyl_piston = 0.08;         % Friction coefficient between cylinder
                                           and the piston [-]


    % Slipper
    R_G = 0.009175;                     % Outer radius of the sealing land [m]
    r_G = 0.00495;                      % Inner radius of the sealing land [m]
    A_in_G = pi*r_G^2;                  % Area of the slipper pocket [m^2]
    m_G = 0.01323;                      % Mass of the slipper [kg]
    distance_G = 0.00739;               % Distance between spherical joint and
                                           centre of gravity of the slipper [m]
    A_slipper=pi*R_G^2-A_in_G;          % Area of the sealing land [m^2]
    HB_1=0.729;                         % Hydrostatic balance [-]

else
    % Piston
    piston_m = 0.108;                   % Mass (piston, slipper, collar,
                                           eddy current sensor) [kg]
    piston_r = 0.00848;                 % Piston radius [m]
    piston_A = pi*piston_r^2;           % Piston area [m^2]
    friction_cyl_piston = 0.08;         % Friction coefficient between cylinder
                                           and the piston [-]
```

```
    % Slipper
    R_G = 0.010;                    % Outer radius of the sealing land [m]
    r_G = 0.00645;                  % Inner radius of the sealing land [m]
    A_in_G = pi*r_G^2;              % Area of the slipper pocket [m^2]
    m_G = 0.01359;                  % Mass of the slipper [kg]
    distance_G = 0.00625;           % Distance between spherical joint and
                                       centre of gravity of the slipper [m]
    A_slipper=pi*R_G^2-A_in_G;      % Area of the sealing land [m^2]
    HB_1=0.923;                     % Hydrostatic balance [-]
end

% Vectors from FSI
Pressure_level=
[0 2.5 5 10 20 30 40]*1e6;                  % [Pa]
Output_force=
[0 200.1564 400.8582 835.1028 1773.9594 2871.054 3808.404]; % [N], slipper B
Output_force2=
[0 211.6224 452.3148 1016.046 2212.47 3325.374 3995.964];   % [N], slipper D
Output_flow=
[0 0.004065902 0.007727178 0.016247988 0.057641777 0.12454339 0.218551053];
                                            % [l/min], slipper B
Output_flow2=
[0 0.015339791 0.027154146 0.060795334 0.220312417 0.57939346 0.997054483];
                                            % [l/min], slipper D
Radius_change=
[0 1.26 2.5 3.72 4.94]*1e-6;                % [m], slipper B
Radius_change2=
[0 1.26 2.482 3.871 5.5]*1e-6;              % [m], slipper D
Pressure_r=
[0 10 20 30 40]*1e6;                        % [Pa]
```

APPENDIX C: Overview of the simulation model

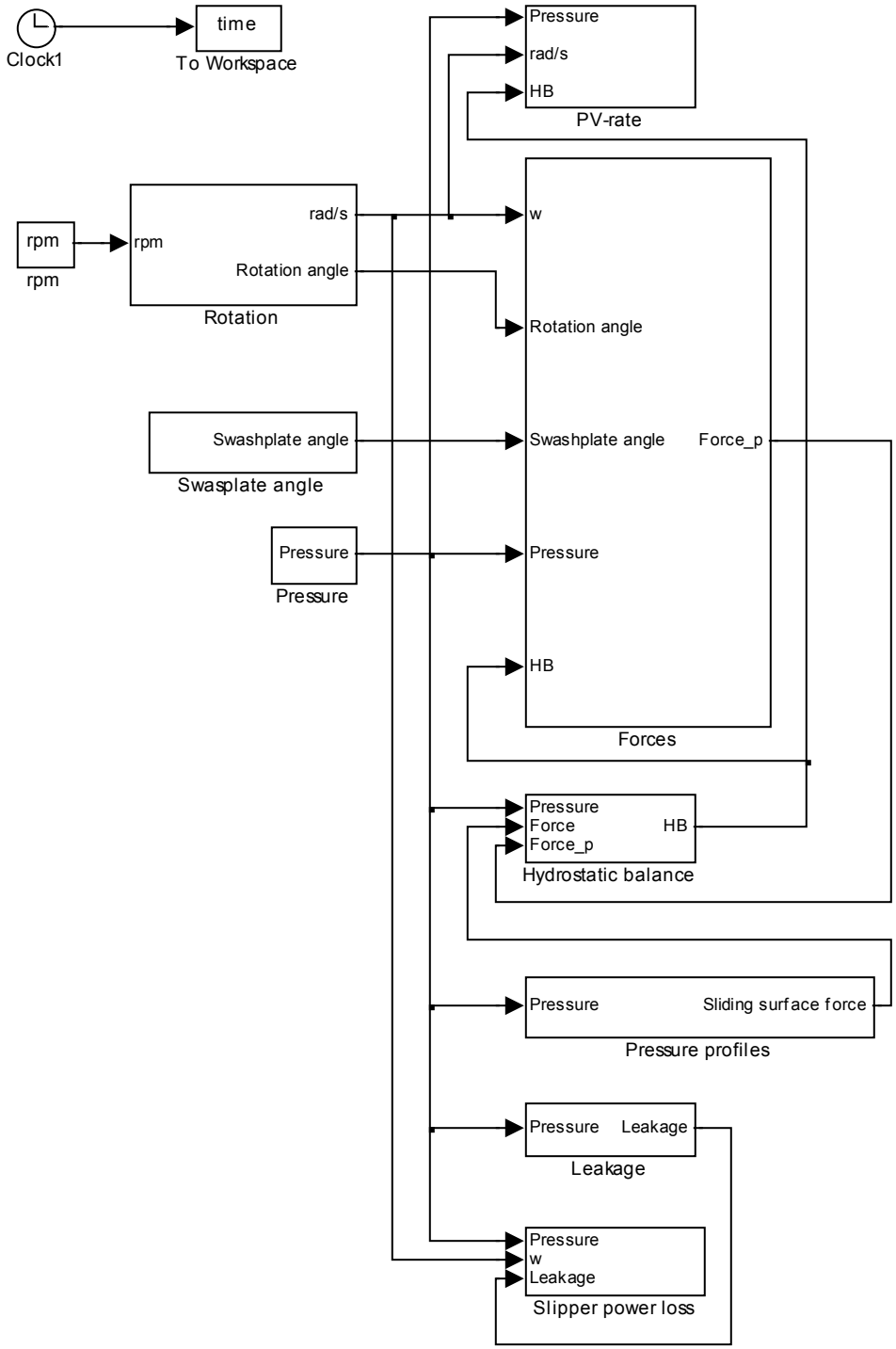

Tampereen teknillinen yliopisto
PL 527
33101 Tampere

Tampere University of Technology
P.O.B. 527
FI-33101 Tampere, Finland

ISBN 978-952-15-2867-5
ISSN 1459-2045